Monte Carlo Adjoint Transport and Adjoint Activation for Biological Dose Calculations and Pathway Analysis

Amir Ebrahim Jaber

May 2012

UWFDM-1412

M.S. thesis.

FUSION TECHNOLOGY INSTITUTE

UNIVERSITY OF WISCONSIN

MADISON WISCONSIN

Monte Carlo Adjoint Transport and Adjoint Activation for Biological Dose Calculations and Pathway Analysis

Amir Ebrahim Jaber

Fusion Technology Institute
University of Wisconsin
1500 Engineering Drive
Madison, WI 53706

http://fti.neep.wisc.edu

May 2012

UWFDM-1412

M.S. thesis.

Monte Carlo Adjoint Transport

and Adjoint Activation

for Biological Dose Calculations and Pathway Analysis

By

Amir Ebrahim Jaber

A thesis submitted in partial fulfillment of

the requirements for the degree of

Masters of Science

(Nuclear Engineering and Engineering Physics)

At the

UNIVERSITY OF WISCONSIN-MADISON

2012

© Copyright by Amir E. Jaber 2012

All Rights Reserved

Abstract

Radioactive decay from the buildup of radioisotopes produced from neutron activation is a major concern in the design and analysis of nuclear systems. For instance, the biological dose that results from gamma decay has significant implications to the safety of the maintenance crew of fission and fusion power plants. The forward multi-step method is an accurate approach to evaluating the delayed gamma dose caused by neutron activation. On the other hand, the adjoint method (that is applied to photon transport) provides techniques of analysis not directly achievable using the forward method as it allows for a direct source-dependent evaluation of the biological dose at a detector placed at a particular location of interest. Additionally, the adjoint method is also applicable to neutron activation in order to indicate the amount of stable isotopes that transmute to different radioisotopes. The Monte Carlo method of radiation transport facilitates the analysis of realistic and complex 3-D problems with flexible modeling capabilities. This thesis applies adjoint methods of Monte Carlo transport and neutron activation to multi-dimensional analyses of fusion systems. The application of adjoint photon transport reveals the biological dose at a detector as a function of time after shutdown. Furthermore, the results of adjoint neutron activation indicate the stable parent isotopes responsible for the production of the radioisotopes undergoing gamma decay that contribute to the biological dose.

Acknowledgements

I want to thank my advisor Dr. Douglass Henderson for supervising the work for this thesis. I am appreciative that he always made himself available in his busy schedule to meet with me. Also, my gratitude belongs to Dr. Laila El-Guebaly for guiding and directing much of my research. My sincere thanks belong to her and the Department of Energy for funding this work.

I want to thank the students and staff of the Fusion Technology Institute for helping develop my knowledge and abilities in computational analysis and nuclear engineering research.

I could not have completed this work without the love and support of my wife-to-be, Dewaa. Her friendship and patience throughout this process did not cease for a moment. My appreciation for all she has done is immeasurable.

Most of all, I am grateful for my truly incredible parents, Ebrahim and Amal Jaber, who have sacrificed so much to give me everything I have in life.

Table of Contents

List of Figures

List of Tables

Introduction

The main objective of this thesis is to use adjoint methods of Monte Carlo photon transport and neutron activation for biological dose calculations on a 3-D fusion power plant design.

The first chapter of this thesis focuses on background information. It discusses the importance of characterizing and understanding the effects of neutron irradiation on materials as the motivation for advancing capabilities for accurate biological dose calculations. This chapter provides the needed information to conceptually understand techniques involving the use of adjoint methods for determining the dose. Two rigorous multi-step methods of calculating dose are presented with emphasis on the use and benefits of using adjoint photon transport. A comparison of deterministic and probabilistic codes is included to present the motivation for pursuing the Monte Carlo method for radiation transport. Additionally, adjoint neutron activation is examined as a unique technique for transmutation pathway analysis to aide in the materials selection process for nuclear systems.

The second chapter contains the mathematical theory relevant to the application of the adjoint transport and activation equations to analysis of physical systems. More specifically, derivations are included that reveal the exact responses from forward methods can be otherwise obtained using adjoint methods. The responses sought after are

the detector response due to photon transport and the isotopic response due to neutron activation.

A number of computational codes and nuclear data sets are used to perform the dose calculations, and the third chapter is devoted to discussing each individually. A deterministic transport code is used to benchmark 1-D problems. A CAD-based Monte Carlo radiation transport code provides the platform for analyzing 3-D geometries. Additionally, a code for neutron activation and an auxiliary code package developed for performing 3-D activation calculations are utilized for various simulations. The nuclear cross section data is taken from two data libraries. The last set of information is the conversion factors for translating gamma-ray fluxes to dose equivalent values.

The fourth chapter is dedicated to presenting the results obtained using the adjoint methods for photon transport and neutron activation. Three physical models are investigated within this chapter. The first problem is an infinite slab geometry. This simple problem is used to understand the Monte Carlo adjoint transport method and benchmark with a deterministic code. The second problem is the ARIES-CS fusion power plant design. This problem is modeled as a series of concentric infinite 1-D cylinders and is also benchmarked with a deterministic code. Lastly, a 3-D model of a fusion design from the Princeton Plasma Physics Laboratory (PPPL) is used to demonstrate the use of adjoint methods for analysis of a 3-D problem. The impact of penetrations on the biological dose was investigated for this problem.

Chapter five contains the conclusions and recommendations as a result of the research performed within this thesis. A number of conclusions regarding the use of adjoint methods for dose calculations are provided. Additionally, improvements on this research and suggestions for future research are offered.

Chapter 1

Background

Nuclear design and analysis requires an understanding of the effects of neutron irradiation. Neutrons will interact with constituent isotopes of a material in several ways. One way is that neutrons cause nuclear reactions with isotopes that transmute the stable isotopes into radioactive isotopes (or radioisotopes) and subsequently cause a stable material to become radioactive. This process is called neutron activation. Materials are often composed of several isotopes that can experience many reactions, thereby causing the buildup of numerous radioisotopes within a material that was originally non-radioactive. Each radioisotope within the activated material will decay with different characteristics. The characteristics of radioactive decay, such as radioactive byproducts, half-life, and decay energy, will greatly influence the design, operation, and safety of fission and fusion power plant designs due to the need for extended shutdown period before accessing the machine, increased cooling requirements to remove the decay heat, or the possibility of high-level waste production at the end of the lifetime of the plant. It is important to understand the radioactive decay in order to implement the proper safety measures in designing nuclear systems.

As a radioisotope decays, it releases radiation that is hazardous to living and non-living entities. The biological dose is a measure of the severity of the damage that the radiation has on living beings. This work concentrates on the dose resulting from gamma decay of radioisotopes. Gamma-rays are the most penetrating type of radiation after plant shutdown and have the largest impact on the dose. Therefore, they must be well shielded to minimize exposure to personnel. The shutdown maintenance schedule for a fission or fusion power plant design will be heavily dictated by the dose because it will determine the cooling time required to allow remote maintenance or reach hands-on safety limits for maintenance personnel. The cooling time is normally a few days after shutdown. Longer cooling times are undesirable and may suggest expensive remote-handling equipment to perform the needed maintenance shortly after shutdown. Therefore, it is necessary to accurately quantify the dose in the process of designing a nuclear system to determine the access scheme for the plant.

The dose can be determined using a rigorous multi-step method that involves performing a sequence of neutron and photon calculations for a particular geometry, set of materials, and neutron source. One form of the multi-step method requires creating the photon source distribution from an activation calculation and then using this source for a photon transport calculation to obtain a photon flux distribution in energy and space. Then, established factors for converting photon flux to dose equivalent values (henceforth, flux-to-dose factors) are used as the detector response function to convert the photon flux values to dose rates. In summary, neutron and gamma radiation transport

calculations and a neutron activation calculation are performed within this sequence and information from each of the calculations is carried on in the process. The multi-step method that uses forward photon transport for biological dose is illustrated in Figure 1.

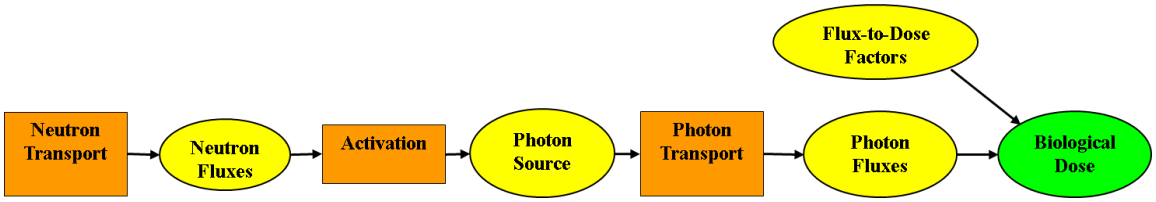

Figure 1: This figure shows the sequence of steps to be taken to determine the biological dose at any location and specific time after shutdown using the forward method. The orange rectangular steps in the sequence represent calculations and the yellow ellipses represent data transfer steps.

The sequence using exclusively forward transport methods is tailored towards directly determining the dose for all spatial locations for an initial neutron source. One forward photon transport calculation can determine the dose throughout a geometric model. However, the forward method would need to be applied for every cooling time that the dose is required since the photon source is continually changing with time.

An alternative multi-step method implements adjoint photon transport. The detector response function is used as the adjoint source, and an adjoint photon transport calculation is performed to determine the adjoint flux distribution in energy and space. The adjoint flux represents the importance or contribution to the detector response should there exist a photon of a given energy at a specified position in the geometric model. The

adjoint flux is then incorporated into the actual photon source generated from the activation calculation in order to determine the dose. The adjoint flux will exist in every bin of the phase-space whereas the actual photon source may not, which results in some bins that do not contribute to the dose. There are again two transport calculations and one activation calculation in this alternative multi-step method. This sequence is shown in Figure 2.

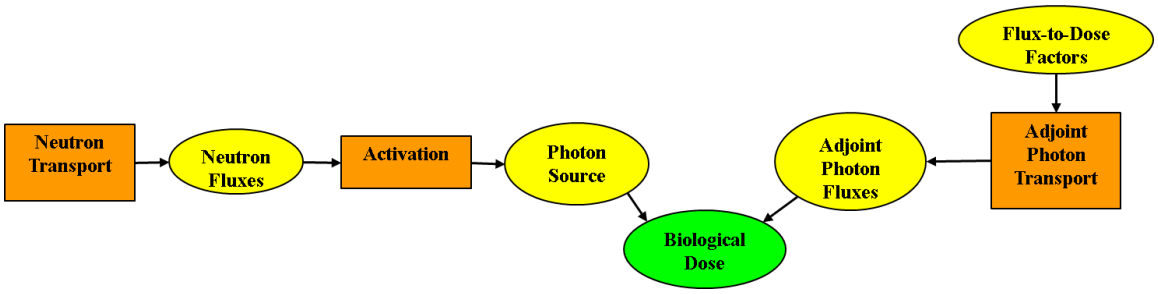

Figure 2: This figure shows the sequence of steps to be taken to determine the biological dose at specific location and all times after shutdown using the adjoint method. The orange rectangular steps in the sequence represent calculations and the yellow ellipses represent data transfer steps.

The sequence using adjoint transport is capable of directly determining the dose at a given detector for multiple cooling times for an initial neutron source. The photon source at any cooling time can be easily determined using simple exponential decay laws and the half-lives of the radioisotopes that have been created. This feature is often desired because it more directly indicates the time-dependent dose at a specific detector location. A time-dependent evaluation of the dose is important in the safety analysis of any component of a nuclear system that will require maintenance during its lifetime.

However, an adjoint transport calculation would need to be performed for every spatial location that the dose is needed. The methodology demonstrated in this thesis is more suited towards analysis that requires the dose for more cooling times than spatial locations.

The most common radiation transport techniques are deterministic and probabilistic methods, of which the most common are the discrete ordinates method and the Monte Carlo method, respectively. Deterministic methods are well suited for obtaining a global solution over the entire domain of the phase-space for a problem. The limitations of deterministic methods rest in that they are inherently multi-group in energy rather than continuous in energy and most of them cannot depict solutions for realistic and complex 3-D geometries. The discrete ordinates method requires the geometric model to be defined using an orthogonal grid, whether it is Cartesian, cylindrical, or spherical. It becomes quite difficult to develop 3-D geometric models of complex fusion power plant designs using only this convention. On the other hand, the Monte Carlo method is well suited for modeling 3-D complex geometries. Monte Carlo is a statistical process that becomes quite difficult to obtain accurate solutions in regions of low flux or as the bin size within the phase-space decreases. Nevertheless, the Monte Carlo method is used for the work presented here for its unique ability to model 3-D geometries fairly accurately.

On a separate topic, the adjoint method can also be applied to neutron activation. To understand adjoint activation, it is necessary to first discuss the forward method for

activation analysis. A forward activation model requires a definition of the geometry, material compositions, phase-space neutron flux distribution, irradiation schedule, and cross section data. The geometric model will be defined with various regions that are assigned group-wise neutron fluxes whose boundaries are determined by the cross section data. The neutron fluxes are typically determined from simulations using radiation transport codes. This information is used to construct activation diagrams or trees that are used to generate the radioisotope inventory. An activation tree is a tool that can show reactions or decays that create pathways for all possible daughter isotopes. Additionally, the activation tree reveals the corresponding relative concentrations of each radioisotope as determined from the activation and decay data. Each reaction or decay is considered a branch of the activation tree, and has a probability of occurring based on the cross sections or half-lives of the radioisotopes. Figure 3 illustrates an example activation tree where the stable isotope Fe-56 is activated by neutrons to different radioisotopes that subsequently transmute or decay until a stable isotope is reached or the relative concentration of the next daughter isotope is below some threshold of interest. Such an activation diagram is normally constructed conceptually for each initial isotope in the activation calculation.

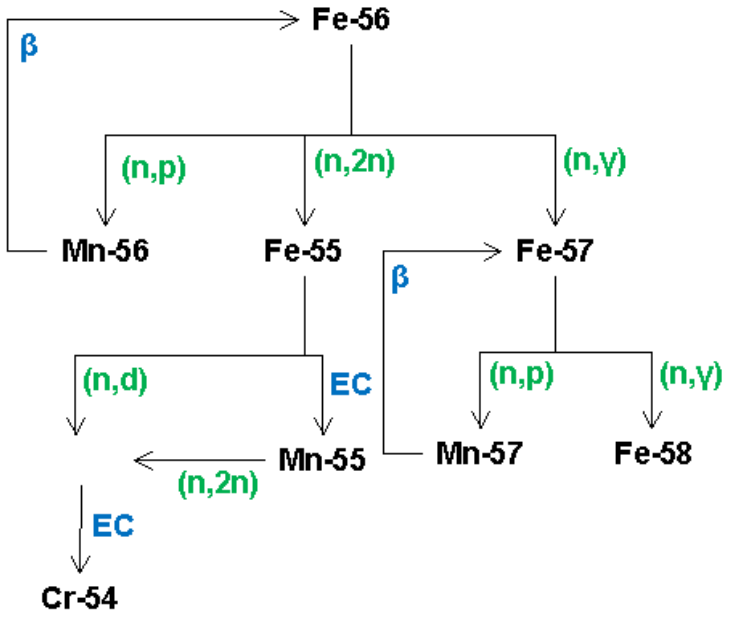

Figure 3: A sample forward activation tree.

The motivation for pursuing the adjoint method for activation is to determine isotopic importance to the activation level. Forward activation cannot directly determine individual parent isotope percent importance or contribution to a particular radioisotope production. It does not answer the question of how much of a certain radioisotope is produced from an isotope in the original material definition. This question is answered using the adjoint method for performing activation analysis. Adjoint activation reveals the source of the dominant radioisotopes that contribute the largest amount to an activation parameter, which is the dose in this case. Whereas adjoint photon transport indicates the photon contribution of surrounding materials to the dose, adjoint activation

reveals the contribution to the dose due to the existence of an isotope in the original material definition. This information is of great importance to the materials selection process. The design process can be enhanced by understanding which of the initial isotopes in the material definition is responsible for producing the undesirable radioisotopes. The implications of the adjoint activation are that optimal material compositions can be determined to minimize safety and environmental impacts. For example, the isotopic compositions can be tailored to ensure low decay heat (that requires a minimal cooling period) or low dose (that allows quick maintenance) for safe repairs or component replacement shortly after shutdown.

To perform adjoint activation, a target radioisotope known to be produced in the forward calculation must be specified. To facilitate the analysis, one can perform a forward activation calculation prior to an adjoint calculation, since this step will determine the dominant radioisotopes contributing to various activation parameters. However, this extra step is not necessary if the target radioisotope is known already. The activation tree is constructed for the target isotope based on adjoint cross section data. All possible pathways from which the target can be produced are created along with relative concentrations of the parent isotopes. An example adjoint tree for the radioisotope Mn-54 is shown in Figure 4.

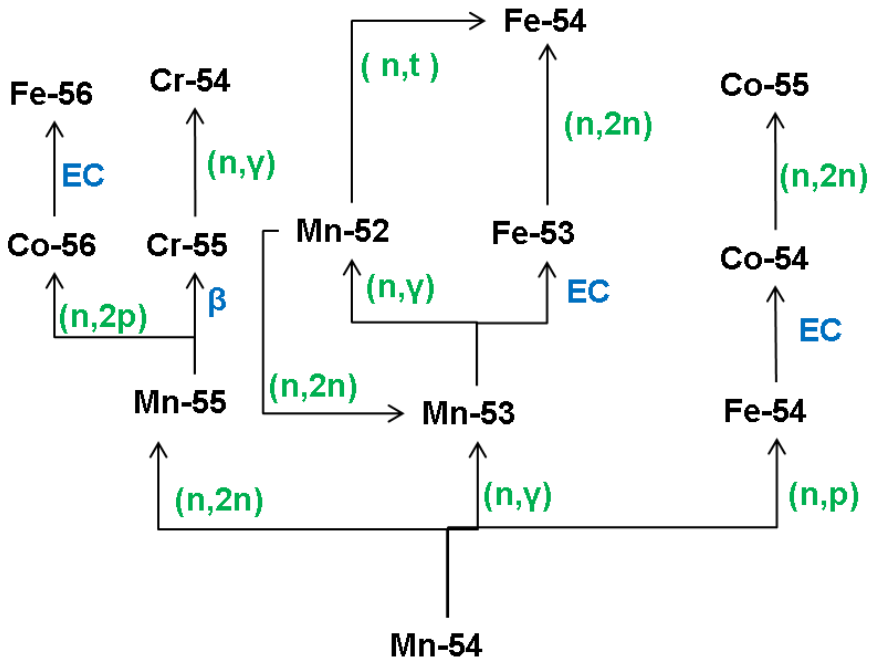

Figure 4: A sample adjoint activation tree.

An important note is that the creation of the activation tree is independent of the material definition used in an actual model. This feature mirrors adjoint transport in that the creation of the adjoint flux distribution is independent of the actual photon source. The adjoint activation tree will contain adjoint isotope densities that represent the importance of all possible isotopes that can lead to the target radioisotope. The isotope importance can be interpreted as the fraction of initial isotopes which will become a radioisotope at the end of activation. The initial isotope number density multiplied by the adjoint isotope density gives the actual number density of the initial isotopes that contribute to the production of a radioisotope. There will be pathways in the adjoint

activation tree that lead to an isotope not included in the material definition. As mentioned earlier, the same behavior is observed in adjoint transport in that the adjoint photon flux will exist within the entire phase-space of the geometric model, but there may not be photons that correspond to every individual bin of the phase-space of the adjoint flux. For adjoint activation, the multiplication of the initial nuclide density by the adjoint isotope density results in an isotope having zero importance for isotopes that are absent in the material definition of a specific model.

In summary, the use of adjoint methods for photon transport and neutron activation provides unique techniques of analysis not directly achievable using forward methods. The work performed in this thesis and discussed in Chapter 4 demonstrates the powerful applications of the adjoint method to the analysis of fusion power plant designs.

Chapter 2

Theory

The implications of the adjoint method applied to photon transport and neutron activation to nuclear design and analysis are investigated in this thesis. Therefore, it is relevant to examine the theory of the adjoint method that illustrates the manner to which techniques using adjoint methods can provide the same response as calculations using forward methods. The derivations of the adjoint operators themselves are not particularly relevant and therefore are not included here. However, the derivations for the adjoint transport operator and adjoint activation operator can be found in Ref [1] and Ref [2], respectively. Instead, the derivations shown here reveal how the adjoint equations for transport and activation can be applied to the analysis of physical systems.

First, some general properties of the adjoint method that will be applied to both transport and activation must be discussed. Equation 1 generally defines the inner product of two arbitrary functions $\psi(x)$ and $\phi(x)$ as the integral over the domain:

$$\langle \psi, \phi \rangle = \int \psi(x)\phi(x)dx. \quad (1)$$

Now say that $\psi(x)$ has an arbitrary mathematical operator **H** applied to it and create a new inner product shown by equation 2:

$$\langle \boldsymbol{H}\psi, \phi \rangle = \int [H\psi(x)]\phi(x)dx. \quad (2)$$

If the operator is not self-adjoint, then the adjoint operator $\mathbf{H}^{+}$ can be defined to operate on ϕ^{+}, an adjoint function, and this new inner product will be equivalent to the original result of **H** operating on ψ. This equality relationship is shown in equation 3:

$$\langle \boldsymbol{H}\psi, \phi \rangle = \langle \psi, \boldsymbol{H}^{+}\phi^{+} \rangle. \tag{3}$$

This equation is known as the adjoint identity and will be used later within this chapter.

The implementation of the adjoint transport equation will be examined first. First the forward transport operator **L** is defined as

$$\begin{aligned} L\psi = {} & \left[\hat{\Omega} \cdot \vec{\nabla} + \Sigma(\vec{r}, E)\right]\psi\left(r, \hat{\Omega}, E\right) \\ & - \iint_{E', \Omega'} \Sigma_s\left(\vec{r}, E' \to E, \hat{\Omega}' \to \hat{\Omega}\right)\psi\left(\vec{r}, E', \hat{\Omega}'\right) d\Omega' \, dE' \, , \end{aligned} \tag{4}$$

where the terms to the right side of the equals sign represent particle streaming, collision, and scattering, respectively. The transport equation in operator notation with an arbitrary initial source q_0 is represented as

$$L\psi = q_0. \tag{5}$$

The forward transport operator is not self-adjoint, so the adjoint transport operator must be derived. The adjoint transport operator is

$$\begin{aligned} L^{+}\psi^{+} = {} & \left[-\hat{\Omega} \cdot \vec{\nabla} + \Sigma(\vec{r}, E)\right]\psi^{+}\left(r, \hat{\Omega}, E\right) \\ & - \iint_{E', \Omega'} \Sigma_s\left(\vec{r}, E \to E', \hat{\Omega} \to \hat{\Omega}'\right)\psi^{+}\left(\vec{r}, E', \hat{\Omega}'\right) d\Omega' \, dE' \end{aligned} \tag{6}$$

An arbitrary detector response can be described using the solution of a forward transport equation. The response *R* is evaluated as the integral of the response function (typically, cross sections) and the forward transport solution (flux distribution). Multiplication by

the detector volume yields units of the response in number of reactions per unit time. This relationship is depicted in equation 7:

$$R = V_d \int \Sigma_d \phi(\vec{r}, E) dE. \tag{7}$$

The corresponding adjoint transport equation in operator notation for an arbitrary detector response is given in equation 8:

$$L^+ \psi^+ = \mathrm{V}_d \Sigma_d \delta(\vec{r} - \vec{r}_d). \tag{8}$$

The forward source is replaced with the adjoint source, which is the detector response function, $\mathrm{V}_d \Sigma_d \delta(\vec{r} - \vec{r}_d)$.

The next step is to take the inner product of the adjoint transport solution ψ^+ and equation 6, and then separately take the inner product of the forward transport solution ψ and equation 8. The resulting two equations are

$$\langle \psi^+, L\psi \rangle = \langle \psi^+, q_0 \rangle \text{ , and} \tag{9}$$

$$\langle \psi, L^+ \psi^+ \rangle = \langle \psi, \mathrm{V}_d \Sigma_d \delta(\vec{r} - \vec{r}_d) \rangle. \tag{10}$$

These equations can be subtracted and then by using the adjoint identity, the left hand side is eliminated. The result shown in equation 11 reveals the equivalence of the detector response using forward and adjoint transport methods:

$$R = \langle \psi^+, q_0 \rangle = \langle \psi, \mathrm{V}_d \Sigma_d \delta(\vec{r} - \vec{r}_d) \rangle. \tag{11}$$

In theory, equation 11 shows that the same detector response can be obtained from both forward and adjoint transport in the multi-step method for dose calculations. This relationship agrees with the claim in Chapter 1 that the inner product of the adjoint solution and initial source evaluates to the detector response, which could otherwise be

found using forward transport methods by evaluating the inner product of the forward solution and the detector response function. With respect to dose calculations, the initial source q_0 is the photon source resulting from neutron activation, and the detector response $\Sigma_d \delta(\vec{r} - \vec{r}_d)$ is the flux-to-dose conversion factors.

Switching the focus from radiation transport to neutron activation, the exact same methodology just followed shows the equality of forward and adjoint methods in determining the isotopic response due to neutron activation. To begin, the forward activation operator is given by equation 12:

$$L = \frac{d}{dt} - \bar{\bar{A}}(t), \tag{12}$$

where $\frac{d}{dt}$ is simply a time derivative and $\bar{\bar{A}}(t)$ is a bi-diagonal transmutation matrix containing terms for production and destruction of isotopes. The forward activation equation in operator notation is:

$$LN(t) = N_0 \delta(t - t_0), \tag{13}$$

where *N(t)* is the forward activation solution, N_0 is the initial source represented as a delta function in time, and t_0 is time at the beginning of irradiation. The forward activation solution is the isotopic relative concentrations of the isotopes in the forward activation tree. Stated differently, it is the fraction of an isotope at a cooling time t_f relative to a unit quantity of an isotope at the beginning of the irradiation period t_0. The initial source is the number densities of the isotopes experiencing neutron irradiation.

The forward activation operator is not self-adjoint, so the adjoint operator also must be derived. The adjoint activation operator is shown in equation 14:

$$L^{+} = -\frac{d}{dt} - \bar{\bar{A}}(t). \tag{14}$$

With the adjoint operator, the corresponding adjoint activation equation in operator notation is:

$$L^{+}N^{+}(t) = N_f \delta\left(t - t_f\right), \tag{15}$$

where N^{+} is the adjoint activation solution, the forward source N_0 is replaced with the adjoint source N_f, and t_f is any cooling time at the end of irradiation. The adjoint activation function can be interpreted as the isotopic importance or relative concentrations of the isotopes in the adjoint activation tree, as discussed in Chapter 1. In other words, the adjoint function represents the fraction of isotopes at the beginning of the irradiation period t_0 that become a specific target isotope at some cooling time t_f.

The response R sought after for activation is fundamentally the isotopic number densities and is the integral shown in equation 16:

$$R = \int N(t) N_f \delta\left(t - t_f\right) dt. \tag{16}$$

Now, by taking the inner product of the adjoint activation solution N^{+} and equation 13 and then separately taking the inner product forward activation solution N with equation 15, two equations are created that mirror equations 9 and 10. These two relationships are shown in equations 17 and 18:

$$\langle N^{+}, LN \rangle = \langle N^{+}, N_0 \delta(t - t_0) \rangle \text{, and} \tag{17}$$

$$\langle N, L^{+}N^{+}\rangle = \langle N, N_f\delta(t - t_f)\rangle. \quad (18)$$

These equations can be subtracted and then again by using the adjoint identity, the left hand side is eliminated. The result is shown in equation 19 and reveals the equivalence of the activation isotopic response using forward and adjoint activation methods:

$$R = \langle N^{+}, N_0\delta(t - t_0)\rangle = \langle N, N_f\delta(t - t_f)\rangle. \quad (19)$$

Equation 19 appears in the same format as equation 11. It shows that forward and adjoint activation can be used to obtain the same isotopic response. The inner product of the adjoint solution N^{+} and initial source N_0 evaluates to the same response that could otherwise be found using forward activation methods by evaluating the inner product of the forward solution N and adjoint source N_f.

Chapter 3

Codes and Nuclear Data

A collection of computational tools and data libraries was used to perform the sequence of calculations mentioned in Chapter 1. Specifically, two radiation transport codes, a neutron activation code, a solid-modeling software platform, an auxiliary code package, and three sets of nuclear data libraries were used to carry out the analyses. This chapter discusses each of these individually and the capacity to which they were applied to the analysis.

3.1 Codes

3.1.1 PARTISN 5.97

PARTISN version 5.97 [3] was one of the computational codes utilized to perform radiation transport simulations. Los Alamos National Laboratory (LANL) develops the PARTISN code, and it is distributed by the Radiation Safety Information

Computational Center (RSICC) at Oak Ridge National Laboratory (ORNL). PARTISN is a time-dependent parallel neutral particle transport code system that is capable of performing forward neutron transport and adjoint photon transport simulations needed for to determine biological dose.

PARTISN is a deterministic code that utilizes the discrete ordinates method of solving the Boltzmann transport equation. Deterministic codes are more effective at obtaining accurate global solutions in comparison to probabilistic codes. However, most deterministic codes are limited to an orthogonal grid, as is the case for PARTISN, and hence their ability to model complex 3-D systems is limited. A focus of this thesis is using the Monte Carlo probabilistic method for radiation transport for its geometric flexibility in representing 3-D complex geometries. However, PARTISN was used to benchmark results of simple 1-D problems obtained using the Monte Carlo method to assure that the Monte Carlo adjoint transport simulations are being implemented correctly.

3.1.2 Cubit 12.2

Cubit is a solid modeling and mesh generation software platform developed and released by Sandia National Laboratories [4]. Cubit provides the ability to build and prepare 3-D models that can be used for CAD-based Monte Carlo radiation transport. The physical models used for calculating the dose were constructed in Cubit.

Cubit is not a necessary platform to draft the models, but it is required to prepare the models before performing Monte Carlo transport simulations. Cubit has an ability to detect and eliminate mathematically identical surfaces of adjacent volumes through the use of the imprint and merge functions. Inadequate CAD models with overlapping volumes cause incomplete imprinting and merging that results in failed simulations or inaccurate results. Cubit can also group volumes and surfaces in order to define material densities, boundary conditions, and tallies for the transport simulation. The solid models drafted by Cubit are subsequently used by the DAGMC code to perform the CAD-based Monte Carlo simulation.

3.1.3 DAGMC

The Directly Accelerated Geometry Monte Carlo (DAGMC) code [5] is a software component of Mesh-Oriented database (MOAB) [6] that provides the ability to perform Monte Carlo radiation transport on complex 3-D geometries created by solid modeling software. DAGMC is developed by the Computational Nuclear Engineering Research Group (CNERG) at the University of Wisconsin-Madison. This code translates a CAD model into a faceted 3-D geometry that can be interpreted by radiation transport codes to perform ray-tracing and geometry operations. DAGMC is coupled to the radiation transport code Monte Carlo N-Particle (MCNP) version 5 [7]. MCNP is developed by LANL and distributed by RSICC at ORNL. Using Cubit's abilities to

prepare the 3-D model and assign groups, the user is only required to create a portion of the data cards associated with a typical input for the native MCNP code.

3.1.4 ALARA 2.9.0

Analytic and Laplacian Adaptive Radioactivity Analysis (ALARA) version 2.9.0 is an activation code developed by the University of Wisconsin-Madison [8,9]. ALARA calculates the induced activation resulting from neutron irradiation by modeling the nuclear system in space, time, and isotopic composition and then numerically solving the system of linear first order ordinary differential equations (ODE). The system of ODE accounts for the production and destruction of isotopes through transmutation and decay. The solution to the system of ODE is the final radioactive isotopic inventory of the problem that is modeled.

ALARA can be provided with supplemental data to modify the output and provide specific activation parameters such as waste disposal rating and decay heat. Additionally, ALARA has the capability to determine the group-wise photon source resulting from gamma decay of radioisotopes when provided with the necessary gamma decay yield data. The photon source can be calculated for several cooling times within one simulation. As mentioned in Chapter 1 and derived in Chapter 2, a photon source and adjoint flux can be combined to determine the biological dose. With the time-dependent photon source calculated internal to ALARA, the group-wise multiplication to determine

the dose can be performed if provided with a phase-space solution for the adjoint flux as well as the volume of the detector.

The second component of this thesis is using adjoint activation for determining the importance or contribution of isotopes at the beginning of activation pathway to the biological dose. ALARA is capable of performing adjoint activation when provided with two additional pieces of information not included in the forward activation calculation. First, it must be provided with an adjoint data library, which can be formed from the forward data library using proper inversions of cross section data. The adjoint data library represents daughter-to-parent rather than parent-to-daughter cross sections. Second, ALARA must be given a target radioisotope within a specific material to begin calculation of the adjoint isotopic number densities.

ALARA's ability to calculate biological dose using adjoint fluxes in addition to its ability to perform the adjoint activation for a given target radioisotope made it well suited for the work performed in this thesis.

3.1.5 R2S 3-D Activation Code Package

The Rigorous 2-Step (R2S) 3-D Activation Code Package developed by CNERG at the University of Wisconsin-Madison contains several auxiliary codes that were needed for the dose calculations. Most of the tools within the package are scripts written in the Python language and have been developed to perform data handling and formatting

between MCNP and ALARA. For example, one of the tools extracts the phase-space neutron flux data stored in a MCNP mesh tally file (meshtal) and reformats it to the ALARA neutron flux file (fluxin). Another is a tool to convert 3-D geometry and material information stored on a Cartesian mesh into a corresponding portion of an ALARA input. Geometry and materials information is obtained through the use of a code that overlays a Cartesian mesh onto CAD geometry and determine material volume fractions using ray-tracing techniques [10].

3.2 Nuclear Data Libraries

3.2.1 FENDL-2.1

The nuclear transport and activation data for all but one aspect of this analysis was taken from Fusion Evaluated Nuclear Data Library (FENDL) version 2.1 [11,12]. PARTISN and ALARA used the group-wise FENDL data that is arranged in 175 neutron groups and 42 photon groups. The neutron group boundaries can be seen on the EMESH cards of the MCNP forward neutron transport inputs included in the Appendix. The 42-group photon boundaries are tabulated in Section 3.2.3. MCNP forward neutron calculations used the FENDL continuous energy data.

3.2.2 ENDF/B-V

Currently, MCNP does not allow for continuous energy adjoint photon transport. It requires multi-group treatment of particles when operating in adjoint mode, and a 42-group FENDL2.1 library for MCNP was not available at the time this work was performed. The MCNP Data Team supports only one set of data suited to multi-group photon transport, so this was the nuclear data used in the implementation of Monte Carlo adjoint transport. This data contains a 12-group photon library taken mostly from the Evaluated Nuclear Data Library (ENDF/B-V) [13]. The group structure is shown in Section 3.2.3.

3.2.3 ANSI/ANS 1977

Flux-to-dose conversion factors are taken from the American National Standard Institute (ANSI) report ANSI/ANS-6.1.1-1977 [14]. They are needed as the detector response functions for determining the dose. The ANSI report provides an empirical fit to experimental data for the flux-to-dose factors as a function of photon energy. Two sets of multi-group flux-to-dose factors were needed due to the 42-group adjoint transport in PARTISN and 12-group adjoint transport in MCNP. The empirical relation and group-wise factors are overlapped graphically in Figure 5. Additionally, the 12-group and 42-

group factors are presented in Table 1 and Table 2. The energy group boundaries were determined from the 42-group and 12-group photon libraries mentioned previously.

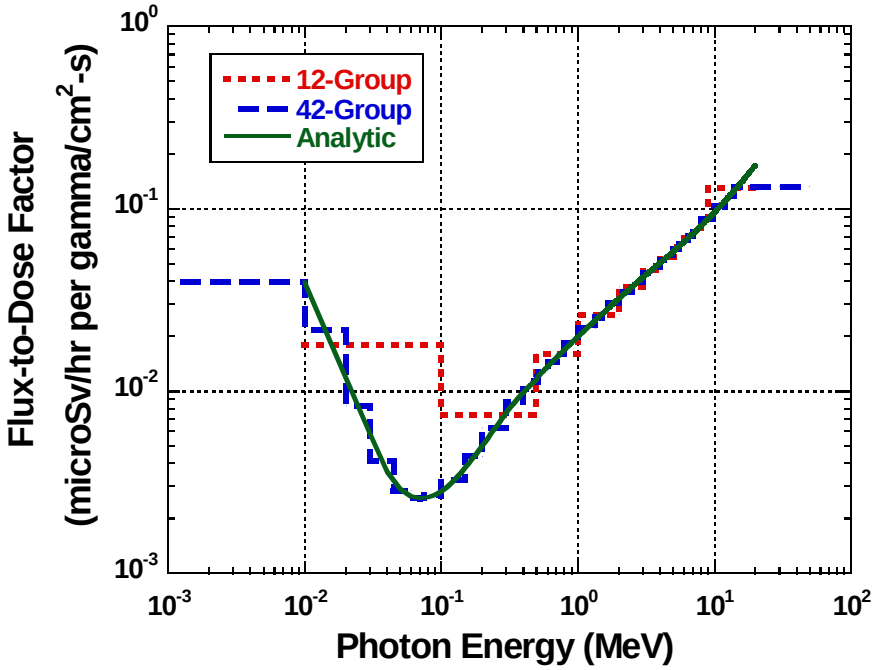

Figure 5: Flux-to-Dose Factors. This figure shows the analytic solution of the flux-to-dose factors and the group-wise values used for multi-group adjoint photon transport.

Table 1: 12-Group flux-to-dose factors used for MCNP5 adjoint photon transport

Group	Lower Bound (MeV)	Upper Bound (MeV)	Flux-to-Dose Conversion Factors (microSv/hr per g/cm^2-s)
1	9	20	1.295E-01
2	8	9	8.401E-02
3	7	8	7.663E-02
4	6	7	6.926E-02
5	5	6	6.191E-02
6	4	5	5.430E-02
7	3	4	4.636E-02
8	2	3	3.725E-02
9	1	2	2.629E-02
10	0.5	1	1.601E-02
11	0.1	0.5	7.410E-03
12	0.01	0.1	1.786E-02

Table 2: 42-Group flux-to-dose conversion factors used for PARTISN adjoint photon transport

Group	Lower Bound (MeV)	Upper Bound (MeV)	Flux-to-Dose Conversion Factors (microSv/hr per g/cm^2-s)
1	30.000	50.000	1.331E-01
2	20.000	30.000	1.331E-01
3	14.000	20.000	1.325E-01
4	12.000	14.000	1.178E-01
5	10.000	12.000	1.026E-01
6	8.000	10.000	8.772E-02
7	7.500	8.000	7.847E-02
8	7.000	7.500	7.478E-02
9	6.500	7.000	7.110E-02
10	6.000	6.500	6.743E-02
11	5.500	6.000	6.375E-02
12	5.000	5.500	6.007E-02
13	4.500	5.000	5.601E-02
14	4.000	4.500	5.227E-02
15	3.500	4.000	4.832E-02
16	3.000	3.500	4.412E-02
17	2.500	3.000	3.960E-02
18	2.000	2.500	3.469E-02
19	1.660	2.000	3.019E-02
20	1.500	1.660	2.731E-02
21	1.340	1.500	2.536E-02
22	1.330	1.340	2.430E-02
23	1.000	1.330	2.205E-02
24	0.800	1.000	1.833E-02
25	0.700	0.800	1.604E-02
26	0.600	0.700	1.442E-02
27	0.512	0.600	1.281E-02
28	0.510	0.512	1.202E-02
29	0.450	0.510	1.128E-02
30	0.400	0.450	1.032E-02
31	0.300	0.400	8.759E-03
32	0.200	0.300	6.306E-03
33	0.150	0.200	4.391E-03
34	0.100	0.150	3.277E-03
35	0.075	0.100	2.682E-03
36	0.070	0.075	2.578E-03
37	0.060	0.070	2.601E-03
38	0.045	0.060	2.844E-03
39	0.030	0.045	4.115E-03
40	0.020	0.030	8.267E-03
41	0.010	0.020	2.144E-02
42	0.001	0.010	3.961E-02

Chapter 4

Results and Discussion

Biological dose calculations using the adjoint method for photon transport and neutron activation are performed for three different physical systems. The first two problems are 1-D problems that were benchmarked with the PARTISN code. The first of these is a 1-D infinite slab of ferritic steel (FS). The second problem is the ARIES-Compact Stellerator (CS). It is a fusion power plant design that is modeled as a series of concentric infinite cylinders. The third calculation is performed on a model of a 3-D spherical tokamak (ST) designed by the PPPL. The impact of including a diagnostic penetration on the biological dose is evaluated for this 3-D problem.

4.1 1-D Slab Problem

The first biological dose calculation is performed on a model representing a 1-D infinite slab. The dimensions of the slab are shown in Figure 6.

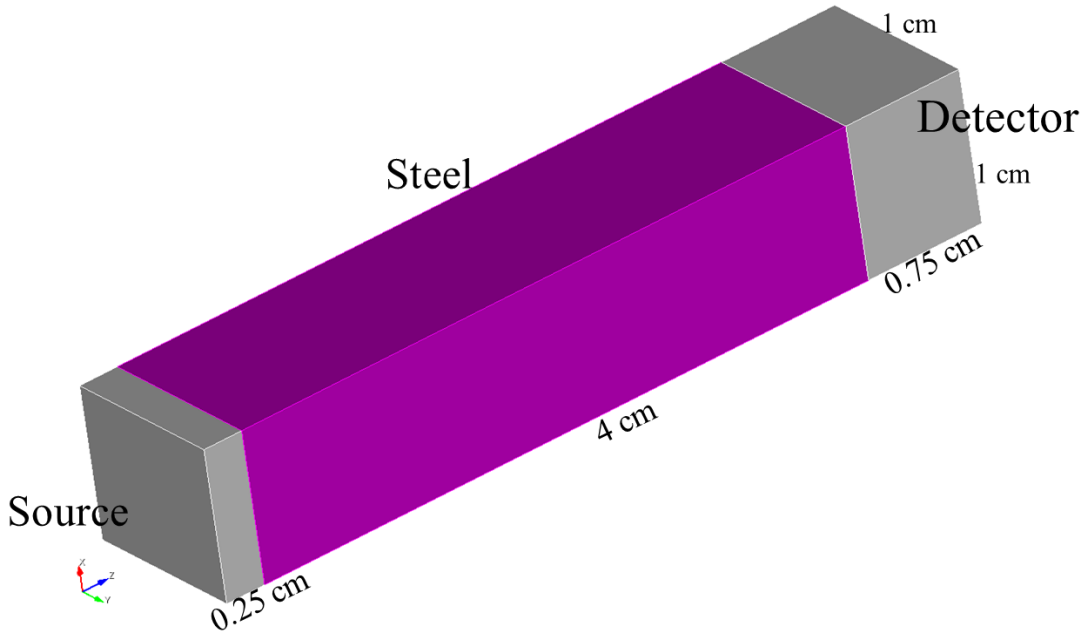

Figure 6: 1-D Slab geometry. This shows the dimensions and location of the source and detector regions.

The volumetric source consists of 14.1 MeV isotropic neutrons. Reflecting boundary conditions are assigned to the surfaces parallel to the z-axis in order to model an infinite slab for the Monte Carlo simulation. Vacuum boundary conditions are assigned to the surfaces at z = 0 cm and z = 5 cm. The 4 cm thick volume is filled with F82H ferritic steel with a density of 7.89 g/cm^3 and elemental composition of atom percentages given in Table 3 for the transport simulations. The isotopic compositions of the elements are defined using natural abundances. The steel composition for the activation calculations included impurities in the material definition.

Table 3: Elemental composition of steel in 1-D slab

Element	Atom Percent
Fe	90.6%
Cr	8.1%
W	0.6%
C	0.5%
V	0.2%

The first step in the multi-step method is to perform a forward neutron transport calculation to determine the phase-space neutron flux distribution. The group-wise neutron flux is tallied at six intervals along the z-axis. This step is performed using PARTISN and MCNP. The total neutron flux summed over all energies falls as the distance within the material increases, as expected. Figure 7 illustrates the total neutron flux versus distance from the source at z = 0 cm. The first interval is not shown since it is within the source and irrelevant to activation. One billion histories are simulated in the MCNP calculation, which yielded an average relative error of 6.6×10^{-5} for the neutron flux. Excellent agreement between PARTISN and MCNP was found with a discrepancy that remains below 1% at each interval.

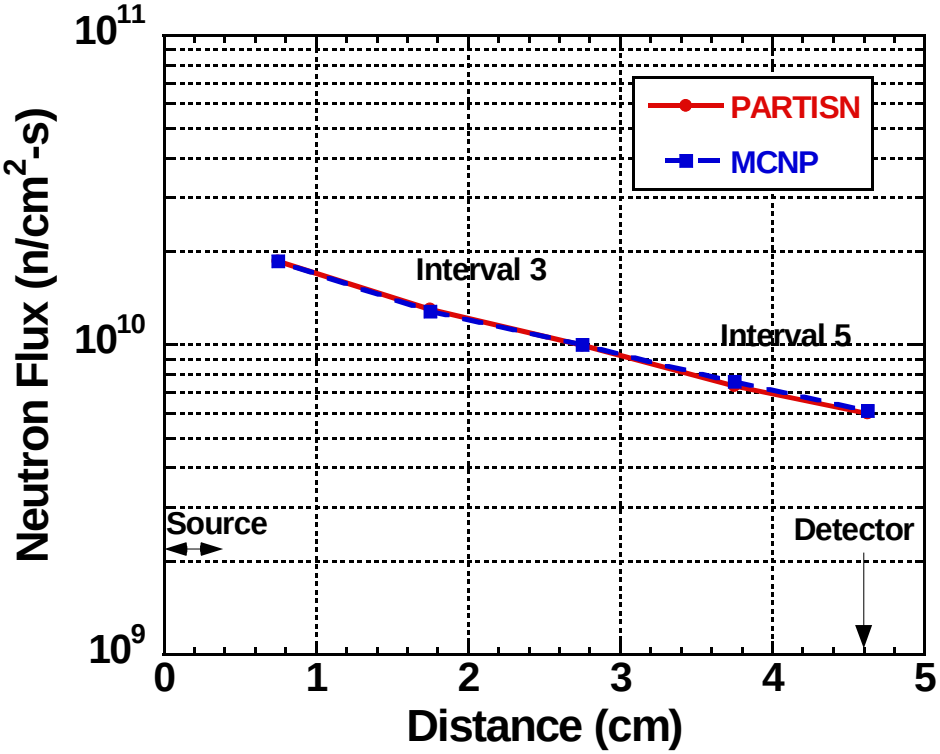

Figure 7: Forward neutron flux for the 1-D slab calculated from PARTISN and MCNP.

The neutron flux is broken down into a spectrum of 175-group neutron fluxes based on the FENDL-2.1 175-group boundaries. The spectrum reveals detailed information regarding the neutron energies at given locations within the model. The group-wise fluxes at the interval 3 located at z = 1.75 cm is shown in Figure 8. The thermal energy neutron flux is roughly six orders of magnitude less than the fast neutron flux, which suggests a large significance of threshold reactions (with E_n>0.1 MeV) in the activation.

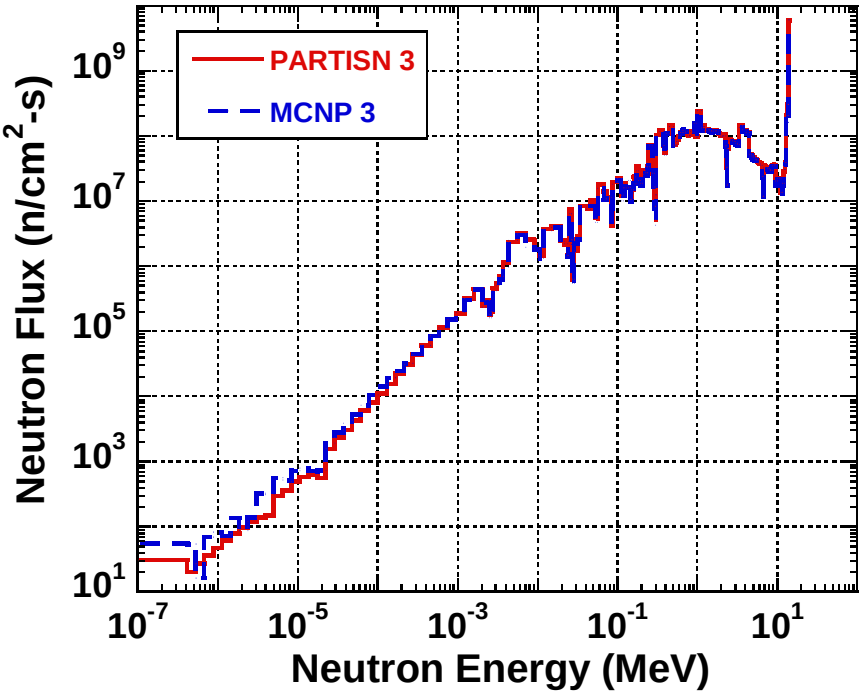

Figure 8: Group-wise neutron flux at interval 3 located at z = 1.75 cm from PARTISN and MCNP.

A comparison of the neutron spectra from PARTISN and MCNP is included to find the energy groups with the largest discrepancies. The relative fraction of the group-wise neutron flux values calculated using the two transport codes at two different locations is shown in Figure 9. The locations are the planes at the z = 1.75 cm and z = 3.75 cm corresponding to intervals 3 and 5, respectively. The relative fraction is calculated as the PARTISN flux minus the MCNP flux then divided by the PARTISN flux. The discrepancy among the high energy fluxes remains below 5% while the largest

discrepancy between the two fluxes occurs below 0.1 eV where the statistical error is relatively large (20%-80%) for the MCNP low energy flux, as explained below.

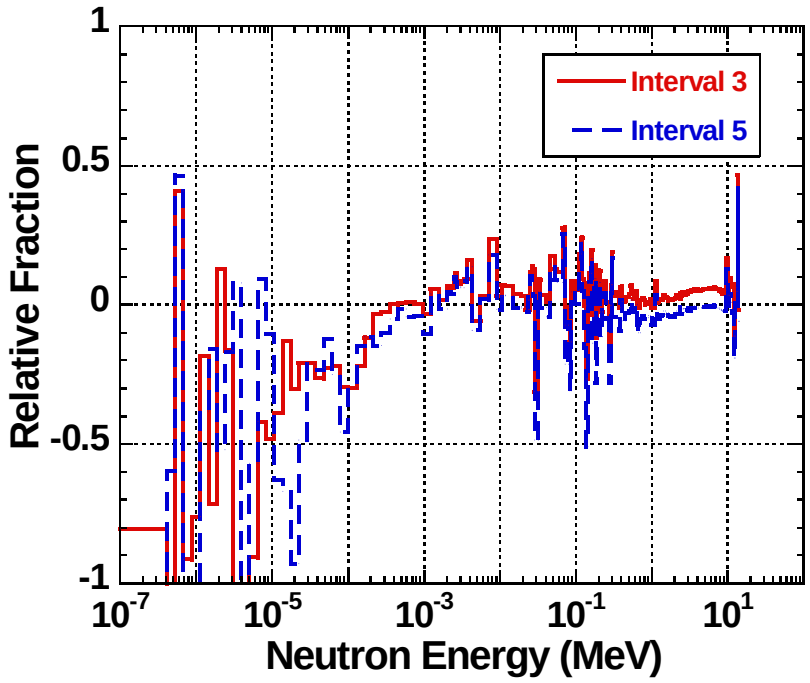

Figure 9: Relative fraction of MCNP from PARTISN of group-wise neutron flux for two intervals of the slab geometry.

To help explain the larger discrepancy at thermal energies, the statistical error of the MCNP results are examined. Figure 10 shows the relative statistical error of the group-wise MCNP neutron fluxes at the two previously examined locations within the slab. The statistical error of the group-wise MCNP flux values increases dramatically at thermal energies. The large statistical error exists because the 4 cm of ferritic steel will not thermalize the neutrons significantly, hence there are fewer scores contributing to the thermal energy tallies causing the large statistical errors in the MCNP results.

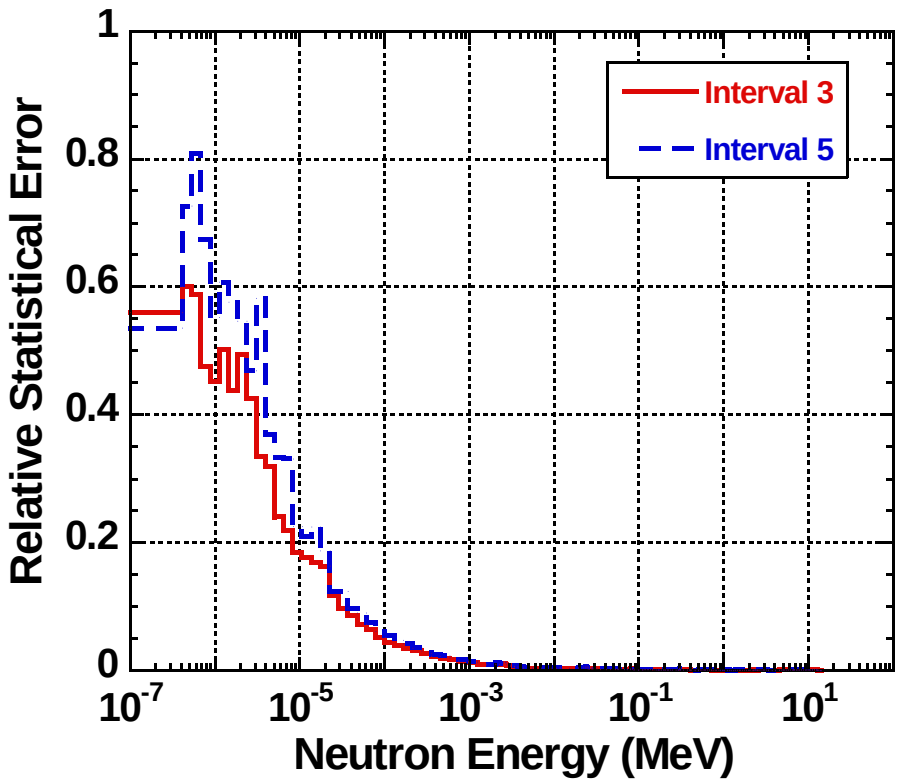

Figure 10: Statistical errors of group-wise neutron fluxes at two locations within steel. The statistical error of the MCNP calculation increases at low neutron energies due to relatively smaller thermal fluxes.

The adjoint photon calculation was performed using the flux-to-dose conversion factors as the adjoint source. The group-wise adjoint flux solution is shown in Figure 11 for two locations within the slab. The results show that at locations further from the detector (interval 3), the adjoint flux is lower, which is to be expected since the importance of photons further from the detector is lower. The discrepancy between the integrals of the adjoint flux spectra at interval 5 is 0.4%, and it increases to 12.3% at

interval 3. This behavior is to be expected since interval 5 is closer to the adjoint source, and MCNP tally results exhibit lower statistical uncertainty when closer to a source.

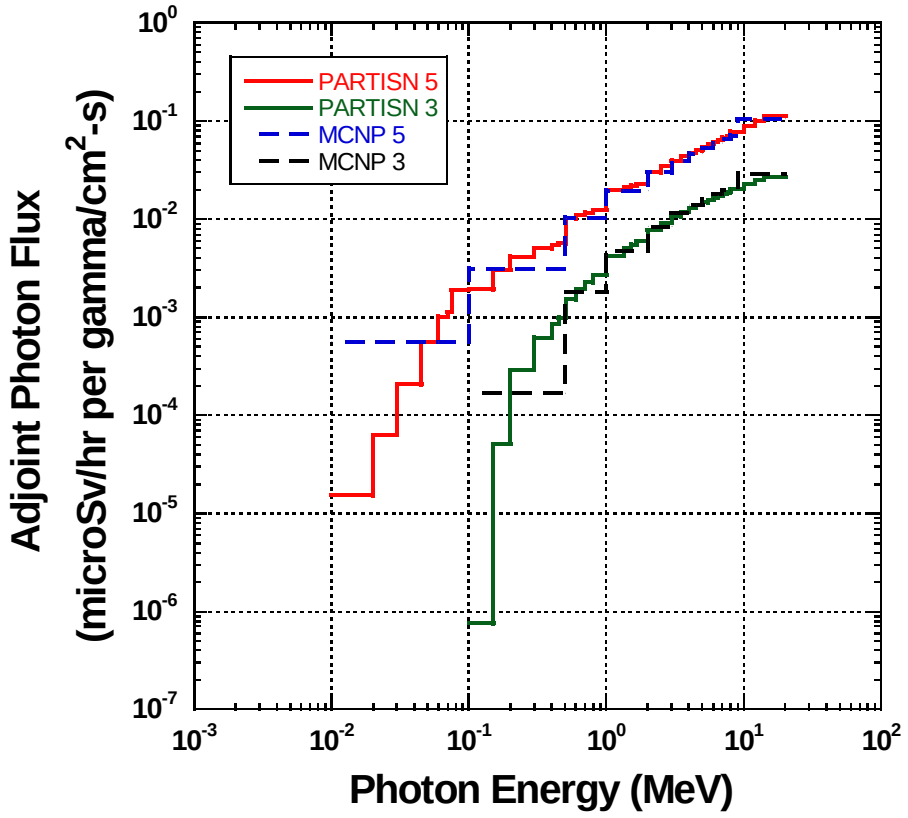

Figure 11: Group-wise adjoint photon flux for PARTISN (42 photon groups) and MCNP (12 photon groups) at two intervals within the steel. Interval 5 is closer to the detector and has the larger adjoint fluxes.

The forward neuron fluxes are used within the ALARA code for neutron activation and generation of the photon source. The spatial distribution of the photon source immediately after shutdown resulting from the neutron fluxes of both transport codes is shown in Figure 12 for one location within the slab. The discrepancy of the

photon source created using neutron fluxes from PARTISN and MCNP is less than 3% at each location within the slab.

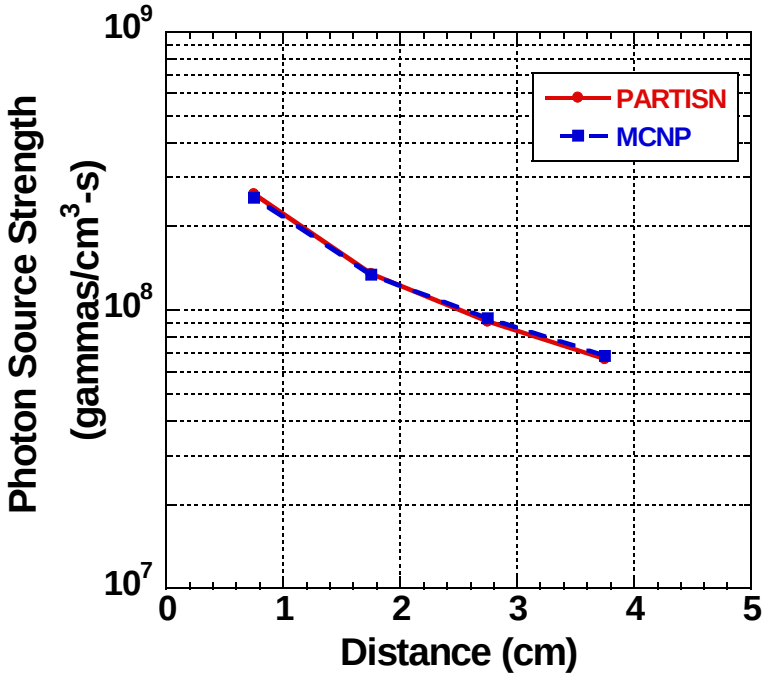

Figure 12: Total photon source immediately after shutdown versus distance. Photon source is generated using neutron fluxes from PARTISN and MCNP. The discrepancy at each interval is less than 3%.

The group-wise photon source values are investigated as well to examine any possible discrepancies. The group boundaries of the photon source resulting from the two transport codes was required to be the same as the boundaries of the nuclear data used for the adjoint photon transport. Therefore, the photon source created using MCNP neutron fluxes is binned according to the 12-group boundaries whereas the photon source from

PARTISN neutron fluxes is binned according to the 42-group boundaries, as shown in Figure 13.

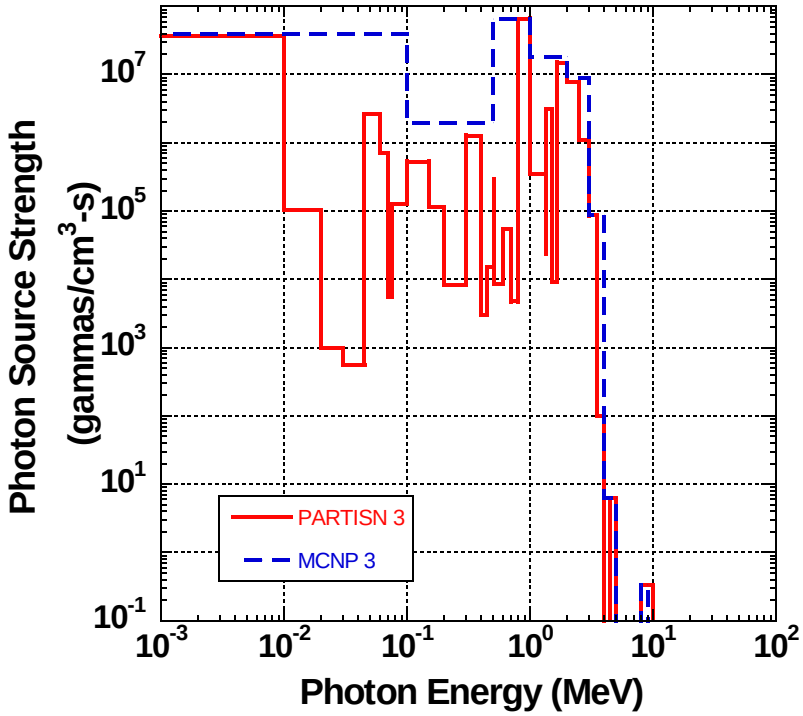

Figure 13: Group-wise photon source at interval 3. Group boundaries for MCNP and PARTISN needed to correspond to the group boundaries of the adjoint fluxes.

The photon source shown in Figure 13 has been evaluated at the shutdown cooling time. However, the ALARA code can generate the photon source for many user-specified cooling times at once. Within one simulation, ALARA generates the photon source at 23 different cooling times ranging from zero seconds to 100 years after shutdown. The dose is then calculated using a group-wise multiplication of the photon source and adjoint photon fluxes followed by division by the detector volume. The

biological dose trend is shown in Figure 14. The discrepancy between the dose generated using MCNP and PARTISN fluxes is 15.4% through one day after shutdown and 32.7% through 100 years after shutdown. The reasons for such discrepancies in the results throughout the analysis are explained at the end of Section 4.2 since the reasons apply to the next problem as well.

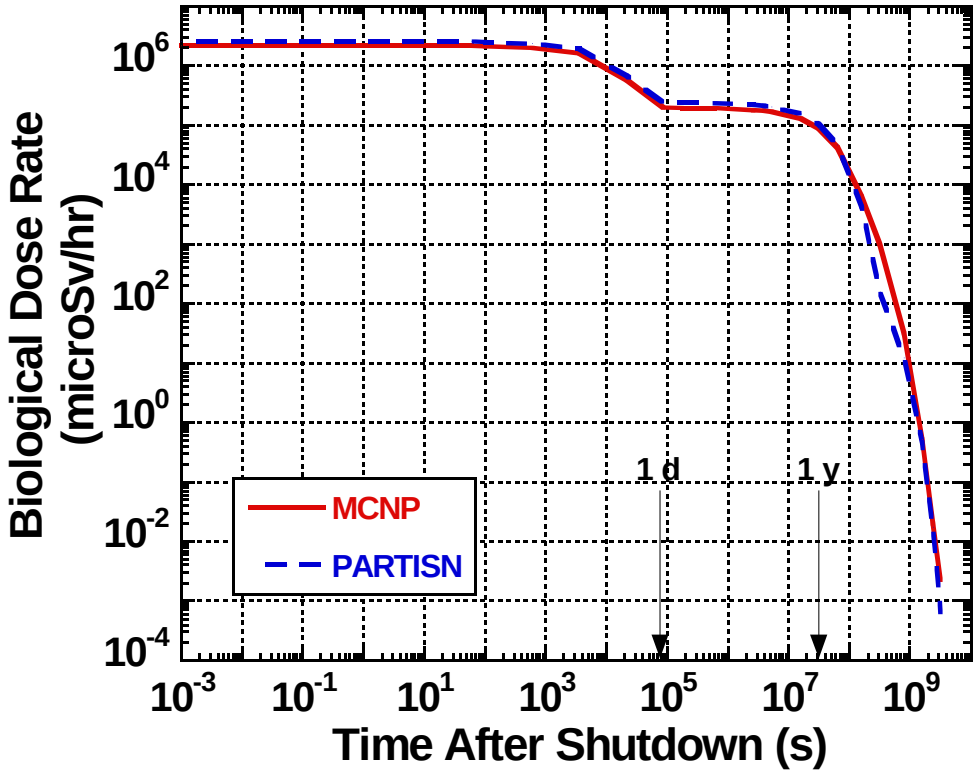

Figure 14: Biological dose versus time for the 1-D slab geometry. The dose is calculated using fluxes from MCNP and PARTISN.

Figure 15 displays the dose at each spatial location that contributes to the dose at the detector at one day after shutdown. This information indicates which spatial location is contributing the most to the dose. Interval 5 (closest to the detector) is found to be responsible for 51% of the total dose at one day after shutdown (~2 x10^5 microSv/hr), so it will be the focus of further analysis.

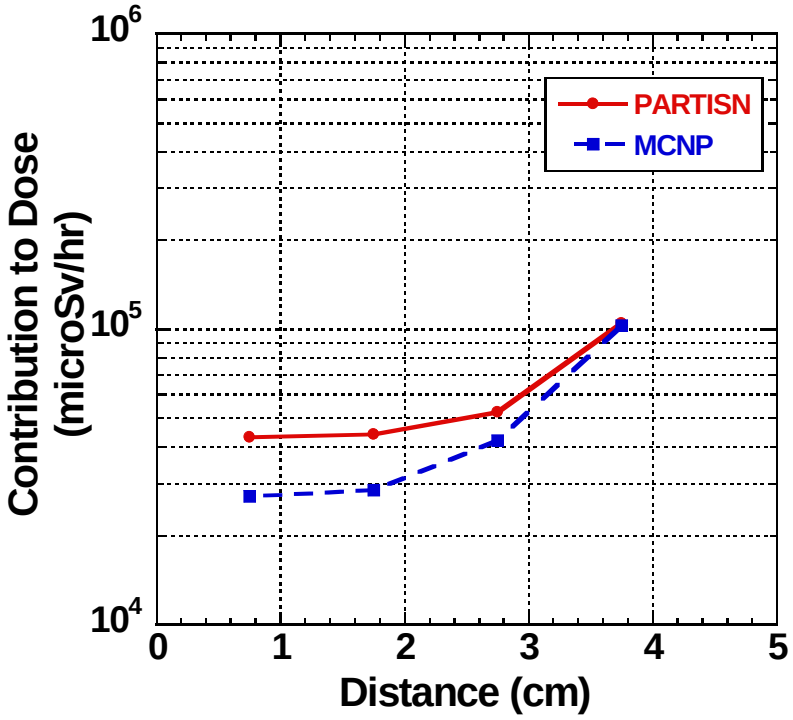

Figure 15: Contribution to total dose at the detector versus distance. The interval closest to the detector (interval 5) contributes the 51% to the total dose.

Adjoint activation calculations are then performed to determine the stable isotopes contributing to the production of the dominant radioisotopes for the biological dose. Interval 5 (closest to the detector) is studied to see which radioisotopes dominate the dose

at one day after shutdown – a relevant time for maintenance. Table 4 lists the radioisotopes and their contribution to the total dose. The three most dominant radioisotopes are Mn-54, Fe-55 and Cr-51. These isotopes will be used as the target radioisotope within ALARA for the construction of the adjoint activation tree discussed in Chapter 1.

Table 4: Forward activation results for 1-D slab geometry. This table contains a list of radioisotopes dominating dose at 1 day after shutdown

Isotope	Dose Rate (microSv/hr)	Contribution to Total
total	1.007E+05	-
mn-54	8.439E+04	83.8%
fe-55	1.065E+04	10.6%
cr-51	3.281E+03	3.3%
co-58	7.777E+02	0.8%
w-181	6.073E+02	0.6%
sc-48	2.831E+02	0.3%
co-57	1.858E+02	0.2%
co-60	1.296E+02	0.1%
ta-182	1.177E+02	0.1%
fe-59	8.247E+01	0.1%
v-49	7.870E+01	0.1%
w-187	5.735E+01	0.1%

Adjoint activation results indicate which stable isotopes dominate the production of the significant radioisotopes. Table 5, Table 6, and Table 7 reveal the results from the adjoint activation for the slab problem. The most dominant radioisotope Mn-54 is being

produced from Fe-54 via a (n,p) reaction. Fe-55 is produced from Fe-56 whereas the Cr-51 is from Cr-52, both with (n,2n) reaction. These reactions are threshold reactions with the main constituents of the F82H steel, indicating that the high energy neutrons are mostly responsible for the radioisotope production that dominates the dose shortly after shutdown.

Table 5: Adjoint activation results for 1-D slab with Mn-54 target. This table contains a list of the parent isotopes that are responsible for the production of Mn-54.

Isotope	Dose Rate (microSv/hr)	Contribution to Total
total	8.439E+04	-
fe-54	8.439E+04	100.00%

Table 6: Adjoint activation results for 1-D slab with Fe-55 target. This table contains a list of the parent isotopes that are responsible for the production of Fe-55.

Isotope	Dose Rate (microSv/hr)	Contribution to Total
total	1.065E+04	-
fe-56	1.061E+04	99.86%
fe-54	1.275E+01	0.12%
ni-58	1.291E+00	0.01%

Table 7: Adjoint activation results for 1-D slab with Cr-51 target. This table contains a list of the parent isotopes that are responsible for the production of Cr-51.

Isotope	Dose Rate (microSv/hr)	Contribution to Total
total	3.281E+03	-
cr-52	2.641E+03	78.46%
fe-54	7.202E+02	21.40%
cr-50	4.568E+00	0.14%

4.2 ARIES-CS 1-D Cylindrical Problem

Biological dose calculations are performed on a model of the ARIES-CS fusion power plant design [15]. The dose calculations using the multi-step method with adjoint transport have been perform and published previously using deterministic transport codes [16]. Thus, it was another suitable benchmark problem for using Monte Carlo transport.

The ARIES-CS fusion power plant design is modeled as a series of concentric infinite cylinders for the MCNP calculation as shown in Figure 16.

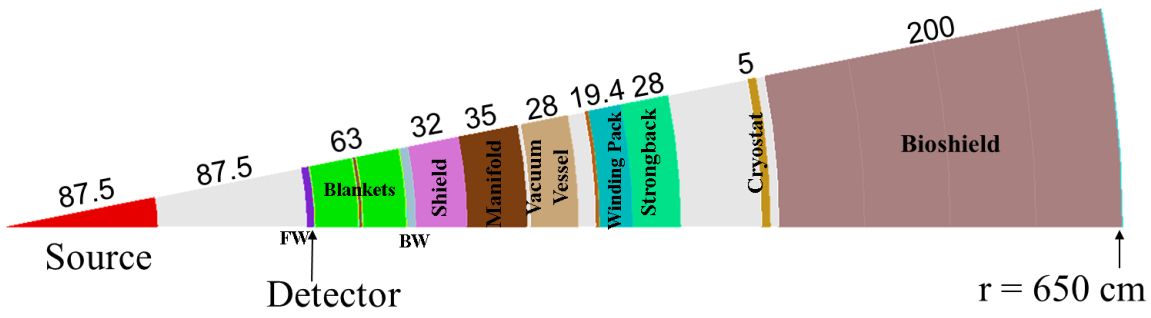

Figure 16: ARIES-CS 1-D cylindrical geometry with radial zones and thicknesses in cm. Reflecting boundaries are placed on the sides of the wedge as well as on top and bottom in order to represent infinite cylinders.

The DAGMC model is constructed to represent infinitely long cylinders by taking advantage of reflecting boundary conditions at the side surfaces of the sliced cylinders as well as on the top and bottom surfaces of the cylinders. Each radial zone is assigned homogeneous composition to replicate accurate shielding characteristics. The homogeneous material composition of every zone is provided separately within the MCNP, PARTISN, and ALARA inputs included in the Appendix. The volumetric source consists of 14.1 MeV D-T isotropic neutrons placed within the first cylinder with 87.5 cm radius measured from the axis at r = 0 cm. The detector is placed immediately behind the first wall (FW) in the region ranging from r = 178.8 cm to r = 179.0 cm. Analog Monte Carlo is poor at obtaining reliable and detailed solutions for large shielding problems, so the detector is placed behind the FW to avoid excessively long computational time despite the fact that a detector behind the magnets or vacuum vessel would be more relevant place for maintenance.

The same sequence of calculations performed for the slab problem is applied here. The first calculation is to determine the forward neutron flux distribution. The spatial distribution of the total neutron flux summed over all energies from PARTISN and MCNP simulations is shown in Figure 17. MCNP was simulated with 4 x 10^6 histories. The discrepancy between the two codes remains below 1% through a distance of 300 cm. The average relative error of the MCNP results through a distance of 300 cm is 0.1%. MCNP did not report usable flux values past 325 cm, however the dose at the detector will not be affected by photons created from such far distances, which will be confirmed later.

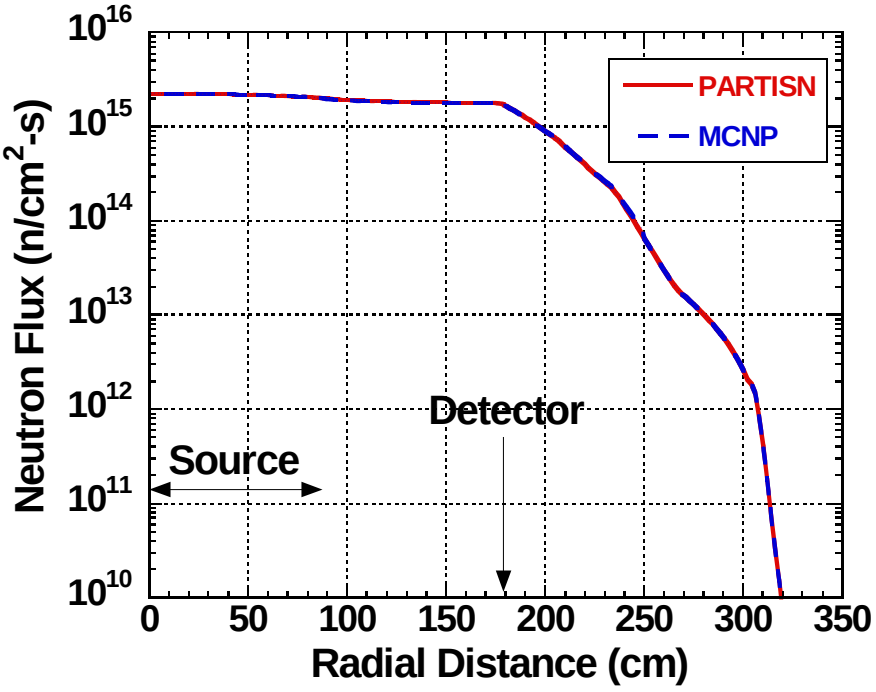

Figure 17: Forward neutron flux distribution from MCNP and PARTISN for the ARIES-CS model.

A comparison of the group-wise neutron flux values at the detector (interval 103) is included to show the spectrum distribution. The average discrepancy of the spectra obtained from PARTISN and MCNP is 2.42% for energies above 10^{-4} MeV. Below this energy, MCNP produced zero values since there were no neutrons that contributed to the tally for the number of histories used.

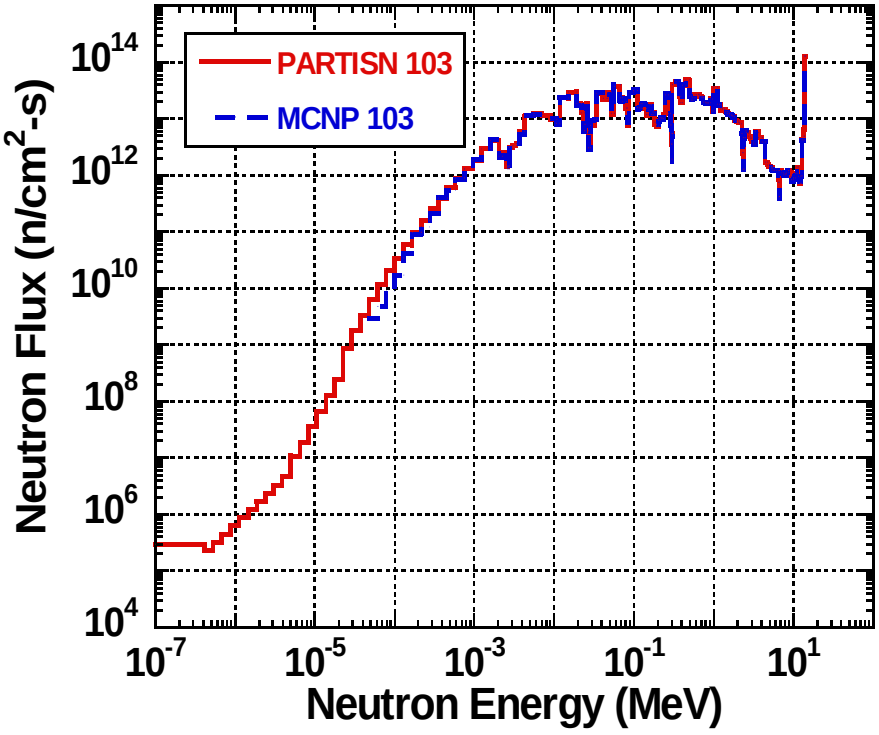

Figure 18: Group-wise forward neutron flux at detector location. Interval 103 corresponds to a radial distance of 178.8 cm.

The discrepancy of the neutron flux at the detector between the two transport codes for all 175 groups of the FENDL group-wise neutron data is shown in Figure 19.

Also, the statistical errors of the MCNP results are provided in Figure 20. These figures illustrate the poor accuracy of the Monte Carlo method in determining reliable low energy fluxes in a high energy dominated region behind the FW of ARIES-CS.

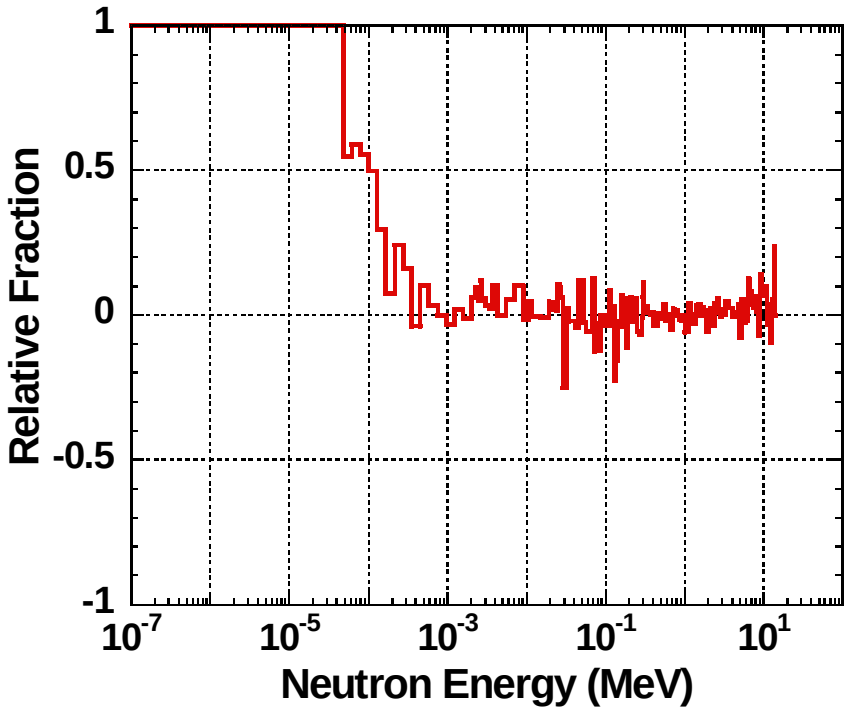

Figure 19: Relative fraction of group-wise neutron flux values calculated from PARTISN and MCNP at a radial distance of 178.8 cm.

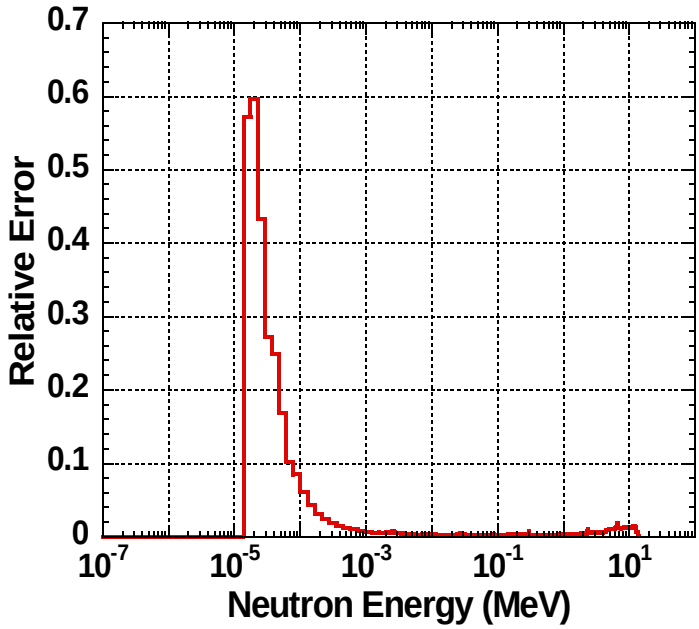

Figure 20: Group-wise relative errors of MCNP neutron flux values at interval 103 or a radial distance of 178.8 cm.

Adjoint transport is performed to determine the phase-space distribution of the adjoint photon flux. The group-wise adjoint photon flux distribution at the detector is shown in Figure 21 to agree by visual inspection. With more scrutiny, the discrepancy between the integral of the group-wise adjoint flux from PARTISN and MCNP is 2.4%, which also suggests good agreement.

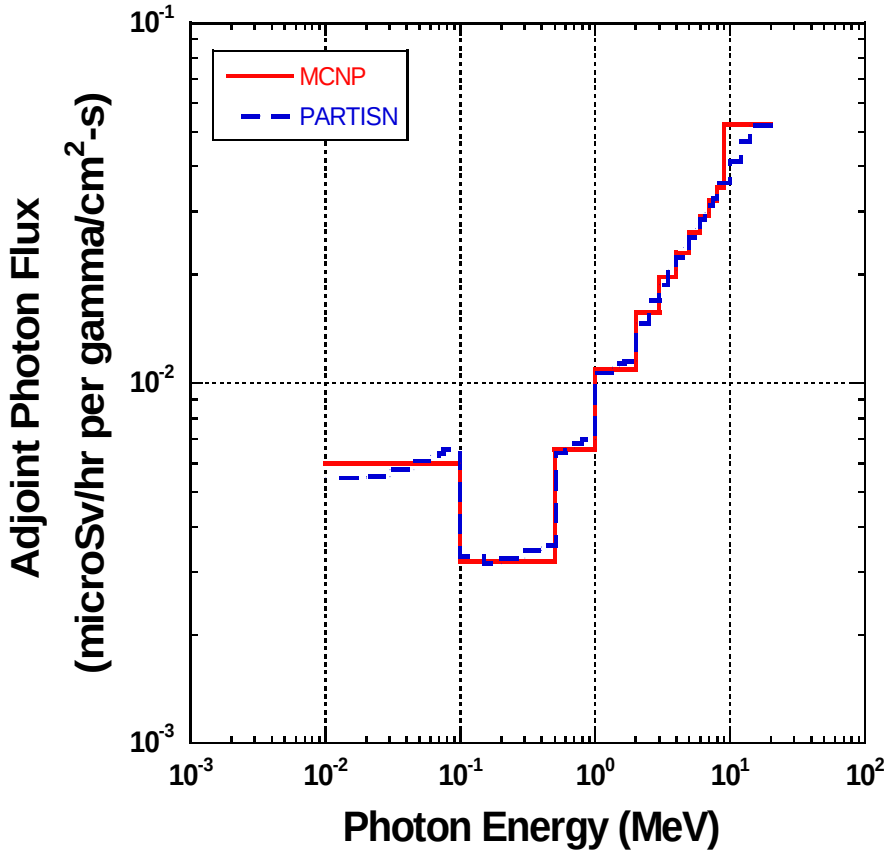

Figure 21: Group-wise adjoint photon flux calculated using MCNP and PARTISN. The adjoint flux is calculated at interval 103 or a radial distance of 178.8 cm.

The photon source evaluated immediately after shutdown at the interval nearest the detector within the FW is provided in Figure 22. The photon source generated using forward neutron fluxes from PARTISN and MCNP. Visual inspection shows good agreement and the discrepancy of the total photon source shown is 2.9%.

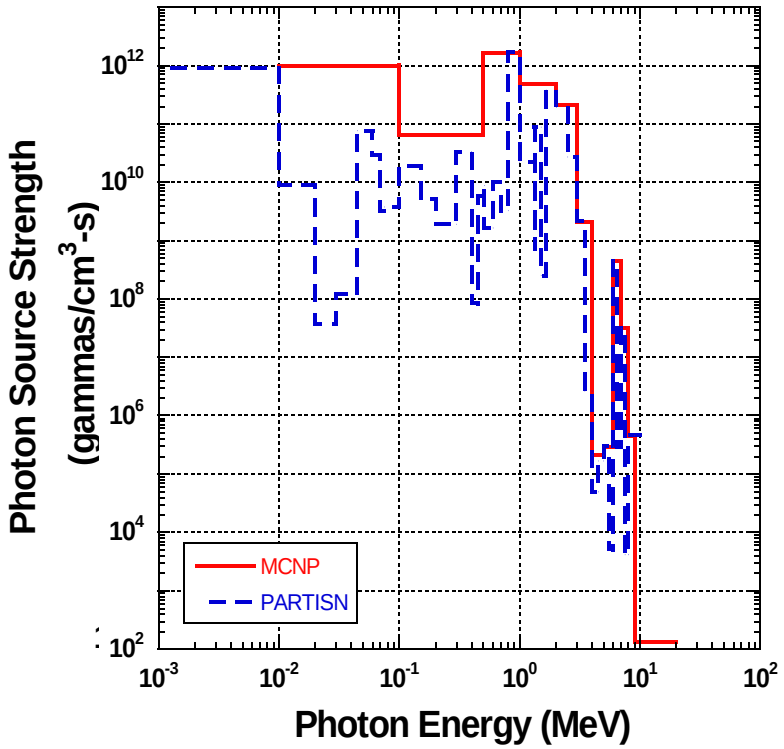

Figure 22: Group-wise photon source at shutdown using forward neutron fluxes from PARTISN and MCNP.

After calculating the phase-space solution of the adjoint photon flux with MCNP and PARTISN and time-dependent photon source within ALARA, the dose behind the FW of the ARIES-CS is evaluated. Figure 23 illustrates the trend in the biological dose for the ARIES-CS using forward neutron fluxes and adjoint photon fluxes from both transport codes used in this analysis. The average discrepancy is 17.6% through a cooling time of one day after shutdown and 27.3% through 100 years after shutdown.

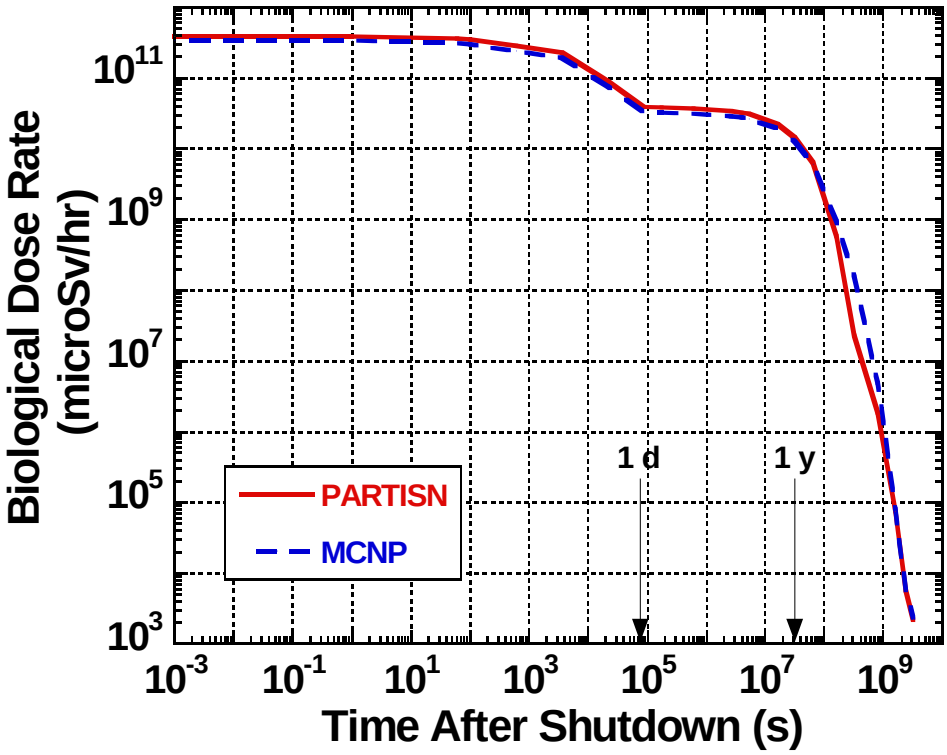

Figure 23: Biological dose rate of ARIES-CS at detector located behind FW for various cooling times using fluxes from MCNP and PARTISN.

The discrepancy in the biological dose results calculated using fluxes from PARTISN and MCNP can be attributed to multiple factors. As shown, there were discrepancies between each PARTISN and MCNP transport calculation. The forward neutron fluxes were calculated using continuous energy nuclear data in MCNP whereas PARTISN performed neutron transport using 175-group nuclear data. The difference in data will be responsible for some of the discrepancy because the 175-group data may not

resolve a significant feature in the cross section for any number of the isotopes used in this model. Also, the group structure of the adjoint data was different between PARTISN and MCNP. PARTISN was implemented with a 42-group adjoint source whereas MCNP used a 12-group adjoint source, which created a modeling difference.

To determine if the discrepancy is due to the forward neutron fluxes or the adjoint photon fluxes, the PARTISN adjoint fluxes were used in combination with the MCNP neutron fluxes to determine the dose. By doing this, the average discrepancy in the biological dose data reduces to 2.7% when compared to the results calculated using only fluxes from PARTISN. Separately, the PARTISN neutron fluxes were used in combination with the MCNP adjoint photon fluxes and yielded an average discrepancy of 15.3% when compared to the dose using only PARTISN fluxes.

There is also a large discrepancy in the results at 10 - 100 years after shutdown. Spectral differences in the PARTISN and MCNP caused variations in the radioisotope production that revealed itself in the large discrepancy in the biological dose. The radioisotope production at this time is examined, and the presence of Fe-55 radioisotope with 2.73 year half-life is found to be mostly responsible for the relatively larger biological dose in the MCNP results. The production of Fe-55 is a result of the high energy neutron reactions with Fe-54 in the FW.

Next, the adjoint activation calculations are to be performed. The dose as a function of radial distance is examined to determine the radial locations that contribute the most to the dose behind the FW. The results shown in Figure 24 indicate that the

locations closest to the detector contribute the most, which is to be expected. The FW is found to contribute 28.2% to the total dose at the detector and will be the focus of the adjoint activation analysis.

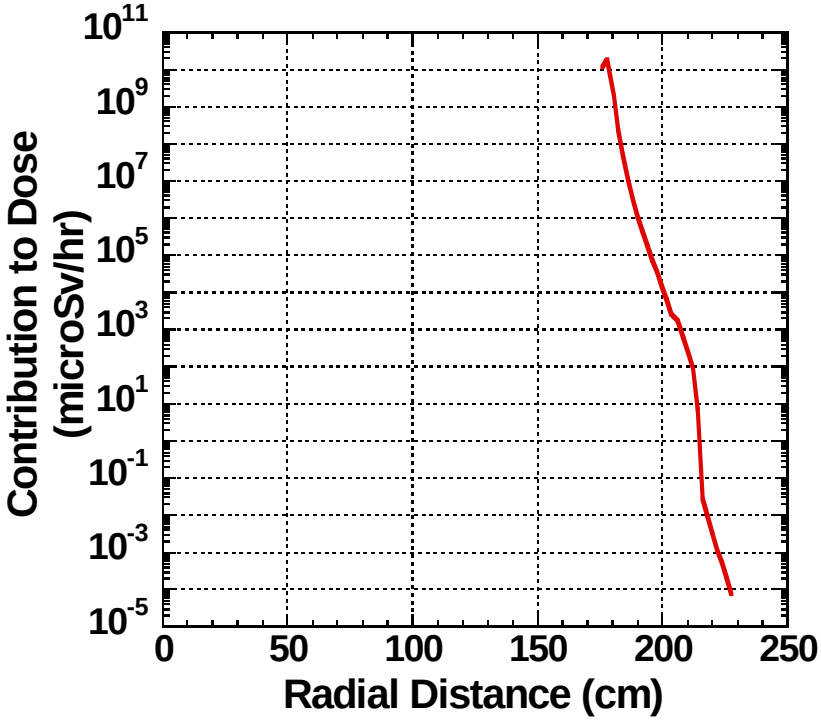

Figure 24: Contribution of radial locations to the dose at the detector. The contribution peaks in materials adjacent to the detector.

The forward activation calculation indicates the dominant radioisotopes within the FW that contribute to the biological dose at the detector. The FW is a homogeneous composition of ferritic steels, so it is expected that some radioisotopes appear as were seen in the slab problem. The three dominant radioisotopes are Mn-54, Fe-55, and Y-88

as shown in Table 8. These three radioisotopes will be used as the target within ALARA for the adjoint calculations.

Table 8: ARIES-CS forward activation results for one day after shutdown using MCNP forward neutron fluxes.

Isotope	Dose Rate (microSv/hr)	Contribution to Total
total	1.91E+10	
mn-54	1.34E+10	70.3%
fe-55	1.69E+09	8.9%
y-88	1.21E+09	6.3%
ta-182	7.59E+08	4.0%
cr-51	5.44E+08	2.8%
w-187	3.01E+08	1.6%
fe-59	2.44E+08	1.3%
mn-52	1.71E+08	0.9%
mn-56	1.67E+08	0.9%
co-58	1.41E+08	0.7%
re-184	1.18E+08	0.6%
sc-48	9.62E+07	0.5%
w-181	9.29E+07	0.5%
co-57	2.72E+07	0.1%
co-60	2.34E+07	0.1%
v-49	1.27E+07	0.1%
re-186	1.25E+07	0.1%
sc-46	1.08E+07	0.1%
re-184m	9.81E+06	0.1%

Comparable results are found for ARIES-CS as for the slab since the material compositions are similar. Tables 9, 10, and 11 reveal the results from the adjoint activation for the ARIES-CS problem. The most dominant radioisotope Mn-54 is mostly produced from Fe-54 via a (n,p) reaction. Fe-55 is mostly produced from Fe-56 whereas

the Y-88 is from Y-89, both via (n,2n) reaction. Again, it is revealed that threshold reactions are mostly responsible for the activation that dominates the dose.

Table 9: Adjoint activation results for ARIES-CS with Mn-54 target. This table contains a list of the parent isotopes that are responsible for the production of Mn-54.

Isotope	Dose Rate (microSv/hr)	Contribution to Total
total	1.34E+10	-
fe-54	1.23E+10	91.77%
fe-56	7.69E+08	5.75%
mn-55	3.31E+08	2.48%

Table 10: Adjoint activation results for ARIES-CS with Fe-55 target. This table contains a list of the parent isotopes that are responsible for the production of Fe-55.

Isotope	Dose Rate (microSv/hr)	Contribution to Total
total	1.69E+09	-
fe-56	1.65E+09	97.78%
fe-54	3.67E+07	2.17%
fe-57	5.09E+05	0.03%

Table 11: Adjoint activation results for ARIES-CS with Y-88 target. This table contains a list of the parent isotopes that are responsible for the production of Y-88.

Isotope	Dose Rate (microSv/hr)	Contribution to Total
total	1.21E+09	-
y-89	1.21E+09	100%

To compare the importance of the thermal neutron contribution to the biological dose, the forward activation calculation is performed to provide a breakdown of the constituent radioisotopes produced using PARTISN neutron fluxes at one day after shutdown. Table 12 shows a list of the radioisotopes and the contribution to the total. The thermal neutron reactions increase the dose rate resulting from Ta-182 due to (n,gamma) reactions with the impurity Ta-181. The percentage of the total dose rate of the Ta-182 decreases due to an increase in the other radioisotopes as well, specifically Mn-54 and Y-88, however the total dose rate from Ta-182 increases compared to the results using MCNP fluxes shown in Table 8.

Table 12: ARIES-CS forward activation results for one day after shutdown using PARTISN forward neutron fluxes.

Isotope	Dose Rate (microSv/hr)	Contribution to Total
total	2.16E+10	-
mn-54	1.75E+10	80.8%
y-88	1.52E+09	7.0%
ta-182	6.28E+08	2.9%
cr-51	5.86E+08	2.7%
w-187	3.15E+08	1.5%
fe-59	2.09E+08	1.0%
mn-56	2.03E+08	0.9%
mn-52	1.88E+08	0.9%
co-58	1.66E+08	0.8%
re-184	1.32E+08	0.6%
sc-48	9.31E+07	0.4%
co-60	2.20E+07	0.1%
w-181	1.25E+07	0.1%
sc-46	1.11E+07	0.1%

4.3 PPPL ST-FNSF 3-D Problem

The final problem of analysis using adjoint methods of transport and activation is a PPPL fusion design, the Spherical Tokamak Fusion Nuclear Science Facility (ST-FNSF). This problem is realistically modeled using Cubit to construct the 3-D complex geometry. Since PARTISN cannot easily model this geometry, it was not possible to benchmark results as was performed for the slab and ARIES-CS problem. Therefore, the impact on the biological dose of including a penetration in the blanket was investigated instead.

The ST-FNSF is modeled as the upper half of a $1/10^{th}$ blanket sector of the full 360^{o} model. Cubit is used to assign surfaces and cells to groups in order to define materials and boundary conditions. Reflecting boundaries are placed on the sides of the sector and at the midplane. The neutron source is placed within the plasma region and is modeled using a three-region nested source [17] and is normalized to a fusion power of 160 MW. This design consists of a dual-coolant lithium lead (DCLL) blanket placed on the outboard (OB). The OB radial build consists of a 3.8 cm FW, 43.2 cm homogenized blanket I, 3 cm BW, 5 cm gap, 50 cm homogenized blanket II, and 50 cm outer shield. The FW has a composition of 8% ODS-FS, 27% F82H, and 65% He. The homogenized

blankets consist of components comprised of lithium lead (LiPb), F82H, and silicon carbide (SiC). The dimensions and exact compositions of the components are based on the ARIES-ACT-DCLL fusion power plant design [18]. The outer shield is 80% ODS-FS. The IB radial build consists of a 3.5 cm FW, 8.7 cm vacuum vessel (VV), and 48.1 cm center stack. The divertor is 7.7 cm thick made of 28% W alloy, 8% W, 11% ODS-FS, and 53% He. A 3 cm thick stabilizing shell made of W is placed between the OB blankets. Isometric images of the ST model with and without the blanket penetration are shown in Figure 25. The penetration model is 50 cm wide and 40 cm tall from the midplane with a 3 cm thick FS lining.

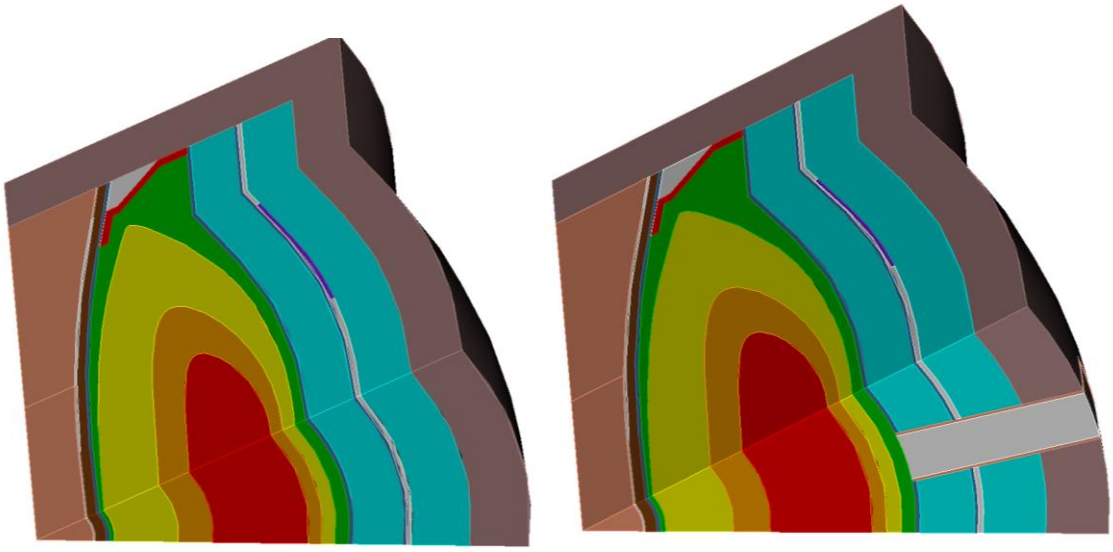

Figure 25: Isometrics of the ST-FNSF design used for 3-D dose calculations without (left) and with (right) the blanket penetration.

A volume detector is placed between the OB blankets along the side of the penetration and in the exact same location in the model without the penetration. Figure 26

shows the volume detector placed within each variation of the model. The adjoint source will be placed within this volume for the adjoint transport calculation.

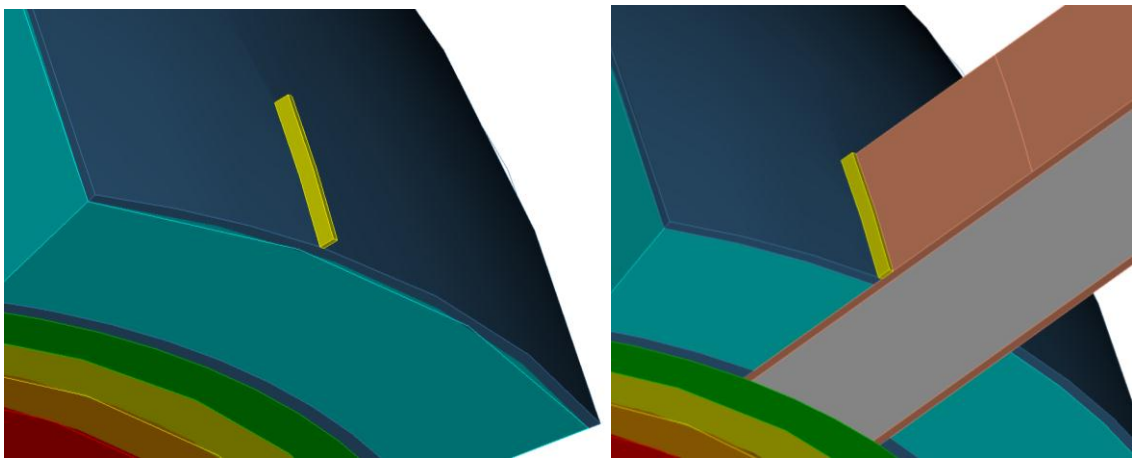

Figure 26: Isometric images showing the location of the volume detector for two variations of the ST-FNSF model for dose calculations.

The first calculation is to obtain the phase-space forward neutron flux distribution for both models. An MCNP mesh tally was used to overlay a 20x20x20 Cartesian mesh in order to obtain the spatial flux distribution. The forward neutron transport is simulated using 100 million histories. Figure 27 and Figure 28 show the distribution of the neutron flux summed over all energies taken at two planes within the 3-D model without the penetration. It is clear the flux is largest within the neutron source region and drops as the distance into the shielding increases. Figure 29 and Figure 30 show the neutron flux distribution taken at the same two planes for the 3-D model with the penetration. The penetration is shown to increase the neutron flux in the adjacent regions by approximately an order of magnitude.

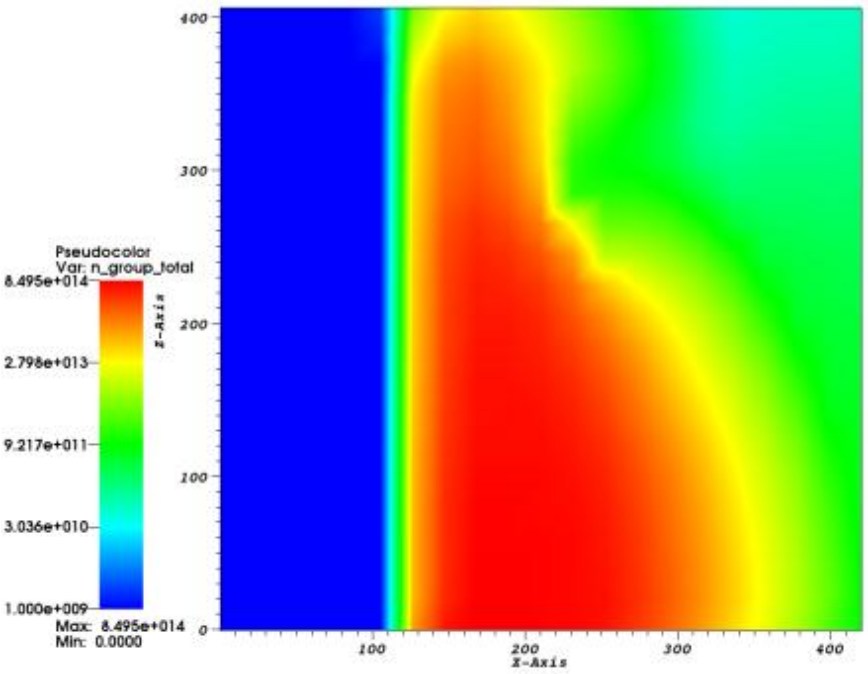

Figure 27: Surface plot of distribution of neutron flux summed over all energies at y=100 cm (adjacent to the detector) for ST-FNSF variation without the penetration.

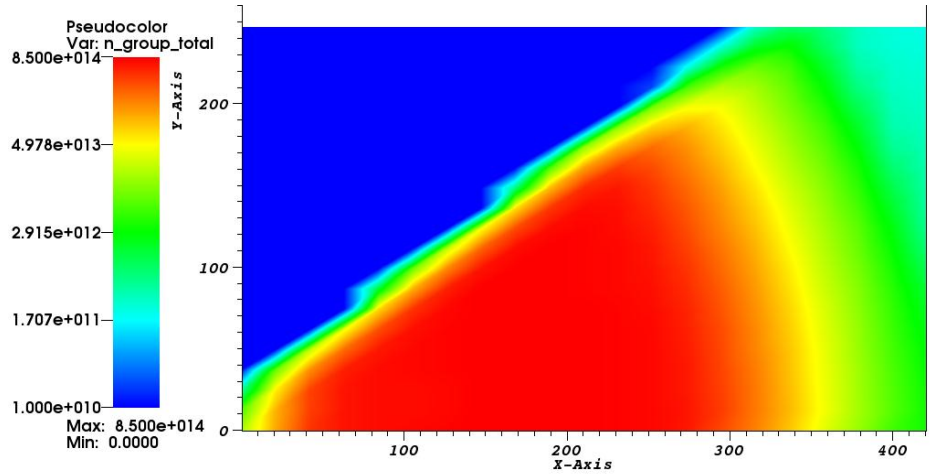

Figure 28: Surface plot of distribution of neutron flux summed over all energies taken at the midplane for ST-FNSF variation without the penetration.

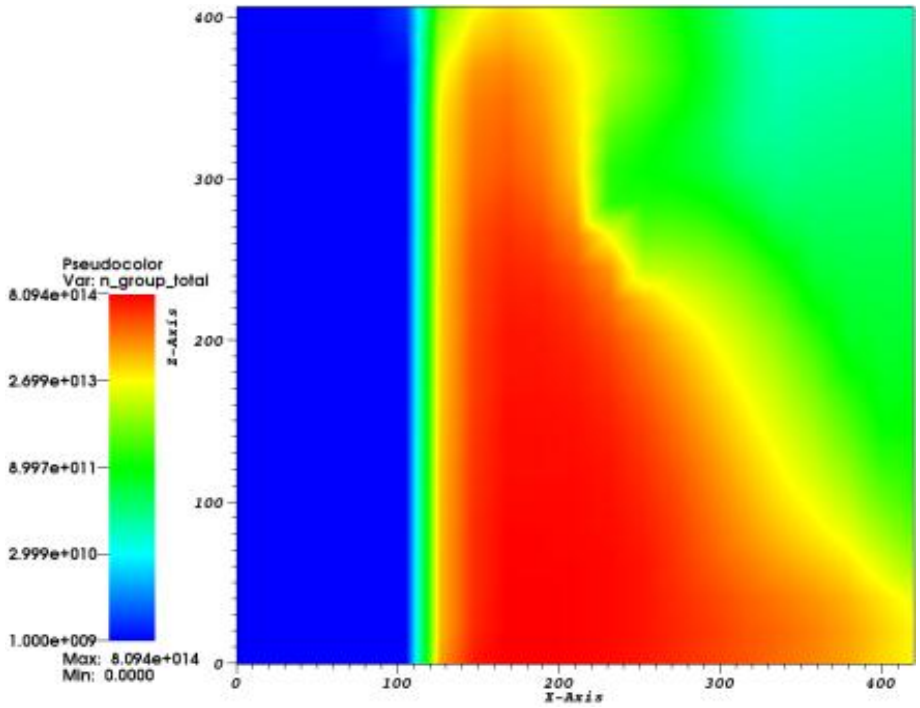

Figure 29: Distribution of neutron flux summed over all energies taken at y=100 cm (adjacent to the detector) for ST-FNSF variation with the penetration.

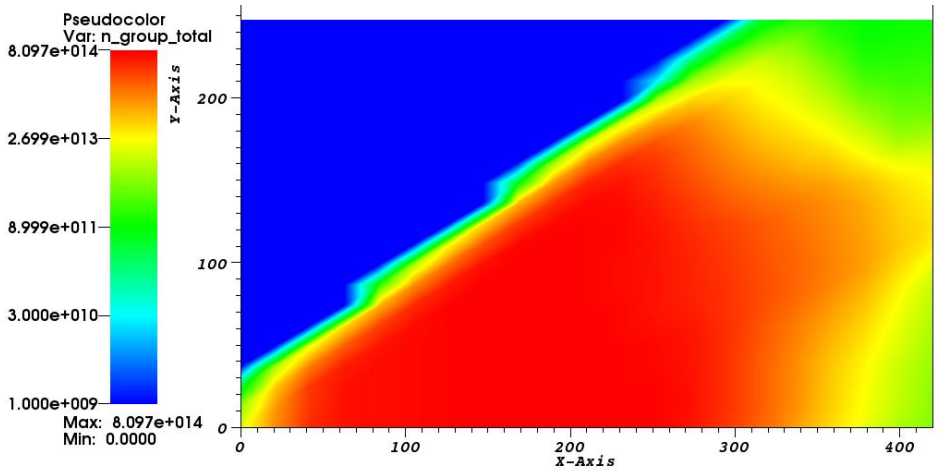

Figure 30: Distribution of neutron flux summed over all energies at midplane for ST-FNSF variation with the penetration.

A group-wise evaluation of the neutron flux at the detector is included to examine the spectral shifts caused by the design variation. The group-wise neutron flux at the detector with the penetration is shown to have larger high energy fluxes than without the penetration, which is to be expected due to the absence of shielding material. The average statistical error of the neutron flux at energy bins that recorded results for both variations is around 5%.

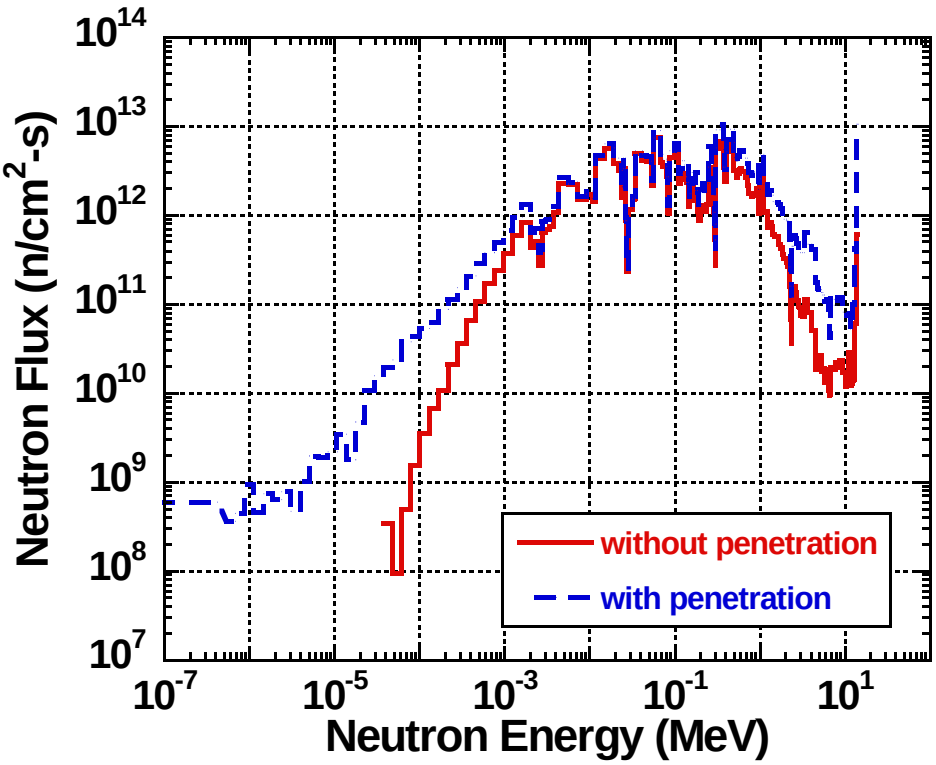

Figure 31: Neutron spectrum at the detector for the two ST-FNSF design variations.

The adjoint photon Monte Carlo transport calculation is performed to obtain the phase-space distribution of the adjoint flux within the same 20x20x20 grid used for neutron transport. Figure 32 and Figure 33 show the result of the transport calculation for the models without and with the penetration, respectively. The adjoint flux is shown at two planes corresponding to locations nearest the detector since that is where the adjoint flux will be largest. The adjoint photon flux generally increases in the model for same reason that the neutron flux increases, which is in locations where there is less shielding between the source and tally regions.

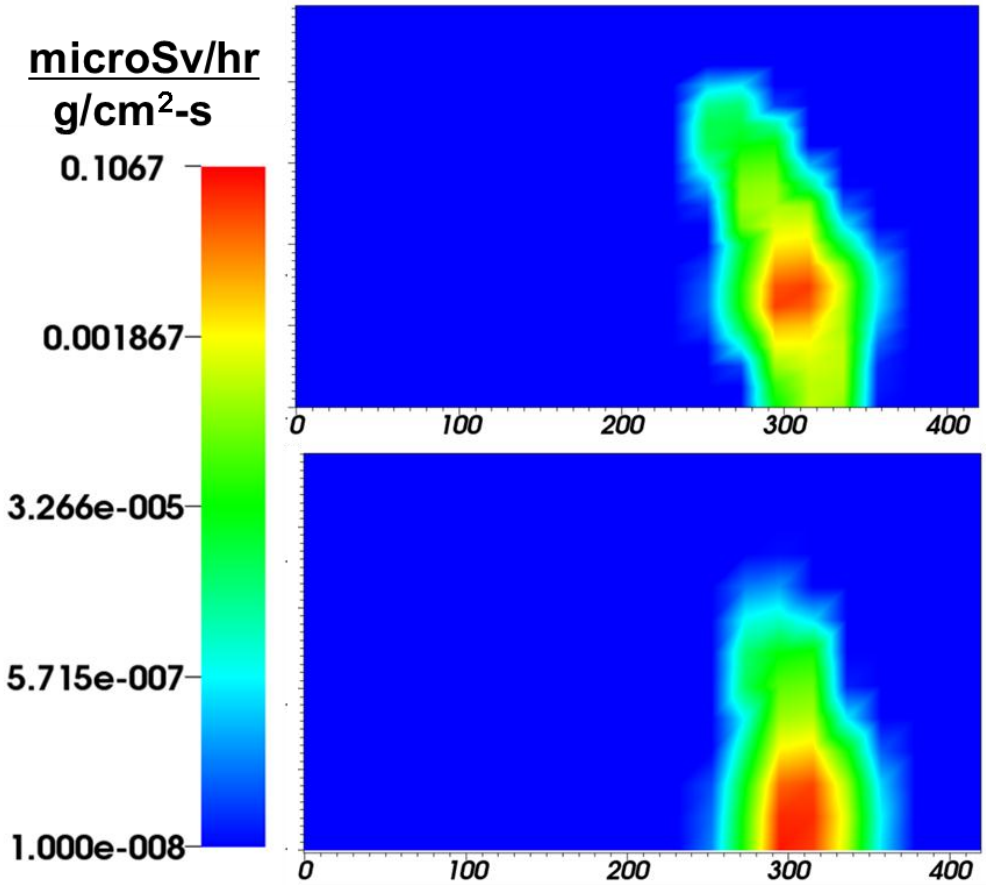

Figure 32: Side view taken at y=70 cm (top) and midplane cross section (bottom) of adjoint photon flux summed over all energies for ST-FNSF without penetration.

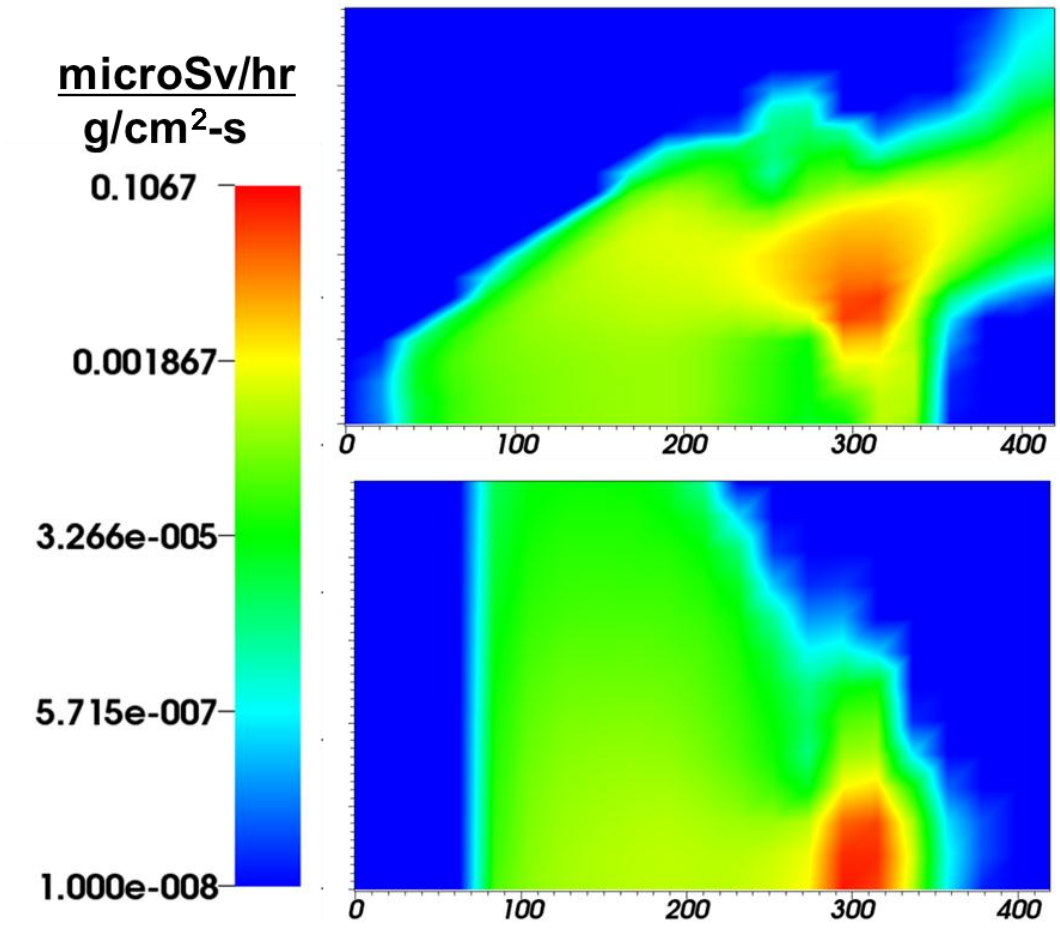

Figure 33: Side view taken at y = 70 cm (top) and midplane cross section (bottom) of adjoint photon flux summed over all energies for ST-FNSF with penetration.

The biological dose at the detector is determined for the 3-D model with the design variations. The dose with the penetration is found to be about an order of magnitude larger than without the penetration. The neutron flux will determine the photon source strength within each of the two models and since the total neutron flux was

found to be approximately an order of magnitude larger near the detector, the same increase in biological dose is to be expected.

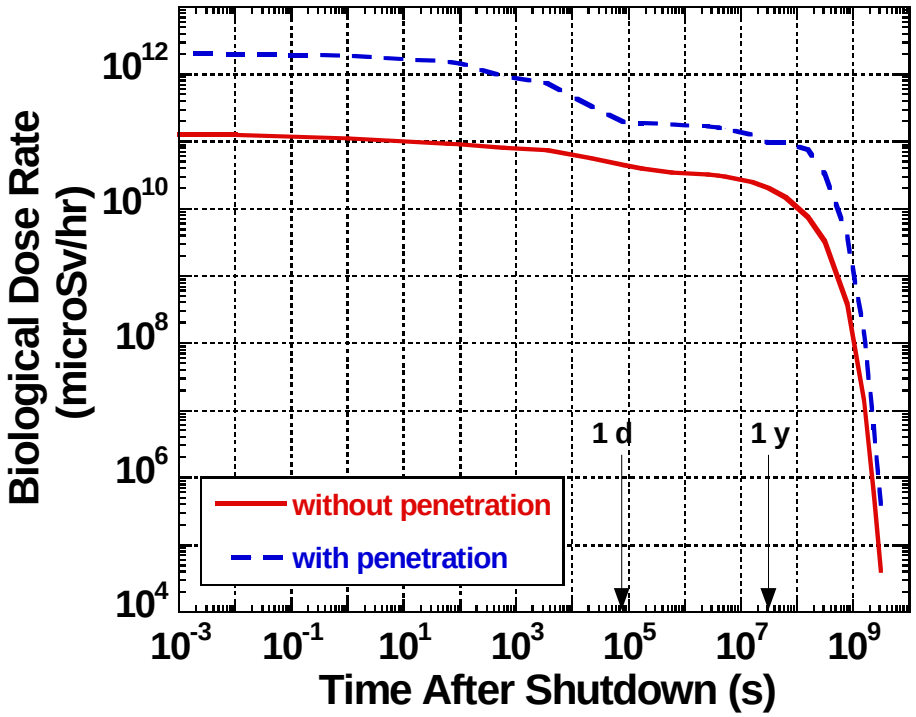

Figure 34: ST-FNSF Biological dose rate as a function of time after shutdown for models with and without penetration.

The spatial location within the 20x20x20 grid that contributes the most to the dose is located in order to proceed with the adjoint activation calculation. The dominating mesh element is found to be adjacent to the detector, and it contributes 36.6% to the total dose at the detector. The radioisotopes produced within this interval are examined to determine appropriate targets to be used in adjoint activation. The three dominant radioisotopes are Fe-55, Mn-54, and Cr-51.

Table 13: Dominant radioisotopes contributing to the dose at one day after shutdown at the detector for the ST-FNSF design with the penetration.

Isotope	Dose Rate (microSv/hr)	Contribution to Total
total	6.05E+10	-
fe-55	2.60E+10	43.0%
mn-54	2.21E+10	36.5%
cr-51	3.17E+09	5.2%
w-187	2.75E+09	4.6%
ta-182	2.31E+09	3.8%
w-181	1.44E+09	2.4%
fe-59	1.06E+09	1.8%
pb-203	5.67E+08	0.9%
co-58	2.79E+08	0.5%
mn-56	2.35E+08	0.4%
v-49	1.82E+08	0.3%
co-57	8.83E+07	0.1%
co-60	7.82E+07	0.1%
re-184	4.60E+07	0.1%
re-186	3.23E+07	0.1%

Comparable results are found for ST-FNSF problem as for ARIES-CS and the slab problem since the material surrounding the detector is mostly ferritic steel. Tables 14, 15, and 16 display the results from the adjoint activation for 3-D problem. The stable isotopes contributing to the production of the dominate radioisotopes are found to Fe-56, Fe-54, and Cr-52, which are the main constituents of steel.

Table 14: Adjoint activation results for ST-FNSF design with Fe-55 target. This table contains a list of the parent isotopes that are responsible for the production of Fe-55.

Isotope	Dose Rate (microSv/hr)	Contribution to Total
total	2.60E+10	-
fe-56	2.45E+10	94.16%
fe-54	1.52E+09	5.83%
ni-58	3.22E+06	0.01%

Table 15: Adjoint activation results for ST-FNSF design with Mn-54 target. This table contains a list of the parent isotopes that are responsible for the production of Mn-54.

Isotope	Dose Rate (microSv/hr)	Contribution to Total
total	2.21E+10	-
fe-54	2.20E+10	99.525%
fe-56	1.05E+08	0.474%
cr-54	1.61E+05	0.001%

Table 16: Adjoint activation results for ST-FNSF design with Cr-51 target. This table contains a list of the parent isotopes that are responsible for the production of Cr-51.

Isotope	Dose Rate (microSv/hr)	Contribution to Total
total	3.17E+09	-
cr-52	2.22E+09	70.0%
fe-54	6.14E+08	19.4%
cr-50	3.38E+08	10.7%

Chapter 5

Conclusions and Recommendations

The application of adjoint methods offers powerful tools to analysis of physical systems. Monte Carlo adjoint transport provides a means of investigating realistic and complex 3-D systems such as fusion power plant designs. Adjoint photon transport with flux-to-dose conversion factors as the adjoint source is capable of more directly determining a time-dependent biological for a given detector as demonstrated in this thesis. Additionally, the use of adjoint activation provides incredibly significant information relevant to the materials selection and isotopic tailoring by indicating the contribution of stable isotopes to activation parameters.

After completion of this thesis, a few recommendations have surfaced for future work with the adjoint methods. As mentioned in Chapter 1, the limitation of the adjoint method used here is that it can only be used to give the response for one spatial location. A suggestion for future research is to implement multiple adjoint sources within a Monte Carlo transport code. In theory, multiple adjoint sources might allow for the dose to be determined for more than one location at a time, thereby eliminating the disadvantage of

the adjoint transport method over the forward transport method. Also, it is recommended to use a larger multi-group or a continuous energy photon library for the adjoint Monte Carlo transport simulation rather than the readily available 12-group photon library released with MCNP. This improvement would add greater robustness and accuracy to the adjoint solutions and allow for a better comparison with deterministic codes. Lastly, analog MCNP was shown to be inefficient in obtaining statistically accurate thermal neutron fluxes in fast neutron dominated systems. It is suggested to introduce variance reduction techniques that increase the efficiency of the Monte Carlo method in determining thermal neutron fluxes should they be relevant to the biological dose. The impact of the thermal neutrons on the biological dose will be dependent on the isotopic composition of each system, so wise judgment would be necessary prior to implementing such a method.

References

1. A. White, “Transmutation and Activation Analysis of Fusion Power Plants,” Ph.D. Thesis, University of Wisconsin, 1985.
2. G. Bell, S. Glasstone, “Nuclear Reactor Theory,” Robert E. Krieger Publishing Compnay, New York, 1979.
3. R. Alcouffe et al., “PARTISN: A Time Dependent, Parallel Neutral Particle Transport Code System,” Los Alamos National Laboratory Report, LA-UR-08-07258 (2008).
4. “Cubit Geometry and Mesh Generation Toolkit version 12.2.” Sandia National Laboratories (2010). Available at: http://cubit.sandia.gov.
5. “DAGMC Users Guide.” University of Wisconsin-Madison Fusion Technology Institute (2008). Available at: http://cnerg.engr.wisc.edu/cgi-bin/index.cgi/wiki?p=DagmcUsersGuide.
6. T. Tautges et al., “MOAB: A Mesh Oriented Database”. Albuquerque, NM. Sandia National Laboratories, 2004.
7. X-5 Monte Carlo Team, “MCNP-A General Monte Carlo N-Particle Transport Code, Version 5,” Vol. I, LA-UR-03-1987, Los Alamos National Laboratory (April 2003; revised 6/30/2004) and Vol. II, LA-CP-03-0245, Los Alamos National Laboratory (April 2003; revised 6/30/2004).

8. P. Wilson and D. Henderson, "ALARA: Analytic and Laplacian Adaptive Radioactivity Analysis: A Complete Package for Analysis of Induced Activation – Volume I," University of Wisconsin-Madison Fusion Technology Institute Report, UWFDM-1070 (1998). Available at: http://fti.neep.wisc.edu/pdf/fdm1070.pdf.
9. P. Wilson and D. Henderson, "ALARA: Analytic and Laplacian Adaptive Radioactivity Analysis: A Complete Package for Analysis of Induced Activation – Volume II," University of Wisconsin-Madison Fusion Technology Institute Report, UWFDM-1071 (1998). Available at: http://fti.neep.wisc.edu/pdf/fdm1071.pdf.
10. D. Moule, "A Comparison of Mesh Generation Methods for Deterministic Radiation Transport," M.S. Thesis, University of Wisconsin, 2011.
11. D.L. Aldama, A. Trkov, "FENDL-2.1 Update of an Evaluated Nuclear Data Library for Fusion Applications," International Atomic Agency Report INDC(NDC)-467 (2004).
12. A. Pashchenko, H. Wienke, J. Kopecky, J. Sublet and R. Forrest, "FENDL/A-2.0, Nuclear Activation Cross Section Data Library for Fusion Applications," International Atomic Energy Agency Report IAEA-NDS-173 (1998).
13. J. Wagner, et al., "MCNP: Multigroup/Adjoint Capabilities," LA-12704, Los Alamos National Laboratory (April 1994).
14. "American National Standard for Neutron and Gamma-Ray Flux-to-Dose Factors" American Nuclear Society, ANSI/ANS-6.1.1-1977 (1977).

15. L. El-Guebaly, P. Wilson, D. Henderson, M. Sawan, G. Sviatoslavsky, T. Tautges et al., "Designing ARIES-CS Compact Radial Build and Nuclear System: Neutronics, Shielding, and Activation," Fusion Science and Technology 54, No. 3 (2008) 747-770.

16. A. Robinson, L. El-Guebaly, D. Henderson, "Evaluation of Biological Dose for ARIES-CS and Comparison with Approximate Contact Dose Approach," University of Wisconsin-Madison Fusion Technology Institute Report, UWFDM-1375 (2010). Available at: http://fti.neep.wisc.edu/pdf/fdm1375.pdf.

17. R. N. Slaybaugh, P.P.H. Wilson, L.A. El-Guebaly, and E.P. Marriott, "Three-Dimensional Source Models for Toroidal Fusion Energy Systems," *Fusion Engineering and Design*, **84**, Issues 7-11, 1774 (2009).

18. A. Jaber, L. El-Guebaly and L. Mynsberge, "3-D Modeling of Neutron Wall Loading, Tritium Breeding Ratio, and Nuclear Heating Distribution for ARIES-ACT-DCLL Design," University of Wisconsin Fusion Technology Institute Report UWFDM-1408 (2012). Available at: http://fti.neep.wisc.edu/pdf/fdm1408.pdf.

Appendix

A. 1-D Slab Inputs

A.1. 1-D Slab Forward Neutron Transport PARTISN Input

```
1     0     0
   1-D Slab Geometry Forward Neutron Transport 4/19/2012 Amir Jaber
/
/  ---------------- Block 1 (Control and Dimensions) -------------------
    igeom= 1  ngroup= 217  isn= 12  niso= 44  mt= 1
              nzone= 1    im=3  it=6
    maxlcm= 5000000
    maxscm= 1000000
    idimen= 1
    iquad=4
    t
/
/  ---------------- Block 2 (Geometry) ---------------------------------
/
/
/
    xmesh= 0  0.25 4.25 5
    xints=   1  4  1
    zones=   0   1   0
    t
/
/  ---------------- Block 3 (Cross Section) ----------------------------
/
    lib= bxslib
    lng= 175
    maxord= 5  ihm= 227  iht= 10  ihs= 11  ifido= 1  ititl= 1
               i2lp1= 0  savbxs= 1  kwikrd= 1
    names= hnat  h1  d  h3  he3  he4  linat  li6 li7  be9  bnat b10 b11
           c12  n  o16  f19  na23  mgnat  al27  si  p31  snat  cl  knat
           canat  ti  vnat  cr  mn55  fe  co59  ni  cu  ganat  zrnat nb93
           mo  snnat  ta181  w   au197  pb  bi209
    edname= heat  kerma  dame  dpa  tp  he  h
    t
/
/  ---------------- Block 4 (Material Mixing) -------------------------
/
    matls=
         MF82H    fe .07667 c12 .000396 vnat .000187 cr .00685 w .00052 ;
    assign=
         VV        MF82H   1.0 ;
    t
/
/  ---------------- Block 5 (Solver) ---------------------------------
/
     ievt= 0  isct= 5  ith= 0  ibl= 0  ibr= 0 norm=1e10
```

```
     iitl= 200
     fluxp=1
/
/   ----------  source input ----------------------------------------
/
     source= 7z 1 f0
     sourcx= 1 f0
    t
/
/  ---------------- Block 6 ----------------------------------------
/
     pted= 1 zned= 1 resdnt= 1 rsfnam= flux
     rsfe= 7z f1.0 ;
     rsfx= f 1 ;
    t
```

A.2. 1-D Slab Adjoint Photon Transport PARTISN Input

```
  1     0     0
   1-D Slab Geometry Adjoint Photon Transport 4/19/2012 Amir Jaber
/
/  ---------------- Block 1 (Control and Dimensions) -------------------
    igeom= 1  ngroup= 217  isn= 12  niso= 44  mt= 1
              nzone= 1    im=3  it=6
    maxlcm= 5000000
    maxscm= 1000000
    idimen= 1
    t
/
/  ---------------- Block 2 (Geometry) ---------------------------------
/
/
/
    xmesh= 0  0.25 4.25 5
    xints=   1  4  1
    zones=   0   1   0
    t
/
/  ---------------- Block 3 (Cross Section) ---------------------------
/
    lib= bxslib
    lng= 175
    maxord= 5  ihm= 227  iht= 10  ihs= 11  ifido= 1  ititl= 1
               i21p1= 0  savbxs= 1  kwikrd= 1
    names= hnat  h1  d  h3  he3  he4  linat  li6 li7  be9  bnat b10 b11
           c12  n  o16  f19  na23  mgnat  al27  si  p31  snat  cl  knat
           canat  ti  vnat  cr  mn55  fe  co59  ni  cu  ganat  zrnat nb93
           mo  snnat  ta181  w   au197  pb  bi209
    edname= heat  kerma  dame  dpa  tp  he  h
    t
/
```

```
/  ---------------- Block 4 (Material Mixing) -------------------------
/
    matls=
         MF82H    fe .07667 c12 .000396 vnat .000187 cr .00685 w .00052 ;
    assign=
         VV        MF82H   1.0 ;
    t
/
/  ---------------- Block 5 (Solver) ---------------------------------
/
     ievt= 0  isct= 5  ith=1  ibl=0  ibr=0 norm=0
     iitl=300
     fluxp=1
/
/   ----------  source input ----------------------------------------
/  flux to dose conversion factors (1977) microSv/h per g/cm2s
     source= 175r0   2r0  1.325-1  1.178-1  1.026-1  8.772-2
             7.847-2  7.478-2  7.110-2  6.743-2  6.375-2  6.007-2
             5.601-2  5.227-2  4.832-2  4.412-2  3.960-2  3.469-2
             3.019-2  2.731-2  2.536-2  2.430-2  2.205-2  1.833-2
             1.604-2  1.442-2  1.281-2  1.202-2  1.128-2  1.032-2
             8.759-3  6.306-3  4.391-3  3.277-3  2.682-3  2.578-3
             2.601-3  2.844-3  4.115-3  8.267-3  2.144-2  0;
    sourcx= 5z 1 ;
    t
```

A.3. 1-D Slab Forward Neutron Transport MCNP Input

```
c ************************
c Source Definition
c ************************
mode n
sdef par=n erg=14 x=d2 y=d3 z=d4 cel=1
si2 0.001 0.999
sp2 0 1
si3 0.001 0.999
sp3 0 1
si4 0.001 0.2499
sp4 0 1
c
c ************************
c Material Definition
c ************************
c 100% MF82H
m1 26054.21c    0.0044814    &
26056.21c    0.0703478    &
26057.21c    0.0016246    &
26058.21c    0.0002162    &
24050.21c    0.0002976    &
24052.21c    0.0057395    &
24053.21c    0.0006508    &
24054.21c    0.0001620    &
```

```
74182.21c    0.0001384    &
74183.21c    0.0000744    &
74184.21c    0.0001593    &
74186.21c    0.0001478    &
23000.21c    0.0001870    &
6012.21c     0.0003960
c
c ************************
c Tally Definition
c ************************
c
fmesh4:n geom=xyz origin=0 0 0
          imesh=1 iints=1
          jmesh=1 jints=1
          kmesh=    0.25   4.25   5
          kints=  1      4      1
          emesh=1.0000E-07 4.1399E-07 5.3158E-07 6.8256E-07 8.7642E-07
               1.1254E-06 1.4450E-06 1.8554E-06 2.3824E-06 3.0590E-06
               3.9279E-06 5.0435E-06 6.4760E-06 8.3153E-06 1.0677E-05
               1.3710E-05 1.7603E-05 2.2603E-05 2.9023E-05 3.7267E-05
               4.7851E-05 6.1442E-05 7.8893E-05 1.0130E-04 1.3007E-04
               1.6702E-04 2.1445E-04 2.7536E-04 3.5380E-04 4.5400E-04
               5.8295E-04 7.4852E-04 9.6112E-04 1.2341E-03 1.5846E-03
               2.0347E-03 2.2487E-03 2.4852E-03 2.6126E-03 2.7465E-03
               3.0354E-03 3.3546E-03 3.7074E-03 4.3107E-03 5.5308E-03
               7.1017E-03 9.1188E-03 1.0595E-02 1.1709E-02 1.5034E-02
               1.9305E-02 2.1875E-02 2.3579E-02 2.4176E-02 2.4788E-02
               2.6058E-02 2.7000E-02 2.8500E-02 3.1828E-02 3.4307E-02
               4.0868E-02 4.6309E-02 5.2475E-02 5.6562E-02 6.7379E-02
               7.2000E-02 7.9500E-02 8.2500E-02 8.6517E-02 9.8037E-02
               1.1109E-01 1.1679E-01 1.2277E-01 1.2907E-01 1.3569E-01
               1.4264E-01 1.4996E-01 1.5764E-01 1.6573E-01 1.7422E-01
               1.8316E-01 1.9255E-01 2.0242E-01 2.1280E-01 2.2371E-01
               2.3518E-01 2.4724E-01 2.7324E-01 2.8725E-01 2.9452E-01
               2.9720E-01 2.9850E-01 3.0197E-01 3.3373E-01 3.6883E-01
               3.8774E-01 4.0762E-01 4.5049E-01 4.9787E-01 5.2340E-01
               5.5023E-01 5.7844E-01 6.0810E-01 6.3928E-01 6.7206E-01
               7.0651E-01 7.4274E-01 7.8082E-01 8.2085E-01 8.6294E-01
               9.0718E-01 9.6164E-01 1.0026E+00 1.1108E+00 1.1648E+00
               1.2246E+00 1.2873E+00 1.3534E+00 1.4227E+00 1.4957E+00
               1.5724E+00 1.6530E+00 1.7377E+00 1.8268E+00 1.9205E+00
               2.0190E+00 2.1225E+00 2.2313E+00 2.3069E+00 2.3457E+00
               2.3653E+00 2.3852E+00 2.4660E+00 2.5924E+00 2.7253E+00
               2.8650E+00 3.0119E+00 3.1664E+00 3.3287E+00 3.6788E+00
               4.0657E+00 4.4933E+00 4.7237E+00 4.9659E+00 5.2205E+00
               5.4881E+00 5.7695E+00 6.0653E+00 6.3763E+00 6.5924E+00
               6.7032E+00 7.0469E+00 7.4082E+00 7.7880E+00 8.1873E+00
               8.6071E+00 9.0484E+00 9.5123E+00 1.0000E+01 1.0513E+01
               1.1052E+01 1.1618E+01 1.2214E+01 1.2523E+01 1.2840E+01
               1.3499E+01 1.3840E+01 1.4191E+01 1.4550E+01 1.4918E+01
               1.5683E+01 1.6487E+01 1.6905E+01 1.7333E+01 1.9640E+01
fm4 1e10 $ Source strength
nps 1e7
```

A.4. 1-D Slab Adjoint Photon Transport MCNP Input

```
c ************************
c Source Definition
c ************************
mode p
sdef par=p erg=d5 x=d2 y=d3 z=d4 cel=3
si2 0.001 0.999
sp2 0 1
si3 0.001 0.999
sp3 0 1
si4 4.25 5.00
sp4 0 1
si5 h   1.00E-02 1.00E-01    5.00E-01    1.00E+00    2.00E+00
                 3.00E+00    4.00E+00    5.00E+00    6.00E+00
                 7.00E+00    8.00E+00    9.00E+00    2.00E+01
c 1977 Flux-to-Dose Conversion Factors(uSv/hr) - 12 Group Structure
sp5 d   0.00 1.7858E-02  7.4099E-03  1.6011E-02  2.6292E-02
             3.7253E-02  4.6360E-02  5.4299E-02  6.1909E-02
             6.9265E-02  7.6626E-02  8.4008E-02  1.2955E-01
c
c ************************
c Adjoint Options
c ************************
mgopt a 12
cut:p j 20
c
c ************************
c Material Definition
c ************************
c VV 100% MF82H
m1 26000    0.0766700    &
24000       0.0068500    &
74182       0.0001384    &
74183       0.0000744    &
74184       0.0001593    &
74186       0.0001478    &
23000       0.0001870    &
6012        0.0003960
c
c
c ************************
c Tally Definition
c ************************
c
fmesh4:p geom=xyz origin=0 0 0
          imesh=1 iints=1
          jmesh=1 jints=1
          kmesh=    0.25   4.25   5
```

```
          kints=  1      4      1
          emesh = 1.00E-01    5.00E-01    1.00E+00    2.00E+00
                  3.00E+00    4.00E+00    5.00E+00    6.00E+00
                  7.00E+00    8.00E+00    9.00E+00    2.00E+01
fm4 0.47025 $ volume of detector times source strength ( 0.75 * 0.627 )
nps 1e7
```

A.5. 1-D Slab Forward Activation ALARA Input

```
# 1-D Slab Geometry ALARA Input

geometry rectangular

dimension     x      0
       1     0.25
       4     4.25
       1     5
end

mat_loading
       zone0  void
       zone1  mix_1
       zone2  void
end

mixture       mix_1
       material      MF82H         1.0    1.0
end

material_lib  ARIES_matlib
element_lib   ARIES_elelib
data_library alaralib      FENDL2

flux flux_1 forflux_mcnp 1.0 0 default

impurity      5e-5   1e-3

cooling
       .01    s
       1      s
       1      m
       100    s
       10     m
       1      h
       6      h
       1      d
       2      d
       7      d
       30     d
       45     d
       60     d
       .5     y
```

```
       1      y
       2      y
       5      y
       10     y
       25     y
       50     y
       75     y
       100    y
end

dump_file     dump.file

#output interval
#      units Bq cm3
#      photon_source FENDL2
#      phtn-src-part 42 1e4 2e4 3e4 4.5e4  6e4
#          7e4  7.5e4  1e5  1.5e5  2e5  3e5 4e5  4.5e5
#          5.1e5  5.12e5  6e5  7e5  8e5  1e6  1.33e6
#         1.34e6  1.5e6  1.66e6  2e6  2.5e6  3e6  3.5e6
#         4e6  4.5e6  5e6  5.5e6  6e6  6.5e6  7e6  7.5e6
#           8e6  1e7  1.2e7  1.4e7  2e7  3e7  5e7
#       folded_dose FENDL2 0.75
#       adjflux_part 42 1e4 2e4 3e4 4.5e4  6e4
#           7e4  7.5e4  1e5  1.5e5  2e5  3e5 4e5  4.5e5
#           5.1e5  5.12e5  6e5  7e5  8e5  1e6  1.33e6
#          1.34e6  1.5e6  1.66e6  2e6  2.5e6  3e6  3.5e6
#          4e6  4.5e6  5e6  5.5e6  6e6  6.5e6  7e6  7.5e6
#           8e6  1e7  1.2e7  1.4e7  2e7  3e7  5e7
#end

output interval
       units Bq cm3
       photon_source FENDL2
       phtn-src-mcnp 12 1e5 5e5 1e6 2e6 3e6 4e6
                        5e6 6e6 7e6 8e6 9e6 2e7
       folded_dose FENDL2 0.75
       adjflux_mcnp 12 1e5 5e5 1e6 2e6 3e6 4e6
                       5e6 6e6 7e6 8e6 9e6 2e7
end

schedule      total
       .85    y      flux_1 3.9FPYpulsed  0  s
end

pulsehistory  3.9FPYpulsed
       5      .15    y
end

truncation    1e-7
```

B. ARIES-CS Inputs

B.1. ARIES-CS Forward Neutron Transport PARTISN Input

```
    1     0     0
   ARIES-CS - Poloidal geom.- FENDL-2 - 2.6 MW/m2 Av. - LiPb/FS System
/
/  ---------------- Block 1 (Control and Dimensions) -------------------
    igeom= 2  ngroup= 217  isn= 12  niso= 44  mt= 15
              nzone= 15    im=31  it= 333
    maxlcm= 5000000
    maxscm= 1000000
    idimen= 1
    iquad=4
    t
/
/  ---------------- Block 2 (Geometry) ---------------------------------
/
/
/
    xmesh= 0 175 178.8 179 179.5 204.5 205 205.2 206.7 206.9
           207.4 232.4 232.9 233.1 238.1 268.1 303.1
           305.1 333.1 343.1 345.1 345.3 364.7 392.7
           440 445 450 500 550 600 650 650.5
    xints= 100 2 1 1 13 5r1 13 1 1 3 16 18 1 14 2
           1 1 10 15 9 3 2 4r25 1
    zones= 0 5 6 7 9 7 6 8 6 7 9 7 6 10 11 12 0 13
           0 1 4 2 1 0 14 0 4r15 0
    t
/
/  ---------------- Block 3 (Cross Section) ---------------------------
/
    lib= bxslib
    lng= 175
    maxord= 5  ihm= 227  iht= 10  ihs= 11  ifido= 1  ititl= 1
               i2lp1= 0  savbxs= 1  kwikrd= 1
    names= hnat  h1  d  h3  he3  he4  linat  li6 li7  be9  bnat b10 b11
           c12  n  o16  f19  na23  mgnat  al27  si  p31  snat  cl  knat
           canat  ti  vnat  cr  mn55  fe  co59  ni  cu  ganat  zrnat nb93
           mo  snnat  ta181  w   au197  pb  bi209
    edname= heat  kerma  dame  dpa  tp  he  h
    t
/
/  ---------------- Block 4 (Material Mixing) -------------------------
/
    matls=
         ODSFS    fe  .07038 cr .01134  ti .00034 mo .00001 mn55 .00004
```

```
                c12 .000204 si .00017 o16 .000469  ni .0002 w 0.00062 ;
        MF82H   fe .07667 c12 .000396 vnat .000187 cr .00685 w .00052 ;
        B-FS    fe .07412 c12 .000396 vnat .000187 cr .00685 w .00052
                bnat .013213  ;
        h2o     hnat .0656 o16 .0328  ;
        B-h2o   bnat .0004888 hnat .06523 o16 .03335 ;
        G.poly  si .008765 o16 .02898 al27 .003966 mgnat .002 c12 .0212
                hnat .01746 n .0035  ;
        cu      cu .08434 ;
        sic.95  si .0459 c12 .0459  ;
        lipb90  li6 .00479 li7 .000533 pb .026  ; / at 580 oC
        JK2LB   fe .04783 ni .00738 cr .01204 mn55 .01841 c12 .00008
                mo .0005 si .00051 bnat .0000089  ;
        nb3sn   nb93 .04046 snnat .013486 ;
        LHe     he4 .02108 ;
        SS-304  fe .05982 ni .0075 cr .01611 mn55 .00101 c12 .00018
                mo .00016 si .00079 ti .00003  ;
        MildSS  c12 7.96e-4 si 4.25e-4 mn55 3.91e-4 fe .0847  ;
        conc    hnat .007856 o16 .04406 na23 .001053 mgnat .0001514
                al27 .002397 si .01588 snat .00005649 knat .0006951
                canat .002927 fe .0003132  ;
    assign=
        case    JK2LB .95 LHe .05 ;
        WP      JK2LB .185 cu .482 nb3sn .128 G.poly .1 LHe .105 ;
        Cu.     cu 1  ;
        insl.   G.poly 1.  ;
        FW      ODSFS  .08  MF82H  .26  ;
        LiPb    lipb90 1  ;
        SiC     sic.95 1  ;
        Chanl   MF82H .58  ;
        Blkt    lipb90  .84 MF82H .05 sic.95 .04  ;
        BW      MF82H .8  ;
        Shld    MF82H .15 B-FS .75  ;
        Mnfld   MF82H .52 lipb90 .227 sic.95 .013 ;
        VV      MF82H .28 B-FS .23 h2o .49  ;
        Cryost  SS-304  1  ;
        Conc.   conc .85 MildSS .1 ;
    t
/
/  ---------------- Block 5 (Solver) ---------------------------------
/
     ievt= 0  isct= 5  ith= 0  ibl=1  ibr= 0 norm= 1.3e17
     iitl= 100 iitm= 100
     fluxp=1
/
/   ----------  source input ----------------------------------------
/
     source= 7z 1 f0
     sourcx= 50r1 f0
    t
/
/  ---------------- Block 6 ----------------------------------------
/
     pted= 1 zned= 1 resdnt= 1 rsfnam= flux
     rsfe= 7z f1.0 ;
     rsfx= f 1 ;
```

```
    t
```

B.2. ARIES-CS Adjoint Photon Transport PARTISN Input

```
   1     0     0
   ARIES-CS - ADJOINT
/
/  ---------------- Block 1 (Control and Dimensions) -------------------
    igeom= 2  ngroup= 217  isn= 12  niso= 44  mt= 15
              nzone= 15    im=31  it= 333
    maxlcm= 5000000
    maxscm= 1000000
    idimen= 1
    t
/
/  ---------------- Block 2 (Geometry) ---------------------------------
/
/
/
    xmesh= 0 175 178.8 179 179.5 204.5 205 205.2 206.7 206.9
           207.4 232.4 232.9 233.1 238.1 268.1 303.1
           305.1 333.1 343.1 345.1 345.3 364.7 392.7
           440 445 450 500 550 600 650 650.5
    xints= 100 2 1 1 13 5r1 13 1 1 3 16 18 1 14 2
           1 1 10 15 9 3 2 4r25 1
/   No LiPb in adjoint case (6--0)
    zones= 0 5 0 7 9 7 0 8 0 7 9 7 0 10 11 12 0 13
           0 1 4 2 1 0 14 0 4r15 0
    t
/
/  ---------------- Block 3 (Cross Section) ---------------------------
/
    lib= bxslib
    lng= 175
    maxord= 5  ihm= 227  iht= 10  ihs= 11  ifido= 1  ititl= 1
               i2lp1= 0  savbxs= 1  kwikrd= 1
    names= hnat  h1  d  h3  he3  he4  linat  li6 li7  be9  bnat b10 b11
           c12  n  o16  f19  na23  mgnat  al27  si  p31  snat  cl  knat
           canat  ti  vnat  cr  mn55  fe  co59  ni  cu  ganat  zrnat nb93
           mo  snnat  ta181  w   au197  pb  bi209
    edname= heat  kerma  dame  dpa  tp  he  h
    t
/
/  ---------------- Block 4 (Material Mixing) -------------------------
/
    matls=
         ODSFS    fe  .07038 cr .01134  ti .00034 mo .00001 mn55 .00004
                  c12 .000204 si .00017 o16 .000469  ni .0002 w 0.00062 ;
         MF82H    fe .07667 c12 .000396 vnat .000187 cr .00685 w .00052 ;
         B-FS     fe .07412 c12 .000396 vnat .000187 cr .00685 w .00052
                  bnat .013213  ;
```

```
         h2o      hnat .0656 o16 .0328  ;
         B-h2o    bnat .0004888 hnat .06523 o16 .03335 ;
         G.poly   si .008765 o16 .02898 al27 .003966 mgnat .002 c12 .0212
                  hnat .01746 n .0035  ;
         cu       cu .08434 ;
         sic.95   si .0459 c12 .0459  ;
         lipb90   li6 .00479 li7 .000533 pb .026  ; / at 580 oC
         JK2LB    fe .04783 ni .00738 cr .01204 mn55 .01841 c12 .00008
                  mo .0005 si .00051 bnat .0000089  ;
         nb3sn    nb93 .04046 snnat .013486 ;
         LHe      he4 .02108 ;
         SS-304   fe .05982 ni .0075 cr .01611 mn55 .00101 c12 .00018
                  mo .00016 si .00079 ti .00003  ;
         MildSS   c12 7.96e-4 si 4.25e-4 mn55 3.91e-4 fe .0847  ;
         conc     hnat .007856 o16 .04406 na23 .001053 mgnat .0001514
                  al27 .002397 si .01588 snat .00005649 knat .0006951
                  canat .002927 fe .0003132  ;
    assign=
         case     JK2LB .95 LHe .05 ;
         WP       JK2LB .185 cu .482 nb3sn .128 G.poly .1 LHe .105 ;
         Cu.      cu 1  ;
         insl.    G.poly 1.  ;
         FW       ODSFS  .08  MF82H  .26  ;
         LiPb     lipb90 1  ;
         SiC      sic.95 1  ;
         Chanl    MF82H .58  ;
         Blkt     lipb90  .84 MF82H .05 sic.95 .04  ;
         BW       MF82H .8  ;
         Shld     MF82H .15 B-FS .75  ;
         Mnfld    MF82H .52 lipb90 .227 sic.95 .013 ;
         VV       MF82H .28 B-FS .23 h2o .49  ;
         Cryost   SS-304  1  ;
         Conc.    conc .85 MildSS .1 ;
    t
/
/  ---------------- Block 5 (Solver) ---------------------------------
/
     ievt= 0  isct= 5  ith= 1  ibl= 0  ibr= 0 norm= 0
     iitl=100
     fluxp=1
/
/   ----------  source input ----------------------------------------
/  flux to dose conversion factors (1977) microSv/h per g/cm2s
     source= 175r0   2r0  1.325-1  1.178-1  1.026-1  8.772-2
             7.847-2  7.478-2  7.110-2  6.743-2  6.375-2  6.007-2
             5.601-2  5.227-2  4.832-2  4.412-2  3.960-2  3.469-2
             3.019-2  2.731-2  2.536-2  2.430-2  2.205-2  1.833-2
             1.604-2  1.442-2  1.281-2  1.202-2  1.128-2  1.032-2
             8.759-3  6.306-3  4.391-3  3.277-3  2.682-3  2.578-3
             2.601-3  2.844-3  4.115-3  8.267-3  2.144-2  0;
/  use interval 103 for FW biodose to contact dose comparison
     sourcx= 102z 1 f0 ;
    t
```

B.3. ARIES-CS Forward Neutron Transport MCNP Input

```
c ************************
c Source Definition
c ************************
mode n
sdef erg=14 x=d2 y=d3 z=d4 cel=1
si2 0.001 87.499
sp2 0 1
si3 0.001 17.0704
sp3 0 1
si4 0.001 0.999
sp4 0 1
c
c ************************
c Material Definition
c ************************
c Case
m1 26054.21c    0.0026559    &
26056.21c    0.0416916    &
26057.21c    0.0009628    &
26058.21c    0.0001281    &
28058.21c    0.0047729    &
28060.21c    0.0018385    &
28061.21c    0.0000799    &
28062.21c    0.0002548    &
28064.21c    0.0000649    &
24050.21c    0.0004970    &
24052.21c    0.0095838    &
24053.21c    0.0010867    &
24054.21c    0.0002705    &
25055.21c    0.0174895    &
6012.21c    0.0000760    &
42092.21c    0.0000705    &
42094.21c    0.0000439    &
42095.21c    0.0000756    &
42096.21c    0.0000792    &
42097.21c    0.0000454    &
42098.21c    0.0001146    &
42100.21c    0.0000457    &
14028.21c    0.0004469    &
14029.21c    0.0000226    &
14030.21c    0.0000150    &
5010.21c    0.0000017    &
5011.21c    0.0000068    &
2004.70c    0.0010540
c
c WP
m2 26054.21c    0.0005172    &
26056.21c    0.0081189    &
26057.21c    0.0001875    &
```

```
26058.21c    0.0000250    &
28058.21c    0.0009295    &
28060.21c    0.0003580    &
28061.21c    0.0000156    &
28062.21c    0.0000496    &
28064.21c    0.0000126    &
24050.21c    0.0000968    &
24052.21c    0.0018663    &
24053.21c    0.0002116    &
24054.21c    0.0000527    &
25055.21c    0.0034059    &
6012.21c    0.0000148    &
42092.21c    0.0000137    &
42094.21c    0.0000086    &
42095.21c    0.0000147    &
42096.21c    0.0000154    &
42097.21c    0.0000088    &
42098.21c    0.0000223    &
42100.21c    0.0000089    &
14028.21c    0.0008954    &
14029.21c    0.0000453    &
14030.21c    0.0000301    &
5010.21c    0.0000003    &
5011.21c    0.0000013    &
29063.21c    0.0281189    &
29065.21c    0.0125330    &
41093.21c    0.0051789    &
50112.70c    0.0000167    &
50114.70c    0.0000112    &
50115.70c    0.0000059    &
50116.70c    0.0002510    &
50117.70c    0.0001326    &
50118.70c    0.0004181    &
50119.70c    0.0001481    &
50120.70c    0.0005626    &
50122.70c    0.0000799    &
50124.70c    0.0000999    &
8016.21c    0.0028980    &
13027.21c    0.0003966    &
12024.70c    0.0001580    &
12025.70c    0.0000200    &
12026.70c    0.0000220    &
6012.21c    0.0021200    &
1001.70c    0.0017460    &
7014.70c    0.0003487    &
7015.70c    0.0000013    &
2004.70c    0.0022134
c
c Cu
m3 29063.21c    0.0583380    &
29065.21c    0.0260020
c
c Insl.
m4 14028.21c    0.0080840    &
14029.21c    0.0004093    &
14030.21c    0.0002717    &
```

```
8016.21c    0.0289800    &
13027.21c    0.0039660    &
12024.70c    0.0015798    &
12025.70c    0.0002000    &
12026.70c    0.0002202    &
6012.21c    0.0212000    &
1001.70c    0.0174600    &
7014.70c    0.0034872    &
7015.70c    0.0000128
c
c FW
m5 26054.21c    0.0014943    &
26056.21c    0.0234565    &
26057.21c    0.0005417    &
26058.21c    0.0000721    &
24050.21c    0.0001168    &
24052.21c    0.0022524    &
24053.21c    0.0002554    &
24054.21c    0.0000636    &
74182.21c    0.0000492    &
74183.21c    0.0000265    &
74184.21c    0.0000566    &
74186.21c    0.0000525    &
42092.21c    0.0000001    &
42094.21c    0.0000001    &
42095.21c    0.0000001    &
42096.21c    0.0000001    &
42097.21c    0.0000001    &
42098.21c    0.0000002    &
42100.21c    0.0000001    &
25055.21c    0.0000032    &
6012.21c    0.0000163    &
22046.21c    0.0000022    &
22047.21c    0.0000020    &
22048.21c    0.0000201    &
22049.21c    0.0000015    &
22050.21c    0.0000015    &
28058.21c    0.0000109    &
28060.21c    0.0000042    &
28061.21c    0.0000002    &
28062.21c    0.0000006    &
28064.21c    0.0000001    &
8016.21c    0.0000375    &
14028.21c    0.0000125    &
14029.21c    0.0000006    &
14030.21c    0.0000004    &
23000.21c    0.0000486    &
6012.21c    0.0001030
c
c LiPb
m6 3006.70c    0.0047907    &
3007.70c    0.0005323    &
82204    0.0003640    &
82206.21c    0.0062660    &
82207.21c    0.0057460    &
82208.21c    0.0136240
```

```
c
c SiC
m7 14028.21c    0.04235478    &
14029.21c    0.00214460    &
14030.21c    0.00142361    &
6012.21c    0.04592300
c
c Chanl
m8 26054.21c    0.0025992    &
26056.21c    0.0408017    &
26057.21c    0.0009423    &
26058.21c    0.0001254    &
24050.21c    0.0001726    &
24052.21c    0.0033289    &
24053.21c    0.0003775    &
24054.21c    0.0000940    &
74182.21c    0.0000803    &
74183.21c    0.0000432    &
74184.21c    0.0000924    &
74186.21c    0.0000857    &
23000.21c    0.0001085    &
6012.21c    0.0002297
c
c Blkt
m9 3006.70c    0.0040242    &
3007.70c    0.0004471    &
82204    0.0003058    &
82206.21c    0.0052634    &
82207.21c    0.0048266    &
82208.21c    0.0114442    &
26054.21c    0.0002241    &
26056.21c    0.0035174    &
26057.21c    0.0000812    &
26058.21c    0.0000108    &
24050.21c    0.0000149    &
24052.21c    0.0002870    &
24053.21c    0.0000325    &
24054.21c    0.0000081    &
74182.21c    0.0000069    &
74183.21c    0.0000037    &
74184.21c    0.0000080    &
74186.21c    0.0000074    &
23000.21c    0.0000094    &
6012.21c    0.0000198    &
14028.21c    0.0016942    &
14029.21c    0.0000858    &
14030.21c    0.0000569    &
6012.21c    0.0018369
c
c BW
m10 26054.21c    0.0035851    &
26056.21c    0.0562782    &
26057.21c    0.0012997    &
26058.21c    0.0001730    &
24050.21c    0.0002381    &
24052.21c    0.0045916    &
```

```
24053.21c    0.0005207    &
24054.21c    0.0001296    &
74182.21c    0.0001107    &
74183.21c    0.0000595    &
74184.21c    0.0001275    &
74186.21c    0.0001183    &
23000.21c    0.0001496    &
6012.21c    0.0003168
c
c Shld
m11 26054.21c    0.0039214    &
26056.21c    0.0615582    &
26057.21c    0.0014216    &
26058.21c    0.0001892    &
24050.21c    0.0002679    &
24052.21c    0.0051656    &
24053.21c    0.0005857    &
24054.21c    0.0001458    &
74182.21c    0.0000208    &
74183.21c    0.0000670    &
74184.21c    0.0001434    &
74186.21c    0.0001330    &
23000.21c    0.0001683    &
6012.21c    0.0003564    &
5010.21c    0.0018140    &
5011.21c    0.0077335
c
c MnFld
m12 26054.21c    0.0023303    &
26056.21c    0.0365809    &
26057.21c    0.0008448    &
26058.21c    0.0001124    &
24050.21c    0.0001548    &
24052.21c    0.0029846    &
24053.21c    0.0003384    &
24054.21c    0.0000842    &
74182.21c    0.0000720    &
74183.21c    0.0000387    &
74184.21c    0.0000829    &
74186.21c    0.0000769    &
23000.21c    0.0000972    &
6012.21c    0.0008029    &
3006.70c    0.0010875    &
3007.70c    0.0001208    &
82204    0.0000826    &
82206.21c    0.0014224    &
82207.21c    0.0013043    &
82208.21c    0.0030926    &
14028.21c    0.0005506    &
14029.21c    0.0000279    &
14030.21c    0.0000185
c
c VV
m13 26054.21c    0.0022512    &
26056.21c    0.0353392    &
26057.21c    0.0008161    &
```

```
26058.21c    0.0001086    &
24050.21c    0.0001518    &
24052.21c    0.0029272    &
24053.21c    0.0003319    &
24054.21c    0.0000826    &
74182.21c    0.0000706    &
74183.21c    0.0000380    &
74184.21c    0.0000813    &
74186.21c    0.0000754    &
23000.21c    0.0000954    &
6012.21c    0.0002020    &
5010.21c    0.0005563    &
5011.21c    0.0023716    &
1001.70c    0.0321440    &
8016.21c    0.0160720
c
c Cryost
m14 26054.21c    0.0034965    &
26056.21c    0.0548872    &
26057.21c    0.0012676    &
26058.21c    0.0001687    &
28058.21c    0.0051058    &
28060.21c    0.0019667    &
28061.21c    0.0000855    &
28062.21c    0.0002726    &
28064.21c    0.0000695    &
24050.21c    0.0007000    &
24052.21c    0.0134984    &
24053.21c    0.0015306    &
24054.21c    0.0003810    &
25055.21c    0.0010100    &
6012.21c    0.0001800    &
42092.21c    0.0000237    &
42094.21c    0.0000148    &
42095.21c    0.0000255    &
42096.21c    0.0000267    &
42097.21c    0.0000153    &
42098.21c    0.0000386    &
42100.21c    0.0000154    &
14028.21c    0.0007286    &
14029.21c    0.0000369    &
14030.21c    0.0000245    &
22046.21c    0.0000024    &
22047.21c    0.0000022    &
22048.21c    0.0000221    &
22049.21c    0.0000017    &
22050.21c    0.0000016
c
c Conc
m15 1001.70c    0.0066776    &
8016.21c    0.0374510    &
11023.21c    0.0008951    &
12024.70c    0.0001017    &
12025.70c    0.0000129    &
12026.70c    0.0000142    &
13027.21c    0.0020375    &
```

```
14028.21c    0.0124884    &
14029.21c    0.0006323    &
14030.21c    0.0004198    &
50112.70c    0.0000005    &
50114.70c    0.0000003    &
50115.70c    0.0000002    &
50116.70c    0.0000070    &
50117.70c    0.0000037    &
50118.70c    0.0000116    &
50119.70c    0.0000041    &
50120.70c    0.0000156    &
50122.70c    0.0000022    &
50124.70c    0.0000028    &
19039.70c    0.0005510    &
19040.70c    0.0000001    &
19041.70c    0.0000398    &
20040.21c    0.0024118    &
20042.70c    0.0000161    &
20043.70c    0.0000034    &
20044.70c    0.0000519    &
20046.70c    0.0000001    &
20048.70c    0.0000047    &
26054.21c    0.0005106    &
26056.21c    0.0080158    &
26057.21c    0.0001851    &
26058.21c    0.0000246    &
6012.21c    0.0000796    &
25055.21c    0.0000391
c
c ************************
c Tally Definition
c ************************
fmesh4:n geom=cyl origin=0 0 0 axs=0 0 1 vec=1 0 0
          imesh=175.0 178.8 179.0 179.5 204.5 205.0 205.2 206.7 206.9
                207.4 232.4 232.9 233.1 238.1 268.1 303.1 305.1 333.1 343.1
                345.1 345.3 364.7 392.7 440 445 450 500 550 600 650.0 650.5
          iints=100 2 1 1 13 1 1 1 1 1 13 1 1 3 16 18 1 14 2 1 1 10 15 9 3 2
                25 25 25 25 1
          jmesh=1 jints=1
          kmesh=1 kints=1
          emesh=1.0000E-07 4.1399E-07 5.3158E-07 6.8256E-07 8.7642E-07
               1.1254E-06 1.4450E-06 1.8554E-06 2.3824E-06 3.0590E-06
               3.9279E-06 5.0435E-06 6.4760E-06 8.3153E-06 1.0677E-05
               1.3710E-05 1.7603E-05 2.2603E-05 2.9023E-05 3.7267E-05
               4.7851E-05 6.1442E-05 7.8893E-05 1.0130E-04 1.3007E-04
               1.6702E-04 2.1445E-04 2.7536E-04 3.5380E-04 4.5400E-04
               5.8295E-04 7.4852E-04 9.6112E-04 1.2341E-03 1.5846E-03
               2.0347E-03 2.2487E-03 2.4852E-03 2.6126E-03 2.7465E-03
               3.0354E-03 3.3546E-03 3.7074E-03 4.3107E-03 5.5308E-03
               7.1017E-03 9.1188E-03 1.0595E-02 1.1709E-02 1.5034E-02
               1.9305E-02 2.1875E-02 2.3579E-02 2.4176E-02 2.4788E-02
               2.6058E-02 2.7000E-02 2.8500E-02 3.1828E-02 3.4307E-02
               4.0868E-02 4.6309E-02 5.2475E-02 5.6562E-02 6.7379E-02
               7.2000E-02 7.9500E-02 8.2500E-02 8.6517E-02 9.8037E-02
               1.1109E-01 1.1679E-01 1.2277E-01 1.2907E-01 1.3569E-01
               1.4264E-01 1.4996E-01 1.5764E-01 1.6573E-01 1.7422E-01
```

```
                1.8316E-01 1.9255E-01 2.0242E-01 2.1280E-01 2.2371E-01
                2.3518E-01 2.4724E-01 2.7324E-01 2.8725E-01 2.9452E-01
                2.9720E-01 2.9850E-01 3.0197E-01 3.3373E-01 3.6883E-01
                3.8774E-01 4.0762E-01 4.5049E-01 4.9787E-01 5.2340E-01
                5.5023E-01 5.7844E-01 6.0810E-01 6.3928E-01 6.7206E-01
                7.0651E-01 7.4274E-01 7.8082E-01 8.2085E-01 8.6294E-01
                9.0718E-01 9.6164E-01 1.0026E+00 1.1108E+00 1.1648E+00
                1.2246E+00 1.2873E+00 1.3534E+00 1.4227E+00 1.4957E+00
                1.5724E+00 1.6530E+00 1.7377E+00 1.8268E+00 1.9205E+00
                2.0190E+00 2.1225E+00 2.2313E+00 2.3069E+00 2.3457E+00
                2.3653E+00 2.3852E+00 2.4660E+00 2.5924E+00 2.7253E+00
                2.8650E+00 3.0119E+00 3.1664E+00 3.3287E+00 3.6788E+00
                4.0657E+00 4.4933E+00 4.7237E+00 4.9659E+00 5.2205E+00
                5.4881E+00 5.7695E+00 6.0653E+00 6.3763E+00 6.5924E+00
                6.7032E+00 7.0469E+00 7.4082E+00 7.7880E+00 8.1873E+00
                8.6071E+00 9.0484E+00 9.5123E+00 1.0000E+01 1.0513E+01
                1.1052E+01 1.1618E+01 1.2214E+01 1.2523E+01 1.2840E+01
                1.3499E+01 1.3840E+01 1.4191E+01 1.4550E+01 1.4918E+01
                1.5683E+01 1.6487E+01 1.6905E+01 1.7333E+01 1.9640E+01
fm4 1.3e17
nps 1e5
```

B.4. ARIES-CS Adjoint Photon Transport MCNP Input

```
c ************************
c Source Definition
c ************************
mode p
sdef erg=d5 x=d2 y=d3 z=d4 cel=4
si2 175.364 178.999
sp2 0 1
si3 0.001 34.921
sp3 0 1
si4 0.001 0.999
sp4 0 1
si5 h   1.00E-02 1.00E-01    5.00E-01    1.00E+00    2.00E+00
                 3.00E+00    4.00E+00    5.00E+00    6.00E+00
                 7.00E+00    8.00E+00    9.00E+00    2.00E+01
c 1977 Flux-to-Dose Conversion Factors(uSv/hr) - 12 Group Structure
sp5 d   0.00 1.7858E-02  7.4099E-03  1.6011E-02  2.6292E-02
             3.7253E-02  4.6360E-02  5.4299E-02  6.1909E-02
             6.9265E-02  7.6626E-02  8.4008E-02  1.2955E-01
c
c ************************
c Adjoint Options
c ************************
mgopt a 12
cut:p j 20
c
c ************************
c Material Definition
c ************************
```

```
c Case
m1 26054        0.0026559    &
26056        0.0416916    &
26057        0.0009628    &
26058        0.0001281    &
28058        0.0047729    &
28060        0.0018385    &
28061        0.0000799    &
28062        0.0002548    &
28064        0.0000649    &
24050        0.0004970    &
24052        0.0095838    &
24053        0.0010867    &
24054        0.0002705    &
25055        0.0174895    &
6012        0.0000760    &
42092        0.0000705    &
42094        0.0000439    &
42095        0.0000756    &
42096        0.0000792    &
42097        0.0000454    &
42098        0.0001146    &
42100        0.0000457    &
14028        0.0004469    &
14029        0.0000226    &
14030        0.0000150    &
5010        0.0000017    &
5011        0.0000068    &
2004        0.0010540
c
c WP
m2 26054        0.0005172    &
26056        0.0081189    &
26057        0.0001875    &
26058        0.0000250    &
28058        0.0009295    &
28060        0.0003580    &
28061        0.0000156    &
28062        0.0000496    &
28064        0.0000126    &
24050        0.0000968    &
24052        0.0018663    &
24053        0.0002116    &
24054        0.0000527    &
25055        0.0034059    &
6012        0.0000148    &
42092        0.0000137    &
42094        0.0000086    &
42095        0.0000147    &
42096        0.0000154    &
42097        0.0000088    &
42098        0.0000223    &
42100        0.0000089    &
14028        0.0008954    &
14029        0.0000453    &
14030        0.0000301    &
```

```
5010        0.0000003    &
5011        0.0000013    &
29063        0.0281189    &
29065        0.0125330    &
41093        0.0051789    &
50112        0.0000167    &
50114        0.0000112    &
50115        0.0000059    &
50116        0.0002510    &
50117        0.0001326    &
50118        0.0004181    &
50119        0.0001481    &
50120        0.0005626    &
50122        0.0000799    &
50124        0.0000999    &
8016        0.0028980    &
13027        0.0003966    &
12024        0.0001580    &
12025        0.0000200    &
12026        0.0000220    &
6012        0.0021200    &
1001        0.0017460    &
7014        0.0003487    &
7015        0.0000013    &
2004        0.0022134
c
c Cu
m3 29063        0.0583380    &
29065        0.0260020
c
c Insl.
m4 14028        0.0080840    &
14029        0.0004093    &
14030        0.0002717    &
8016        0.0289800    &
13027        0.0039660    &
12024        0.0015798    &
12025        0.0002000    &
12026        0.0002202    &
6012        0.0212000    &
1001        0.0174600    &
7014        0.0034872    &
7015        0.0000128
c
c FW
m5 26054        0.0014943    &
26056        0.0234565    &
26057        0.0005417    &
26058        0.0000721    &
24050        0.0001168    &
24052        0.0022524    &
24053        0.0002554    &
24054        0.0000636    &
74182        0.0000492    &
74183        0.0000265    &
74184        0.0000566    &
```

```
74186        0.0000525    &
42092        0.0000001    &
42094        0.0000001    &
42095        0.0000001    &
42096        0.0000001    &
42097        0.0000001    &
42098        0.0000002    &
42100        0.0000001    &
25055        0.0000032    &
6012        0.0000163    &
22046        0.0000022    &
22047        0.0000020    &
22048        0.0000201    &
22049        0.0000015    &
22050        0.0000015    &
28058        0.0000109    &
28060        0.0000042    &
28061        0.0000002    &
28062        0.0000006    &
28064        0.0000001    &
8016        0.0000375    &
14028        0.0000125    &
14029        0.0000006    &
14030        0.0000004    &
23000        0.0000486    &
6012        0.0001030
c
c LiPb
m6 3006        0.0047907    &
3007        0.0005323    &
82204    0.0003640    &
82206        0.0062660    &
82207        0.0057460    &
82208        0.0136240
c
c SiC
m7 14028        0.04235478    &
14029        0.00214460    &
14030        0.00142361    &
6012        0.04592300
c
c Chanl
m8 26054        0.0025992    &
26056        0.0408017    &
26057        0.0009423    &
26058        0.0001254    &
24050        0.0001726    &
24052        0.0033289    &
24053        0.0003775    &
24054        0.0000940    &
74182        0.0000803    &
74183        0.0000432    &
74184        0.0000924    &
74186        0.0000857    &
23000        0.0001085    &
6012        0.0002297
```

```
c
c Blkt
m9 3006        0.0040242    &
3007        0.0004471    &
82204    0.0003058    &
82206        0.0052634    &
82207        0.0048266    &
82208        0.0114442    &
26054        0.0002241    &
26056        0.0035174    &
26057        0.0000812    &
26058        0.0000108    &
24050        0.0000149    &
24052        0.0002870    &
24053        0.0000325    &
24054        0.0000081    &
74182        0.0000069    &
74183        0.0000037    &
74184        0.0000080    &
74186        0.0000074    &
23000        0.0000094    &
6012        0.0000198    &
14028        0.0016942    &
14029        0.0000858    &
14030        0.0000569    &
6012        0.0018369
c
c BW
m10 26054        0.0035851    &
26056        0.0562782    &
26057        0.0012997    &
26058        0.0001730    &
24050        0.0002381    &
24052        0.0045916    &
24053        0.0005207    &
24054        0.0001296    &
74182        0.0001107    &
74183        0.0000595    &
74184        0.0001275    &
74186        0.0001183    &
23000        0.0001496    &
6012        0.0003168
c
c Shld
m11 26054        0.0039214    &
26056        0.0615582    &
26057        0.0014216    &
26058        0.0001892    &
24050        0.0002679    &
24052        0.0051656    &
24053        0.0005857    &
24054        0.0001458    &
74182        0.0000208    &
74183        0.0000670    &
74184        0.0001434    &
74186        0.0001330    &
```

```
23000        0.0001683    &
6012        0.0003564    &
5010        0.0018140    &
5011        0.0077335
c
c MnFld
m12 26054        0.0023303    &
26056        0.0365809    &
26057        0.0008448    &
26058        0.0001124    &
24050        0.0001548    &
24052        0.0029846    &
24053        0.0003384    &
24054        0.0000842    &
74182        0.0000720    &
74183        0.0000387    &
74184        0.0000829    &
74186        0.0000769    &
23000        0.0000972    &
6012        0.0008029    &
3006        0.0010875    &
3007        0.0001208    &
82204    0.0000826    &
82206        0.0014224    &
82207        0.0013043    &
82208        0.0030926    &
14028        0.0005506    &
14029        0.0000279    &
14030        0.0000185
c
c VV
m13 26054        0.0022512    &
26056        0.0353392    &
26057        0.0008161    &
26058        0.0001086    &
24050        0.0001518    &
24052        0.0029272    &
24053        0.0003319    &
24054        0.0000826    &
74182        0.0000706    &
74183        0.0000380    &
74184        0.0000813    &
74186        0.0000754    &
23000        0.0000954    &
6012        0.0002020    &
5010        0.0005563    &
5011        0.0023716    &
1001        0.0321440    &
8016        0.0160720
c
c Cryost
m14 26054        0.0034965    &
26056        0.0548872    &
26057        0.0012676    &
26058        0.0001687    &
28058        0.0051058    &
```

```
28060        0.0019667    &
28061        0.0000855    &
28062        0.0002726    &
28064        0.0000695    &
24050        0.0007000    &
24052        0.0134984    &
24053        0.0015306    &
24054        0.0003810    &
25055        0.0010100    &
6012        0.0001800    &
42092        0.0000237    &
42094        0.0000148    &
42095        0.0000255    &
42096        0.0000267    &
42097        0.0000153    &
42098        0.0000386    &
42100        0.0000154    &
14028        0.0007286    &
14029        0.0000369    &
14030        0.0000245    &
22046        0.0000024    &
22047        0.0000022    &
22048        0.0000221    &
22049        0.0000017    &
22050        0.0000016
c
c Conc
m15 1001        0.0066776    &
8016        0.0374510    &
11023        0.0008951    &
12024        0.0001017    &
12025        0.0000129    &
12026        0.0000142    &
13027        0.0020375    &
14028        0.0124884    &
14029        0.0006323    &
14030        0.0004198    &
50112        0.0000005    &
50114        0.0000003    &
50115        0.0000002    &
50116        0.0000070    &
50117        0.0000037    &
50118        0.0000116    &
50119        0.0000041    &
50120        0.0000156    &
50122        0.0000022    &
50124        0.0000028    &
19039        0.0005510    &
19040        0.0000001    &
19041        0.0000398    &
20040        0.0024118    &
20042        0.0000161    &
20043        0.0000034    &
20044        0.0000519    &
20046        0.0000001    &
20048        0.0000047    &
```

```
26054        0.0005106    &
26056        0.0080158    &
26057        0.0001851    &
26058        0.0000246    &
6012        0.0000796    &
25055        0.0000391
c
c ************************
c Tally Definition
c ************************
fmesh4:p geom=cyl origin=0 0 0
         imesh=175.0 178.8 179.0 179.5 204.5 205.0 205.2 206.7 206.9
               207.4 232.4 232.9 233.1 238.1 268.1 303.1 305.1 333.1 343.1
               345.1 345.3 364.7 392.7 440 445 450 500 550 600 650.0 650.5
          iints=100 2 1 1 13 1 1 1 1 1 13 1 1 3 16 18 1 14 2 1 1 10 15 9 3 2
                25 25 25 25 1
          jmesh=1 jints=1
          kmesh=1 kints=1
          emesh = 1.00E-01    5.00E-01    1.00E+00    2.00E+00
                  3.00E+00    4.00E+00    5.00E+00    6.00E+00
                  7.00E+00    8.00E+00    9.00E+00    2.00E+01
fm4 140.957 $ 224.812 x 0.627
nps 1e6
```

B.5. ARIES-CS Forward Activation ALARA Input

```
##  ARIES-CS Biological Dose Calculation

geometry cylindrical

dimension     r 0.0
       100    175
       2      178.8
       1      179
       1      179.5
       13     204.5
       1      205
       1      205.2
       1      206.7
       1      206.9
       1      207.4
       13     232.4
       1      232.9
       1      233.1
       3      238.1
       16     268.1
       18     303.1
       1      305.1
       14     333.1
       2      343.1
       1      345.1
       1      345.3
```

```
       10     364.7
       15     392.7
       9      440
       3      445
       2      450
       25     500
       25     550
       25     600
       25     650
       1      650.5
end

mat_loading
       zone1  void
       zone2  FW
       zone3  void
       zone4  SiC
       zone5  Blanket
       zone6  SiC
       zone7  void
       zone8  Channel
       zone9  void
       zone10 SiC
       zone11 Blanket
       zone12 SiC
       zone13 void
       zone14 back_wall
       zone15 Shield
       zone16 Manifolds
       zone17 void
       zone18 VV
       zone19 void
       zone20 coil_case
       zone21 poly
       zone22 winding_pack
       zone23 strong_back
       zone24 void
       zone25 cryostat
       zone26 void
       zone27 bioshield
       zone28 bioshield
       zone29 bioshield
       zone30 bioshield
       zone31 void
end

mixture       FW
      material      ODS-MF82H     1.0    .08
      material      MF82H         1.0    .26
end

mixture       SiC
      material      si_c          .95    1
end

mixture       Blanket
```

```
       material      MF82H         1.0    .05
       material      si_c          .95    .04
end

mixture       Channel
       material      MF82H         1.0    .58
end

mixture       back_wall
       material      MF82H         1.0    .80
end

mixture       Shield
       material      MF82H         1.0    .15
       material      B_MF82H       1.0    .75
end

mixture       Manifolds
       material      MF82H         1.0    .52
       material      si_c          .95    .013
end

mixture       VV
       material      MF82H         1.0    .28
       material      B_MF82H       1.0    .23
end

mixture       coil_case
       material      JK2LB         1.0    .95
end

mixture       poly
       material      GFFpoly       1.0    1
end

mixture       winding_pack
       material      JK2LB         1.0    .185
       element       cu            1.0    .482
       material      Nb3Sn         1.0    .128
       material      GFFpoly       1.0    .10
end

mixture       strong_back
       material      JK2LB         1.0    .95
end

mixture       cryostat
       material      JK2LB         1.0    1
end

mixture       bioshield
       material      Ordinary_Concrete   1.0    .85
       material      Mild_Steel          1.0    .10
end

material_lib  ARIES_matlib
```

```
element_lib   ARIES_elelib
data_library alaralib      FENDL2

flux flux_1 forflux_mcnp 1.0 0 default

impurity      5e-6   1e-3

cooling
       .01    s
       1      s
       1      m
       100    s
       10     m
       1      h
       6      h
       1      d
       2      d
       7      d
       30     d
       45     d
       60     d
       .5     y
       1      y
       2      y
       5      y
       10     y
       25     y
       50     y
       75     y
       100    y
end

dump_file     dump.file

#output interval
#       units Bq cm3
#       photon_source FENDL2
#       phtn-src-part 42 1e4 2e4 3e4 4.5e4  6e4
#          7e4  7.5e4  1e5  1.5e5  2e5  3e5 4e5  4.5e5
#          5.1e5  5.12e5  6e5  7e5  8e5  1e6  1.33e6
#         1.34e6  1.5e6  1.66e6  2e6  2.5e6  3e6  3.5e6
#         4e6  4.5e6  5e6  5.5e6  6e6  6.5e6  7e6  7.5e6
#           8e6  1e7  1.2e7  1.4e7  2e7  3e7  5e7
#       folded_dose FENDL2 224.812
#       adjflux_part 42 1e4 2e4
#          3e4  4.5e4  6e4  7e4  7.5e4  1e5  1.5e5  2e5  3e5
#          4e5  4.5e5  5.1e5  5.12e5  6e5  7e5  8e5  1e6  1.33e6
#          1.34e6  1.5e6  1.66e6  2e6  2.5e6  3e6  3.5e6
#          4e6  4.5e6  5e6  5.5e6  6e6  6.5e6  7e6  7.5e6  8e6
#          1e7  1.2e7  1.4e7  2e7  3e7  5e7
#end

output interval
       units Bq cm3
       photon_source FENDL2
       phtn-src-mcnp 12 1e5 5e5 1e6 2e6 3e6 4e6
```

```
                        5e6 6e6 7e6 8e6 9e6 2e7
       folded_dose FENDL2 224.812
       adjflux_mcnp 12 1e5 5e5 1e6 2e6 3e6 4e6
                       5e6 6e6 7e6 8e6 9e6 2e7
end

schedule      total
       .85    y      flux_1 3.9FPYpulsed  0  s
end

pulsehistory  3.9FPYpulsed
       5      .15    y
end

truncation    1e-7
```

C. PPPL ST-FNSF Inputs

C.1. ST-FNSF Forward Neutron Transport MCNP Input

```
PPPL STFNSF - 3/2012 Amir Jaber
c *************************
c Source Definition
c *************************
mode n
sdef erg=14.1 x=d2 y=d3 z=d4 cel=d5
si2 53.44 254.14
sp2 0 1
si3 0.001 149.38
sp3 0 1
si4 0.001 300.9
sp4 0 1
si5 l 3 2 1
sp5 d 0.045 0.325 0.63
c
c ************************
c Material Definitions
c ************************
c
c Breeding Zone
c LiPb: 90% Li-6 (Li 15.7% Pb 84.3% a/o)
m1 3006.21c  0.1413    &
   3007.21c  0.0157    &
  82204      0.0118    &
  82206.21c  0.2032    &
  82207.21c  0.1863    &
  82208.21c  0.4417
c
c Outer Shield
c (80% ODSFS, 20% He)
```

```
m2 26054.21c    0.00329097    &
26056.21c    0.05166117    &
26057.21c    0.00119308    &
26058.21c    0.00015878    &
24050.21c    0.00039418    &
24052.21c    0.00760134    &
24053.21c    0.00086193    &
24054.21c    0.00021455    &
74182.21c    0.00013203    &
74183.21c    0.00007100    &
74184.21c    0.00015198    &
74186.21c    0.00014099    &
42092.21c    0.00000119    &
42094.21c    0.00000074    &
42095.21c    0.00000127    &
42096.21c    0.00000133    &
42097.21c    0.00000076    &
42098.21c    0.00000193    &
42100.21c    0.00000077    &
25055.21c    0.00003200    &
6012.21c     0.00016320    &
22046.21c    0.00002176    &
22047.21c    0.00001986    &
22048.21c    0.00020074    &
22049.21c    0.00001496    &
22050.21c    0.00001469    &
28058.21c    0.00010892    &
28060.21c    0.00004196    &
28061.21c    0.00000182    &
28062.21c    0.00000581    &
28064.21c    0.00000148    &
8016.21c     0.00037520    &
14028.21c    0.00012543    &
14029.21c    0.00000635    &
14030.21c    0.00000422
c
c Divertor Plates
c (28% W alloy, 8% W, 11% ODSFS, 53% He)
m3 6012.21c  0.00002244 &
  26054.21c  0.00045251 &
  26056.21c  0.00710341 &
  26057.21c  0.00016405 &
  26058.21c  0.00002183 &
  24050.21c  0.00005420 &
  24052.21c  0.00104518 &
  24053.21c  0.00011852 &
  24054.21c  0.00002950 &
  74182.21c  0.00001815 &
  74183.21c  0.00000976 &
  74184.21c  0.00002090 &
  74186.21c  0.00001939 &
  42092.21c  0.00000016 &
  42094.21c  0.00000010 &
  42095.21c  0.00000018 &
  42096.21c  0.00000018 &
  42097.21c  0.00000011 &
```

```
   42098.21c  0.00000027 &
   42100.21c  0.00000011 &
   25055.21c  0.00000440 &
   22046.21c  0.00000299 &
   22047.21c  0.00000273 &
   22048.21c  0.00002760 &
   22049.21c  0.00000206 &
   22050.21c  0.00000202 &
   28058.21c  0.00001498 &
   28060.21c  0.00000577 &
   28061.21c  0.00000025 &
   28062.21c  0.00000080 &
   28064.21c  0.00000020 &
    8016.21c  0.00005159 &
   14028.21c  0.00001725 &
   14029.21c  0.00000087 &
   14030.21c  0.00000058
c
c IB and OB FW
c (8% ODSFS, 27% MF82H, 65% He)
m4 26054.21c  0.00153906 &
    26056.21c  0.02416002 &
    26057.21c  0.00055796 &
    26058.21c  0.00007425 &
    24050.21c  0.00011978 &
    24052.21c  0.00230981 &
    24053.21c  0.00026191 &
    24054.21c  0.00006520 &
    74182.21c  0.00005057 &
    74183.21c  0.00002720 &
    74184.21c  0.00005822 &
    74186.21c  0.00005401 &
    42092.21c  0.00000012 &
    42094.21c  0.00000007 &
    42095.21c  0.00000013 &
    42096.21c  0.00000013 &
    42097.21c  0.00000008 &
    42098.21c  0.00000019 &
    42100.21c  0.00000008 &
    25055.21c  0.00000320 &
     6012.21c  0.00012324 &
    23000      0.00005049 &
    22046.21c  0.00000218 &
    22047.21c  0.00000199 &
    22048.21c  0.00002007 &
    22049.21c  0.00000150 &
    22050.21c  0.00000147 &
    28058.21c  0.00001089 &
    28060.21c  0.00000420 &
    28061.21c  0.00000018 &
    28062.21c  0.00000058 &
    28064.21c  0.00000015 &
     8016.21c  0.00003752 &
    14028.21c  0.00001254 &
    14029.21c  0.00000064 &
    14030.21c  0.00000042
```

```
c
c OB blkt I back
c (80% MF82H, 20% He)
m5 6012.21c  0.00031680 &
  26054.21c  0.00358509 &
  26056.21c  0.05627823 &
  26057.21c  0.00129971 &
  26058.21c  0.00017297 &
  24050.21c  0.00023811 &
  24052.21c  0.00459164 &
  24053.21c  0.00052065 &
  24054.21c  0.00012960 &
  74182.21c  0.00011073 &
  74183.21c  0.00005955 &
  74184.21c  0.00012747 &
  74186.21c  0.00011825 &
  23000      0.00014960
c
c VV (90% FS)
m6 26054.21c    0.00403323    &
 26056.21c    0.06331301    &
 26057.21c    0.00146217    &
 26058.21c    0.00019459    &
 24050.21c    0.00026787    &
 24052.21c    0.00516559    &
 24053.21c    0.00058574    &
 24054.21c    0.00014580    &
 74182.21c    0.00012457    &
 74183.21c    0.00006699    &
 74184.21c    0.00014340    &
 74186.21c    0.00013303    &
 23000    0.00016830    &
 6012.21c    0.00035640
c
c VV (27% FS 73% LiPb)
c m6 3006.21c    0.00311221    &
c 3007.21c    0.00034580    &
c 82204    0.00025989    &
c 82206.21c    0.00447390    &
c 82207.21c    0.00410262    &
c 82208.21c    0.00972748    &
c 26054.21c    0.00120997    &
c 26056.21c    0.01899390    &
c 26057.21c    0.00043865    &
c 26058.21c    0.00005838    &
c 24050.21c    0.00008036    &
c 24052.21c    0.00154968    &
c 24053.21c    0.00017572    &
c 24054.21c    0.00004374    &
c 74182.21c    0.00003737    &
c 74183.21c    0.00002010    &
c 74184.21c    0.00004302    &
c 74186.21c    0.00003991    &
c 23000    0.00005049    &
c 6012.21c    0.00010692
c
```

```
c CenterStack - Bottom (10% Water, 90% CuCrZr)
m7 1001.21c    0.006543    &
24050.21c    0.00002994    &
24052.21c    0.00057736    &
24053.21c    0.00006547    &
24054.21c    0.00001630    &
40090.70c    0.00002963    &
40091.70c    0.00000646    &
40092.70c    0.00000988    &
40094.70c    0.00000999    &
40096.70c    0.00000161    &
8016.21c    0.00336060    &
27059.21c    0.00004864    &
14028.21c    0.00001726    &
14029.21c    0.00000087    &
14030.21c    0.00000058    &
29063.21c    0.05149942    &
29065.21c    0.02295398
c
c  CenterStack - Top (6.6% Water, 93.4% CuCrZr)
m8 1001.21c    0.00431838    &
24050.21c    0.00003107    &
24052.21c    0.00059917    &
24053.21c    0.00006794    &
24054.21c    0.00001691    &
40090.70c    0.00003075    &
40091.70c    0.00000671    &
40092.70c    0.00001025    &
40094.70c    0.00001037    &
40096.70c    0.00000167    &
8016.21c    0.00225184    &
27059.21c    0.00005047    &
14028.21c    0.00001791    &
14029.21c    0.00000091    &
14030.21c    0.00000060    &
29063.21c    0.05344495    &
29065.21c    0.02382113
c
c Cooling Channels (58% ODS)
m9 26054.21c    0.00259919    &
26056.21c    0.04080172    &
26057.21c    0.00094229    &
26058.21c    0.00012540    &
24050.21c    0.00017263    &
24052.21c    0.00332894    &
24053.21c    0.00037747    &
24054.21c    0.00009396    &
74182.21c    0.00008028    &
74183.21c    0.00004317    &
74184.21c    0.00009242    &
74186.21c    0.00008573    &
23000    0.00010846    &
6012.21c    0.00022968
c
c Flow Channel Inserts (46% SiC)
m10 14028.21c    0.02050863    &
```

```
14029.21c    0.00103844    &
14030.21c    0.00068933    &
6012.21c    0.02223640
c
c Stabilizing Shell (100% W-TiC)
m11 74182.21c    0.01687049    &
74183.21c    0.00907221    &
74184.21c    0.01942090    &
74186.21c    0.01801640
c
c ACTUAL OB-I Homogenization
m15 3006.21c    0.00337763    &
3007.21c    0.00037529    &
82204    0.00028206    &
82206.21c    0.00485545    &
82207.21c    0.00445251    &
82208.21c    0.01055708    &
14028.21c    0.00153176    &
14029.21c    0.00007756    &
14030.21c    0.00005149    &
6012.21c    0.00168526    &
26054.21c    0.00027672    &
26056.21c    0.00434393    &
26057.21c    0.00010032    &
26058.21c    0.00001335    &
24050.21c    0.00001838    &
24052.21c    0.00035441    &
24053.21c    0.00004019    &
24054.21c    0.00001000    &
74182.21c    0.00000855    &
74183.21c    0.00000460    &
74184.21c    0.00000984    &
74186.21c    0.00000913    &
23000    0.00001155
c
c ACTUAL OB-II Homogenization
m16 3006.21c    0.00308174    &
3007.21c    0.00034242    &
82204    0.00025735    &
82206.21c    0.00443011    &
82207.21c    0.00406246    &
82208.21c    0.00963226    &
14028.21c    0.00123805    &
14029.21c    0.00006269    &
14030.21c    0.00004161    &
6012.21c    0.00140557    &
26054.21c    0.00071545    &
26056.21c    0.01123108    &
26057.21c    0.00025937    &
26058.21c    0.00003452    &
24050.21c    0.00004752    &
24052.21c    0.00091632    &
24053.21c    0.00010390    &
24054.21c    0.00002586    &
74182.21c    0.00002210    &
74183.21c    0.00001188    &
```

```
74184.21c    0.00002544    &
74186.21c    0.00002360    &
23000    0.00002985
c
c ************************
c Tally Definitions
c ************************
fc14 Neutron Flux Tally at Detector
e14 1.0000E-07 4.1399E-07 5.3158E-07 6.8256E-07 8.7642E-07
               1.1254E-06 1.4450E-06 1.8554E-06 2.3824E-06 3.0590E-06
               3.9279E-06 5.0435E-06 6.4760E-06 8.3153E-06 1.0677E-05
               1.3710E-05 1.7603E-05 2.2603E-05 2.9023E-05 3.7267E-05
               4.7851E-05 6.1442E-05 7.8893E-05 1.0130E-04 1.3007E-04
               1.6702E-04 2.1445E-04 2.7536E-04 3.5380E-04 4.5400E-04
               5.8295E-04 7.4852E-04 9.6112E-04 1.2341E-03 1.5846E-03
               2.0347E-03 2.2487E-03 2.4852E-03 2.6126E-03 2.7465E-03
               3.0354E-03 3.3546E-03 3.7074E-03 4.3107E-03 5.5308E-03
               7.1017E-03 9.1188E-03 1.0595E-02 1.1709E-02 1.5034E-02
               1.9305E-02 2.1875E-02 2.3579E-02 2.4176E-02 2.4788E-02
               2.6058E-02 2.7000E-02 2.8500E-02 3.1828E-02 3.4307E-02
               4.0868E-02 4.6309E-02 5.2475E-02 5.6562E-02 6.7379E-02
               7.2000E-02 7.9500E-02 8.2500E-02 8.6517E-02 9.8037E-02
               1.1109E-01 1.1679E-01 1.2277E-01 1.2907E-01 1.3569E-01
               1.4264E-01 1.4996E-01 1.5764E-01 1.6573E-01 1.7422E-01
               1.8316E-01 1.9255E-01 2.0242E-01 2.1280E-01 2.2371E-01
               2.3518E-01 2.4724E-01 2.7324E-01 2.8725E-01 2.9452E-01
               2.9720E-01 2.9850E-01 3.0197E-01 3.3373E-01 3.6883E-01
               3.8774E-01 4.0762E-01 4.5049E-01 4.9787E-01 5.2340E-01
               5.5023E-01 5.7844E-01 6.0810E-01 6.3928E-01 6.7206E-01
               7.0651E-01 7.4274E-01 7.8082E-01 8.2085E-01 8.6294E-01
               9.0718E-01 9.6164E-01 1.0026E+00 1.1108E+00 1.1648E+00
               1.2246E+00 1.2873E+00 1.3534E+00 1.4227E+00 1.4957E+00
               1.5724E+00 1.6530E+00 1.7377E+00 1.8268E+00 1.9205E+00
               2.0190E+00 2.1225E+00 2.2313E+00 2.3069E+00 2.3457E+00
               2.3653E+00 2.3852E+00 2.4660E+00 2.5924E+00 2.7253E+00
               2.8650E+00 3.0119E+00 3.1664E+00 3.3287E+00 3.6788E+00
               4.0657E+00 4.4933E+00 4.7237E+00 4.9659E+00 5.2205E+00
               5.4881E+00 5.7695E+00 6.0653E+00 6.3763E+00 6.5924E+00
               6.7032E+00 7.0469E+00 7.4082E+00 7.7880E+00 8.1873E+00
               8.6071E+00 9.0484E+00 9.5123E+00 1.0000E+01 1.0513E+01
               1.1052E+01 1.1618E+01 1.2214E+01 1.2523E+01 1.2840E+01
               1.3499E+01 1.3840E+01 1.4191E+01 1.4550E+01 1.4918E+01
               1.5683E+01 1.6487E+01 1.6905E+01 1.7333E+01 1.9640E+01
fm14 2.83e18 $ 160 MW
c
fmesh24:n geom=xyz origin=0 0 0
          imesh=420 iints=20
          jmesh=247 jints=20
          kmesh=407 kints=20
          emesh=1.0000E-07 4.1399E-07 5.3158E-07 6.8256E-07 8.7642E-07
               1.1254E-06 1.4450E-06 1.8554E-06 2.3824E-06 3.0590E-06
               3.9279E-06 5.0435E-06 6.4760E-06 8.3153E-06 1.0677E-05
               1.3710E-05 1.7603E-05 2.2603E-05 2.9023E-05 3.7267E-05
               4.7851E-05 6.1442E-05 7.8893E-05 1.0130E-04 1.3007E-04
               1.6702E-04 2.1445E-04 2.7536E-04 3.5380E-04 4.5400E-04
               5.8295E-04 7.4852E-04 9.6112E-04 1.2341E-03 1.5846E-03
```

```
                2.0347E-03 2.2487E-03 2.4852E-03 2.6126E-03 2.7465E-03
                3.0354E-03 3.3546E-03 3.7074E-03 4.3107E-03 5.5308E-03
                7.1017E-03 9.1188E-03 1.0595E-02 1.1709E-02 1.5034E-02
                1.9305E-02 2.1875E-02 2.3579E-02 2.4176E-02 2.4788E-02
                2.6058E-02 2.7000E-02 2.8500E-02 3.1828E-02 3.4307E-02
                4.0868E-02 4.6309E-02 5.2475E-02 5.6562E-02 6.7379E-02
                7.2000E-02 7.9500E-02 8.2500E-02 8.6517E-02 9.8037E-02
                1.1109E-01 1.1679E-01 1.2277E-01 1.2907E-01 1.3569E-01
                1.4264E-01 1.4996E-01 1.5764E-01 1.6573E-01 1.7422E-01
                1.8316E-01 1.9255E-01 2.0242E-01 2.1280E-01 2.2371E-01
                2.3518E-01 2.4724E-01 2.7324E-01 2.8725E-01 2.9452E-01
                2.9720E-01 2.9850E-01 3.0197E-01 3.3373E-01 3.6883E-01
                3.8774E-01 4.0762E-01 4.5049E-01 4.9787E-01 5.2340E-01
                5.5023E-01 5.7844E-01 6.0810E-01 6.3928E-01 6.7206E-01
                7.0651E-01 7.4274E-01 7.8082E-01 8.2085E-01 8.6294E-01
                9.0718E-01 9.6164E-01 1.0026E+00 1.1108E+00 1.1648E+00
                1.2246E+00 1.2873E+00 1.3534E+00 1.4227E+00 1.4957E+00
                1.5724E+00 1.6530E+00 1.7377E+00 1.8268E+00 1.9205E+00
                2.0190E+00 2.1225E+00 2.2313E+00 2.3069E+00 2.3457E+00
                2.3653E+00 2.3852E+00 2.4660E+00 2.5924E+00 2.7253E+00
                2.8650E+00 3.0119E+00 3.1664E+00 3.3287E+00 3.6788E+00
                4.0657E+00 4.4933E+00 4.7237E+00 4.9659E+00 5.2205E+00
                5.4881E+00 5.7695E+00 6.0653E+00 6.3763E+00 6.5924E+00
                6.7032E+00 7.0469E+00 7.4082E+00 7.7880E+00 8.1873E+00
                8.6071E+00 9.0484E+00 9.5123E+00 1.0000E+01 1.0513E+01
                1.1052E+01 1.1618E+01 1.2214E+01 1.2523E+01 1.2840E+01
                1.3499E+01 1.3840E+01 1.4191E+01 1.4550E+01 1.4918E+01
                1.5683E+01 1.6487E+01 1.6905E+01 1.7333E+01 1.9640E+01
fm24 2.83e18 $ 160 MW
c
nps 1e8
lost 200000 200000
prdmp 1e7 1e7
```

C.2. ST-FNSF Adjoint Photon Transport MCNP Input

```
PPPL STFNSF - 3/2012 Amir Jaber
c ************************
c Source Definition
c ************************
mode p
sdef erg=d5 x=d2 y=d3 z=d4 cel=899
si2 305.01 310.8
sp2 0 1
si3 68.8 71.9
sp3 0 1
si4 0.001 39.999
sp4 0 1
si5 h   1.00E-02 1.00E-01    5.00E-01    1.00E+00    2.00E+00
                 3.00E+00    4.00E+00    5.00E+00    6.00E+00
                 7.00E+00    8.00E+00    9.00E+00    2.00E+01
c 1977 Flux-to-Dose Conversion Factors(uSv/hr) - 12 Group Structure
sp5 d   0.00 1.7858E-02  7.4099E-03  1.6011E-02  2.6292E-02
```

```
             3.7253E-02  4.6360E-02  5.4299E-02  6.1909E-02
             6.9265E-02  7.6626E-02  8.4008E-02  1.2955E-01
c
c ************************
c Adjoint Options
c ************************
mgopt a 12
cut:p j 20
c
c ************************
c Material Definitions
c ************************
c
c Breeding Zone
c LiPb: 90% Li-6 (Li 15.7% Pb 84.3% a/o)
m1 3006.21c  0.1413    &
   3007.21c  0.0157    &
  82204      0.0118    &
  82206.21c  0.2032    &
  82207.21c  0.1863    &
  82208.21c  0.4417
c
c Outer Shield
c (80% ODSFS, 20% He)
m2 26054.21c    0.00329097    &
26056.21c    0.05166117    &
26057.21c    0.00119308    &
26058.21c    0.00015878    &
24050.21c    0.00039418    &
24052.21c    0.00760134    &
24053.21c    0.00086193    &
24054.21c    0.00021455    &
74182.21c    0.00013203    &
74183.21c    0.00007100    &
74184.21c    0.00015198    &
74186.21c    0.00014099    &
42092.21c    0.00000119    &
42094.21c    0.00000074    &
42095.21c    0.00000127    &
42096.21c    0.00000133    &
42097.21c    0.00000076    &
42098.21c    0.00000193    &
42100.21c    0.00000077    &
25055.21c    0.00003200    &
6012.21c     0.00016320    &
22046.21c    0.00002176    &
22047.21c    0.00001986    &
22048.21c    0.00020074    &
22049.21c    0.00001496    &
22050.21c    0.00001469    &
28058.21c    0.00010892    &
28060.21c    0.00004196    &
28061.21c    0.00000182    &
28062.21c    0.00000581    &
28064.21c    0.00000148    &
8016.21c     0.00037520    &
```

```
14028.21c    0.00012543    &
14029.21c    0.00000635    &
14030.21c    0.00000422
c
c Divertor Plates
c (28% W alloy, 8% W, 11% ODSFS, 53% He)
m3 6012.21c  0.00002244 &
  26054.21c  0.00045251 &
  26056.21c  0.00710341 &
  26057.21c  0.00016405 &
  26058.21c  0.00002183 &
  24050.21c  0.00005420 &
  24052.21c  0.00104518 &
  24053.21c  0.00011852 &
  24054.21c  0.00002950 &
  74182.21c  0.00001815 &
  74183.21c  0.00000976 &
  74184.21c  0.00002090 &
  74186.21c  0.00001939 &
  42092.21c  0.00000016 &
  42094.21c  0.00000010 &
  42095.21c  0.00000018 &
  42096.21c  0.00000018 &
  42097.21c  0.00000011 &
  42098.21c  0.00000027 &
  42100.21c  0.00000011 &
  25055.21c  0.00000440 &
  22046.21c  0.00000299 &
  22047.21c  0.00000273 &
  22048.21c  0.00002760 &
  22049.21c  0.00000206 &
  22050.21c  0.00000202 &
  28058.21c  0.00001498 &
  28060.21c  0.00000577 &
  28061.21c  0.00000025 &
  28062.21c  0.00000080 &
  28064.21c  0.00000020 &
   8016.21c  0.00005159 &
  14028.21c  0.00001725 &
  14029.21c  0.00000087 &
  14030.21c  0.00000058
c
c IB and OB FW
c (8% ODSFS, 27% MF82H, 65% He)
m4 26054.21c  0.00153906 &
   26056.21c  0.02416002 &
   26057.21c  0.00055796 &
   26058.21c  0.00007425 &
   24050.21c  0.00011978 &
   24052.21c  0.00230981 &
   24053.21c  0.00026191 &
   24054.21c  0.00006520 &
   74182.21c  0.00005057 &
   74183.21c  0.00002720 &
   74184.21c  0.00005822 &
   74186.21c  0.00005401 &
```

```
   42092.21c  0.00000012 &
   42094.21c  0.00000007 &
   42095.21c  0.00000013 &
   42096.21c  0.00000013 &
   42097.21c  0.00000008 &
   42098.21c  0.00000019 &
   42100.21c  0.00000008 &
   25055.21c  0.00000320 &
    6012.21c  0.00012324 &
   23000      0.00005049 &
   22046.21c  0.00000218 &
   22047.21c  0.00000199 &
   22048.21c  0.00002007 &
   22049.21c  0.00000150 &
   22050.21c  0.00000147 &
   28058.21c  0.00001089 &
   28060.21c  0.00000420 &
   28061.21c  0.00000018 &
   28062.21c  0.00000058 &
   28064.21c  0.00000015 &
    8016.21c  0.00003752 &
   14028.21c  0.00001254 &
   14029.21c  0.00000064 &
   14030.21c  0.00000042
c
c OB blkt I back
c (80% MF82H, 20% He)
m5 6012.21c  0.00031680 &
  26054.21c  0.00358509 &
  26056.21c  0.05627823 &
  26057.21c  0.00129971 &
  26058.21c  0.00017297 &
  24050.21c  0.00023811 &
  24052.21c  0.00459164 &
  24053.21c  0.00052065 &
  24054.21c  0.00012960 &
  74182.21c  0.00011073 &
  74183.21c  0.00005955 &
  74184.21c  0.00012747 &
  74186.21c  0.00011825 &
  23000      0.00014960
c
c VV (90% FS)
m6 26054.21c    0.00403323    &
 26056.21c    0.06331301    &
 26057.21c    0.00146217    &
 26058.21c    0.00019459    &
 24050.21c    0.00026787    &
 24052.21c    0.00516559    &
 24053.21c    0.00058574    &
 24054.21c    0.00014580    &
 74182.21c    0.00012457    &
 74183.21c    0.00006699    &
 74184.21c    0.00014340    &
 74186.21c    0.00013303    &
 23000    0.00016830    &
```

```
 6012.21c    0.00035640
c
c VV (27% FS 73% LiPb)
c m6 3006.21c    0.00311221    &
c 3007.21c    0.00034580    &
c 82204    0.00025989    &
c 82206.21c    0.00447390    &
c 82207.21c    0.00410262    &
c 82208.21c    0.00972748    &
c 26054.21c    0.00120997    &
c 26056.21c    0.01899390    &
c 26057.21c    0.00043865    &
c 26058.21c    0.00005838    &
c 24050.21c    0.00008036    &
c 24052.21c    0.00154968    &
c 24053.21c    0.00017572    &
c 24054.21c    0.00004374    &
c 74182.21c    0.00003737    &
c 74183.21c    0.00002010    &
c 74184.21c    0.00004302    &
c 74186.21c    0.00003991    &
c 23000    0.00005049    &
c 6012.21c    0.00010692
c
c CenterStack - Bottom (10% Water, 90% CuCrZr)
m7 1001.21c    0.006543    &
24050.21c    0.00002994    &
24052.21c    0.00057736    &
24053.21c    0.00006547    &
24054.21c    0.00001630    &
40090.70c    0.00002963    &
40091.70c    0.00000646    &
40092.70c    0.00000988    &
40094.70c    0.00000999    &
40096.70c    0.00000161    &
8016.21c    0.00336060    &
27059.21c    0.00004864    &
14028.21c    0.00001726    &
14029.21c    0.00000087    &
14030.21c    0.00000058    &
29063.21c    0.05149942    &
29065.21c    0.02295398
c
c  CenterStack - Top (6.6% Water, 93.4% CuCrZr)
m8 1001.21c    0.00431838    &
24050.21c    0.00003107    &
24052.21c    0.00059917    &
24053.21c    0.00006794    &
24054.21c    0.00001691    &
40090.70c    0.00003075    &
40091.70c    0.00000671    &
40092.70c    0.00001025    &
40094.70c    0.00001037    &
40096.70c    0.00000167    &
8016.21c    0.00225184    &
27059.21c    0.00005047    &
```

```
14028.21c    0.00001791    &
14029.21c    0.00000091    &
14030.21c    0.00000060    &
29063.21c    0.05344495    &
29065.21c    0.02382113
c
c Cooling Channels (58% ODS)
m9 26054.21c    0.00259919    &
26056.21c    0.04080172    &
26057.21c    0.00094229    &
26058.21c    0.00012540    &
24050.21c    0.00017263    &
24052.21c    0.00332894    &
24053.21c    0.00037747    &
24054.21c    0.00009396    &
74182.21c    0.00008028    &
74183.21c    0.00004317    &
74184.21c    0.00009242    &
74186.21c    0.00008573    &
23000    0.00010846    &
6012.21c    0.00022968
c
c Flow Channel Inserts (46% SiC)
m10 14028.21c    0.02050863    &
14029.21c    0.00103844    &
14030.21c    0.00068933    &
6012.21c    0.02223640
c
c Stabilizing Shell (100% W-TiC)
m11 74182.21c    0.01687049    &
74183.21c    0.00907221    &
74184.21c    0.01942090    &
74186.21c    0.01801640
c
c ACTUAL OB-I Homogenization
m15 3006.21c    0.00337763    &
3007.21c    0.00037529    &
82204    0.00028206    &
82206.21c    0.00485545    &
82207.21c    0.00445251    &
82208.21c    0.01055708    &
14028.21c    0.00153176    &
14029.21c    0.00007756    &
14030.21c    0.00005149    &
6012.21c    0.00168526    &
26054.21c    0.00027672    &
26056.21c    0.00434393    &
26057.21c    0.00010032    &
26058.21c    0.00001335    &
24050.21c    0.00001838    &
24052.21c    0.00035441    &
24053.21c    0.00004019    &
24054.21c    0.00001000    &
74182.21c    0.00000855    &
74183.21c    0.00000460    &
74184.21c    0.00000984    &
```

```
74186.21c    0.00000913    &
23000    0.00001155
c
c ACTUAL OB-II Homogenization
m16 3006.21c    0.00308174    &
3007.21c    0.00034242    &
82204    0.00025735    &
82206.21c    0.00443011    &
82207.21c    0.00406246    &
82208.21c    0.00963226    &
14028.21c    0.00123805    &
14029.21c    0.00006269    &
14030.21c    0.00004161    &
6012.21c    0.00140557    &
26054.21c    0.00071545    &
26056.21c    0.01123108    &
26057.21c    0.00025937    &
26058.21c    0.00003452    &
24050.21c    0.00004752    &
24052.21c    0.00091632    &
24053.21c    0.00010390    &
24054.21c    0.00002586    &
74182.21c    0.00002210    &
74183.21c    0.00001188    &
74184.21c    0.00002544    &
74186.21c    0.00002360    &
23000    0.00002985
c
c ************************
c Tally Definitions
c ************************
fmesh4:p geom=xyz origin=0 0 0
          imesh=420 iints=20
          jmesh=247 jints=20
          kmesh=407 kints=20
          emesh = 1.00E-01    5.00E-01    1.00E+00    2.00E+00
                  3.00E+00    4.00E+00    5.00E+00    6.00E+00
                  7.00E+00    8.00E+00    9.00E+00    2.00E+01
fm4 138.408 $ 0.627 * 220.746734
c
nps 1e8
lost 2000 2000
```

The University of Wisconsin - Madison
The Graduate School

Candidate for the degree of **MS**

Nuclear Engineering and Engineering Physics

For: **Spring, 2012**

Jaber, Amir Ebrahim

9030664057

The undersigned report that all degree requirements have been met on 05/14/2012
(Date Completed MMDDYY)

If a thesis will be submitted to Memorial Library, indicate date to be delivered and thesis title.

05/14/2012 Monte Carlo Adjoint Transport and Adjoint Activation for Biological Dose Calculations
(Date MMDDYY) *(Title)*

Will the student continue for a PhD/DMA in the department/program? yes (no) *(circle one)*

We recommend that the above named candidate be awarded the degree indicated

Committee Member Names

Henderson, Douglas

El-Guebaly, Laila

Blanchard, James